Universitat
de Girona

ADVANCES IN THE MODELLING OF THERMOELECTRIC ENERGY HARVESTERS IN WASTE HEAT RECOVERY APPLICATIONS

Eduard Massaguer Colomer

Universitat de Girona

DOCTORAL THESIS

Advances in the modelling of thermoelectric energy harvesters in waste heat recovery applications

EDUARD MASSAGUER COLOMER

Eduard Massaguer Colomer

Universitat de Girona

UNIVERSITAT DE GIRONA

DOCTORAL THESIS

ADVANCES IN THE MODELLING OF THERMOELECTRIC ENERGY HARVESTERS IN WASTE HEAT RECOVERY APPLICATIONS

EDUARD MASSAGUER COLOMER

2016

PROGRAMA DE DOCTORAT EN TECNOLOGIA

Supervised by:

Dr. Josep Ramon Gonzàlez Castro

Dr. Lino Montoro Moreno

THESIS SUBMITTED FOR THE DEGREE OF DOCTOR OF PHILOSOPHY BY UNIVERSITY OF GIRONA

A la meva familia i amics

"Thanks to all those who refused to help me because they made me do it myself"

- Albert Einstein -

ACKNOWLEDGEMENT

Molt probablement aquestes siguin les primeres paraules que hom llegeixi d'aquesta tesi, abans inclús que el seu resum. Aquest treball és la culminació de la meva trajectòria acadèmica, tot i que un no deixa mai d'aprendre. No cal dir que no ha estat un camí fàcil i que, al igual com passa amb les coses realment importants a la vida, molt difícilment les puguem fer sols.

És per aquest motiu que no puc començar de cap més manera que donant les gràcies a aquelles persones que, no només durant el transcurs d'aquests últims anys, sinó també durant les etapes anteriors, m'han ajudat i recolzat en tot allò que, tant bé com he sabut, he anat construint, incús un servidor. És ben cert que no només s'aprèn llegint llibres, sinó també dels altres, compartint moments i experiències. Malauradament, no els acabem transmetent la nostra gratitud amb la freqüència que es mereixen.

Vull començar agraint als meus pares tot el que han fet per mi, n'estic molt orgullós. De vosaltres, del vostre exemple, ho he après tot: a ser constant, perseverant, coherent, a esforçar-me, a posar bona cara als problemes, a no esperar res a canvi... Us puc assegurar que heu fet molt bona feina. Mai podré tornar-vos tot el que m'heu donat.

Agrair també al meu company de viatge tant a dins com a fora de la universitat, el meu germà Albert, el seu suport en tot el que hem anat creant. Sense tu no estaria escrivint aquestes paraules. Espero que hagis après tant de mi com jo de tu.

A la Núria, la meva dona, que sempre m'ha animat a tirar endavant tot allò en el que crec, encara que això suposi passar menys temps junts, al treballar fins tard, i viatjar amunt i avall. Ets el far que guia al mariner per tornar a port.

Un especial agraïment a la família i amics per tots els bons moments que hem passat plegats.

Finalment i com no pot ser d'una altra manera, també donar les gràcies als meus tutors i als companys del grup GREFEMA per la flexibilitat i llibertat que m'heu donat en la elaboració d'aquesta tesi. Ja sabeu que sóc molt exigent amb mi mateix i també amb els que m'envolten. Hem pencat de valent! I quan es treballa en equip es poden fer coses molt grans!

This Ph.D. thesis has been prepared as a compendium of papers, according to the regulations of the University of Girona (Normativa d'ordenació dels ensenyaments universitaris de doctorat de la Universitat de Girona, aprovada pel Consell de Govern en la sessió 3/12 de 26 d'abril de 2012, i modificada pel Consell de Govern en la sessió 5/2013 de 25 de setembre de 2013). This thesis includes two published papers and one submitted paper.

The complete references of the papers comprising this thesis, the impact factors, quartile, and category of the journals according to the 2014 Journal Citation Report are described below.

E Massaguer, A Massaguer, L Montoro, JR Gonzalez. Development and validation of a new TRNSYS type for the simulation of thermoelectric generators. Applied Energy, 134, 65-74, 2014. ISSN 0306-2619 (Impact factor 5,613; Journal 8 of 89; 1st quartile; Energy and Fuels)

E Massaguer, A Massaguer, JR Gonzalez, L Montoro. Modeling analysis of longitudinal thermoelectric energy harvester in low temperature waste heat recovery applications. Applied Energy, 140, 184-195, 2015. ISSN 0306-2619 (Impact factor 5,613; Journal 8 of 89; 1st quartile; Energy and Fuels)

E Massaguer, A Massaguer, T. Pujol, JR Gonzalez. Advances in modeling and analysis of longitudinal thermoelectric energy harvesters. Submitted to Applied Energy. ISSN 0306-2619 (Impact factor 5,613; Journal 8 of 89; 1st quartile; Energy and Fuels)

To whom it may concern,

Dr. Josep Ramon Gonzàlez Castro. Professor in the *Department d'Enginyeria Mecànica i de la Construcció Industrial* at the University of Girona.

And

Dr. Lino Montoro Moreno. Professor in the *Department d'Enginyeria Mecànica i de la Construcció Industrial* at the University of Girona.

CERTIFY that the study entitled *Advances in the modelling of thermoelectric energy harvesters in waste heat recovery applications* has been carried out under their supervision by Eduard Massaguer Colomer to apply for the doctoral degree.

Girona, May 2016

Dr. Josep Ramon Gonzàlez Castro   Dr. Lino Montoro Moreno

Universitat de Girona   Universitat de Girona

Nomenclature

Abbreviation

TEG	Thermoelectric generator
LTEH	Longitudinal thermoelectric energy harvester

Letters

n	Number of thermocouples
e	Length (m)
A	Cross sectional area (m^2)
S	Specific heat capacity (J/kgK)
K	Thermal conductance (W/K)
C	Thermal capacity (J/K))
h	Convective heat transfer coefficient (W/m^2K)
Q	Heat rate (W)
V	Electric voltage (V)
I	Electric current (A)
P	Electric power (W)
R	Electric resistance (Ω)
T	Temperature (K)
y	Axis coordinate (m)

t	Time (s)
$\dot{m}$	Mass flow rate (kg/h)
np	Number of TEGs in parallel
ns	Number of TEGs in series

Greek symbols

α	Seebeck coefficient (V/K)
σ	Electrical resistivity (Ωm)
ρ	Material density (kg(m^3)
λ	Thermal conductivity (W/mK)
η	Efficiency (%)

Subscripts

hp	Hot plate
$tc1,2,3$	Thermal compound
ce	Ceramic substrate
cp	Cold plate
cb	Water-cooling block
h,H	Hot side
c,C	Cold side
p	p-type semiconductor
n	n-type semiconductor
in	Input
L	Load resistance
$c\infty$	Cooling water

oc Open circuit

max Maximum

ss Steady-state

hh Hot side heat exchanger

ch Cold side heat exchanger

cl Copper lid

out Output

amb Ambient air

AVG Average

i Stage number

j Row number

f Fluid

k Iteration number

x

List of Figures

List of Tables

Content

Resum

Els dispositius termoelèctrics poden convertir l'energia tèrmica directament en energia elèctrica, o poden treballar en mode invers i utilitzar l'energia elèctrica per crear un gradient de temperatura per aplicacions de refrigeració o calefacció. L'absència de parts mòbils, l'àmplia gamma de temperatures de funcionament, l'escalabilitat i la seva capacitat modular els fan atractius per a aplicacions de generació d'energia.

La recuperació d'energia de fonts de calor residual pot tenir un paper important en l'estalvi d'energia i reduir la dependència de fonts d'energia primària. Proporcionar un subministrament d'energia sostenible s'està convertint en un problema social important, atès que en els pròxims anys el subministrament de combustible fòssil disminuirà mentre que la demanda energètica augmentarà. És per aquest motiu que en els últims anys s'ha observat un augment en l'interès i en el desenvolupament de tecnologies alternatives. En particular, els materials termoelèctrics han esdevingut el centre d'atenció ja que permeten la conversió directa de calor en energia elèctrica i proporcionen una font alternativa de generació d'energia.

S'ha estudiat el seu ús en tubs d'escapament de vehicles, en aplicacions de cogeneració, i en la recuperació de calor en cicles termodinàmics. Tot i que els dispositius termoelèctrics tenen eficiències relativament baixes, recentment hi ha hagut avenços en materials termoelèctrics que obren la porta a un gran nombre de noves aplicacions. Atès que els avenços en nous materials continuen i per tant s'estendrà el ventall d'aplicacions de

generació d'energia, els sistemes de modelització seran fonamentals per al disseny de la propera generació de recuperadors termoelèctrics.

En aquest treball s'investiga la recuperació termoelèctrica en xarxes de fluids i es proposa una eina genèrica per a la simulació i dimensionament de recuperadors termoelèctrics, els quals, poden ser utilitzats en aplicacions industrials per convertir l'energia tèrmica residual en electricitat.

Els models actuals que es troben en la literatura es basen sovint en aplicacions molt específiques o són massa generals per analitzar realment el comportament de recuperadors en aplicacions reals. El model desenvolupat en aquest treball és altament adaptable pel que permet estudiar un gran nombre de sistemes diferents.

S'ha desenvolupat un model teòric per estimar amb precisió l'energia recuperada tenint en compte les no linealitats de les equacions termoelèctriques i de transferència de calor. Tenint en compte que un recuperador termoelèctric comprèn sempre múltiples mòduls termoelèctrics col·locats en respecte a la direcció de flux, ambdues configuracions sèrie-paral·lel, tant la tèrmica com l'elèctrica, s'han considerat. El model presenta un NRMSE de 0.52% i 0.75% i un RMSE de 2.15×10^{-4}% i 2.9mW per a l'eficiència i la generació elèctrica, respectivament.

El nou model ha estat analitzat i validat sota diversos estats estacionaris i transitoris a partir de dades experimentals. El model de recuperador proposat s'ha codificat per tal de treballar en l'entorn TRNSYS, de manera que pot ser utilitzat en el disseny i optimització de recuperadors termoelèctrics, és fàcilment escalable, permet atendre a una gran varietat d'aplicacions i requisits i, per tant, ajudar a la seva implantació en aplicacions reals. Aquest mòdul servirà per predir el comportament de recuperadors de calor termoelèctrics aplicats en sistemes tèrmics convencionals.

Resumen

Los dispositivos termoeléctricos pueden convertir la energía térmica directamente en energía eléctrica, o pueden trabajar en modo inverso y utilizar la energía eléctrica para crear un gradiente de temperatura para aplicaciones de refrigeración o calefacción. La ausencia de partes móviles, la amplia gama de temperaturas de funcionamiento, la escalabilidad y su capacidad modular los hacen atractivos para aplicaciones de generación de energía.

La recuperación de energía de fuentes de calor residual puede tener un papel importante en el ahorro de energía y reducir la dependencia de fuentes de energía primaria. Proporcionar un suministro de energía sostenible se está convirtiendo en un problema social importante, dado que en los próximos años el suministro de combustible fósil disminuirá mientras que la demanda energética aumentará. Es por este motivo que en los últimos años se ha observado un aumento en el interés y en el desarrollo de tecnologías alternativas. En particular, los materiales termoeléctricos se han convertido en el centro de atención ya que permiten la conversión directa de calor en energía eléctrica y proporcionan una fuente alternativa de generación de energía.

Se ha estudiado su uso en tubos de escape de vehículos, en aplicaciones de cogeneración, y en la recuperación de calor en ciclos termodinámicos. Aunque los dispositivos termoeléctricos tienen eficiencias relativamente bajas, recientemente ha habido avances en materiales termoeléctricos que abren la puerta a un gran número de nuevas aplicaciones. Dado que los avances en nuevos materiales continúan y por tanto se extenderá el abanico de aplicaciones de generación de energía, los sistemas de modelización serán

fundamentales para el diseño de la próxima generación de recuperadores termoeléctricos.

En este trabajo, se investiga la recuperación termoeléctrica en redes de fluidos y se propone una herramienta genérica para la simulación y dimensionado de recuperadores termoeléctricos, los cuales pueden ser utilizados en aplicaciones industriales para convertir la energía térmica residual en electricidad.

Los modelos actuales que se encuentran en la literatura se basan a menudo en aplicaciones muy específicas o son demasiado generales para analizar realmente el comportamiento de recuperadores en aplicaciones reales. El modelo desarrollado en este trabajo es altamente adaptable por lo que permite estudiar un gran número de sistemas diferentes.

Se ha desarrollado un modelo teórico para estimar con precisión la energía recuperada teniendo en cuenta las no linealidades de las ecuaciones termoeléctricas y de transferencia de calor. Teniendo en cuenta que un recuperador termoeléctrico comprende siempre múltiples módulos termoeléctricos colocados en respecto a la dirección de flujo, ambas configuraciones serie-paralelo, tanto la térmica como la eléctrica, se han considerado. El modelo presenta un NRMSE de 0.52% y 0.75% y un RMSE de 2.15×10^{-4}% y 2.9mW para la eficiencia y la generación eléctrica, respectivamente.

El nuevo modelo ha sido analizado y validado bajo diversos estados estacionarios y transitorios a partir de datos experimentales. El modelo de recuperador propuesto se ha codificado para trabajar en el entorno TRNSYS, por lo que puede ser utilizado en el diseño y optimización de recuperadores termoeléctricos, es fácilmente escalable, permite atender a una gran variedad de aplicaciones y requisitos y por tanto ayudar a su implantación en aplicaciones reales. Este módulo servirá para predecir el comportamiento de recuperadores de calor termoeléctricos aplicados en sistemas térmicos convencionales.

Abstract

Thermoelectric devices can convert thermal energy directly into electrical energy, or they can work in reverse and use electrical energy to create a temperature gradient for cooling or heating applications. The absence of moving parts, wide range of operating temperatures, scalability, and modular capabilities makes thermoelectrics attractive for energy generation applications.

Harvesting energy from previously unemployed ambient sources can play an important role in saving energy and reducing the dependency to primary energy sources. Providing a sustainable supply of energy is becoming a major societal problem as fossil fuel supplies decrease while demands increase. Hence, the past few years have witnessed a surge in interest in developing alternative renewable energy technologies. In particular, thermoelectric materials have drawn attention because thermoelectric effects enable direct conversion from thermal to electrical energy, and provide an alternative source of power generation.

They have been considered for use with vehicle exhausts, co-generation, and other energy recovery from lost heat in thermodynamic cycles. Thermoelectric devices have relatively low efficiencies but there have been recent advances in thermoelectric materials potentially opening the door to more power applications. As material advancements continue and a wider range of power generation applications will be considered,

module and system level modelling becomes critical for the design of the next generation of thermoelectric systems.

In this work, we investigate harvesting thermoelectric energy from wasted heat in fluid networks and propose a generic tool for the simulation and sizing of thermoelectric energy harvesters, that can be used in industrial applications to convert expended heat energy into electricity.

Current models found in the literature are often based on very specific applications or are too general in nature to truly explore the optimization of a wide range of potential thermoelectric applications. The model developed in this work is highly customizable permitting the optimization of a large number of varying systems.

We develop a theoretical model to accurately estimate the recovered energy considering the nonlinearities of the thermoelectricity and heat transfer equations. Taking into account that a real thermoelectric energy harvester always comprises multiple thermoelectric modules placed with respect to the flow direction, both thermal and electrical series-parallel configurations have also been considered.

The new model has been analysed and validated under steady and transient states with experimental data. The proposed energy harvesting system is easily scalable, to cater to a variety of applications with different requirements, while improving the energy recovery and operational lifetime of energy sources. The value of RMSE is 2.15×10^{-4} % and 2.9mW for efficiency and electrical output power. The model presents a normalized root mean square error NRMSE of 0.52% and 0.75% for efficiency and electrical output power.

On the other hand, this new model is coded in the TRNSYS environment, hence it can be used in design, performance optimization and further application of thermoelectric energy harvesters. The programmed module will serve as the key component of the software package that will predict the performance of the thermoelectric heat recovery unit used in common thermal systems.

Chapter 1

Introduction

1.1 Introduction

In the present chapter, there is firstly a general introduction about thermoelectric energy harvesting followed by summary of the thesis contents and finally the main objectives of this work are introduced.

This thesis has been prepared as a compendium of papers. Chapter 2 contains a transcription of the published paper "Development and validation of a new TRNSYS type for the simulation of thermoelectric generators". In Chapter 3 there is a transcription of the published paper "Modelling analysis of longitudinal thermoelectric energy harvester in low temperature waste heat recovery applications". Finally, in Chapter 4 a transcription of the published paper "Advances in modeling and analysis of longitudinal thermoelectric energy harvesters" can be found.

In the last chapter a discussion recapitulates and summarizes the main findings. Suggestions for future research and necessary improvements in the modelling systems are made.

1.2 Thermoelectric energy harvesting

A thermoelectric power generator (TEG) is a solid-state device that provides direct energy conversion from thermal energy, due to a temperature gradient, into electrical energy based on Seebeck effect. Also, they can work in reverse mode and use electrical energy to create a temperature gradient for cooling or heating applications.

The absence of moving parts, wide range of operating temperatures, scalability, and modular capabilities makes thermoelectricity attractive for a wide variety of applications, such as power for remote control and monitoring of oil or gas pipelines and production facilities, automotive waste heat recovery, power for navigational aids, spacecraft radioisotope

power supply, telecommunications systems and cathodic protection, and other energy recovery processes [1–6].

Thermoelectric devices have relatively low efficiencies but there have been recent advances in thermoelectric materials potentially opening the door to new power applications [7,8]. As material advancements continue and a wider range of power generation applications will be considered, module and system level modelling becomes critical for the design of the next generation of thermoelectric systems.

TEGs contain two dissimilar thermoelectric materials which are arranged electrically in series and thermally in parallel. The junctions of the different conductors are kept at different temperatures which cause an open circuit electromotive force to develop as follows:

$$V_{oc}(t) = \alpha_{pn} \left(T_{pn,h}(t) - T_{pn,c}(t) \right) \tag{1.1}$$

where α_{pn} is the difference in Seebeck coefficient of the two leg materials and has the units of V/K and $T_{pn,h}$ and $T_{pn,c}$ are the hot and cool side absolute temperatures both measured in Kelvin. Thomas Johann Seebeck, a German physicist, discovered this effect in the early 1800s. When a load is applied, electric current is driven by the temperature difference as heat conducts through the device. In the same time period, an independent discovery from Seebeck's research was made by French physicist, Jean Charles Athanase Peltier. The Peltier Effect is the reverse of the Seebeck Effect; as electric current is applied to a semiconductor, heat is absorbed or released depending on direction of current and the relationship of the Seebeck coefficients. The heat absorption or dissipation may create a temperature gradient depending on thermal loading [9].

An important unit-less metric for evaluating the performance of thermoelectric materials is the thermoelectric figure of merit, ZT. It characterizes the effectiveness of a specific thermoelectric material in

terms of its electrical and thermal material properties. The figure of merit is expressed as

$$ZT = \frac{\alpha^2 \sigma}{\lambda} T \tag{1.2}$$

where α is the Seebeck coefficient, σ is the electrical conductivity λ, is the thermal conductivity, and T is the absolute average temperatura of the material [9]. ZT for materials has remained below one for decades but in recent years, ZT of new materials has reached values greater than two [10]. These increases in the figure of merit are a result of studies in nanostructures of thermoelectric materials. This research has the promise of increasing the figure of merit to even higher values. With values greater than 3, thermoelectrics provide feasible solutions in many applications [11].

Modules consist of a group of thermoelectric semiconductor pairs, called legs or pellets, connected electrically in series and thermally in parallel as is shown in Figure 1.1. The ends of the leg pairs are typically connected by a conductor. On top of these conductors an electrically insulating but thermally conductive material is attached to prevent electrical shorting of the leg pairs, typycally a ceramic substrate.
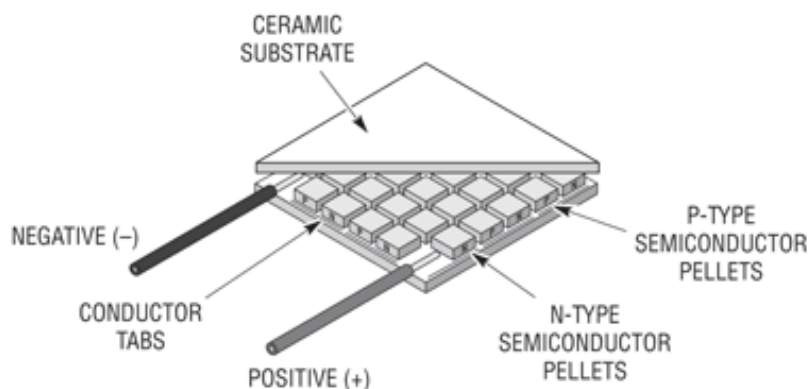
Figure 1.1. Typical one-stage thermoelectric module [12].
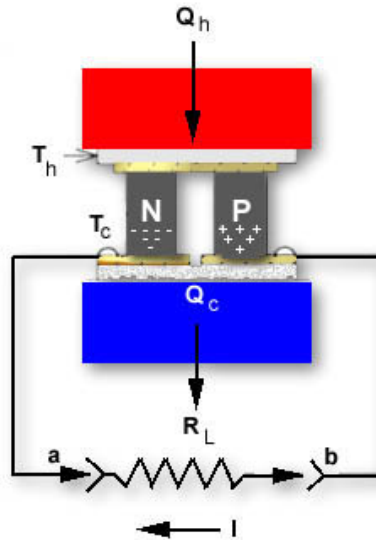
Figure 1.2. Schematic representation of a thermoelectric pair [13].

Figure 1.2 represents a single thermoelectric pair. The heat flowing into the hot surface, Q_h, and out of the cold surface, Q_c, are given by

$$Q_h(t) = K_{pn}\left(T_{pn,h}(t) - T_{pn,c}(t)\right) + \alpha_{pn}I(t)T_{pn,h}(t) - \frac{1}{2}I^2(t)R_{pn} \tag{1.3}$$

$$Q_c(t) = K_{pn}\left(T_{pn,h}(t) - T_{pn,c}(t)\right) + \alpha_{pn}I(t)T_{pn,c}(t) + \frac{1}{2}I^2(t)R_{pn} \tag{1.4}$$

With K_{pn} representing the thermal conductance of the thermoelectric material, I representing the current [6] and R_{pn} the electrical resistance of the thermoelectric module. Module level Seebeck coefficient α_{pn}, module level thermal conductivity λ_{pn} and module level electrical resistance σ_{pn} are the three parameters that define the performance of a thermoelectric module. It must be take into account that a TEG is composed of multiple thermoelectric pairs. Therefore, each parameter have to be multiplied by the number of thermoelectric leg pairs n.

$$K_{pn} = \frac{\lambda_{pn} A_{pn}}{e_{pn}} \tag{1.5}$$

$$\alpha_{pn} = n(\alpha_p - \alpha_n) \tag{1.6}$$

$$\lambda_{pn} = n(\lambda_p + \lambda_n) \tag{1.7}$$

$$R_{pn} = n\left(\frac{\sigma_p e_p}{A_p} + \frac{\sigma_n e_n}{A_n}\right) \tag{1.8}$$

This model operates under the assumptions that there is 1-D thermal transport only, the Seebeck coefficient is constant, and contact resistance of the conducting strips can be ignored. These equations are derived from the heat equation subject to the Seebeck effect equation. The first term is the thermal resistance of the thermoelectric leg pair for the temperature gradient of the boundary surfaces. The second term represents the Peltier effect which is reversible heat absorption or emission at the leg interfaces. The third term is the Joule heating in the semiconductor leg pairs operating at a specific current [14]. Applying conservation of energy gives the following relationship

$$P_{R_L}(t) = Q_h(t) - Q_c(t) = V_{R_L} I = \frac{\alpha_{pn}^2 \left(T_{pn,h}(t) - T_{pn,c}(t)\right)^2 R_L}{\left(R_{pn} + R_L\right)^2} \tag{1.9}$$

where P_{R_L} is the electrical power extracted from the system by the thermoelectric module [15]. Although above equations describe the performance of an individual thermoelectric module subject to $T_{pn,h}$ and $T_{pn,c}$ boundary conditions, more complex formulations are required for modeling entire thermoelectric power units utilizing multiple modules and with thermal resistance between the modules and the heat source and sink.

To boost the waste heat recovery and consequently the output power, energy harvesters are often composed of multiple arrays of TEGs electrically arranged in series-parallel configuration. The way that TEGs are connected strongly affects the electro-thermal outputs of each TEG and the whole harvester as well.

When the heat source comes from a liquid or gas stream, the most used topology is the longitudinal thermoelectric energy harvester LTEH [16], in which TEG modules are located along the energy flow path with the purpose to convert the maximum amount of thermal energy into electrical power.

A basic drawing of a LTEH with insulation surrounding it, solid surfaces holding it in place and a convective medium across these surfaces on the hot and cold side is represented in Figure 1.3.

1. Cold side heat exchanger 2. Thermoelectric generator 3. Hot side heat exchanger
4. Copper lid 5. Thermal compound 6. Ceramic substrate
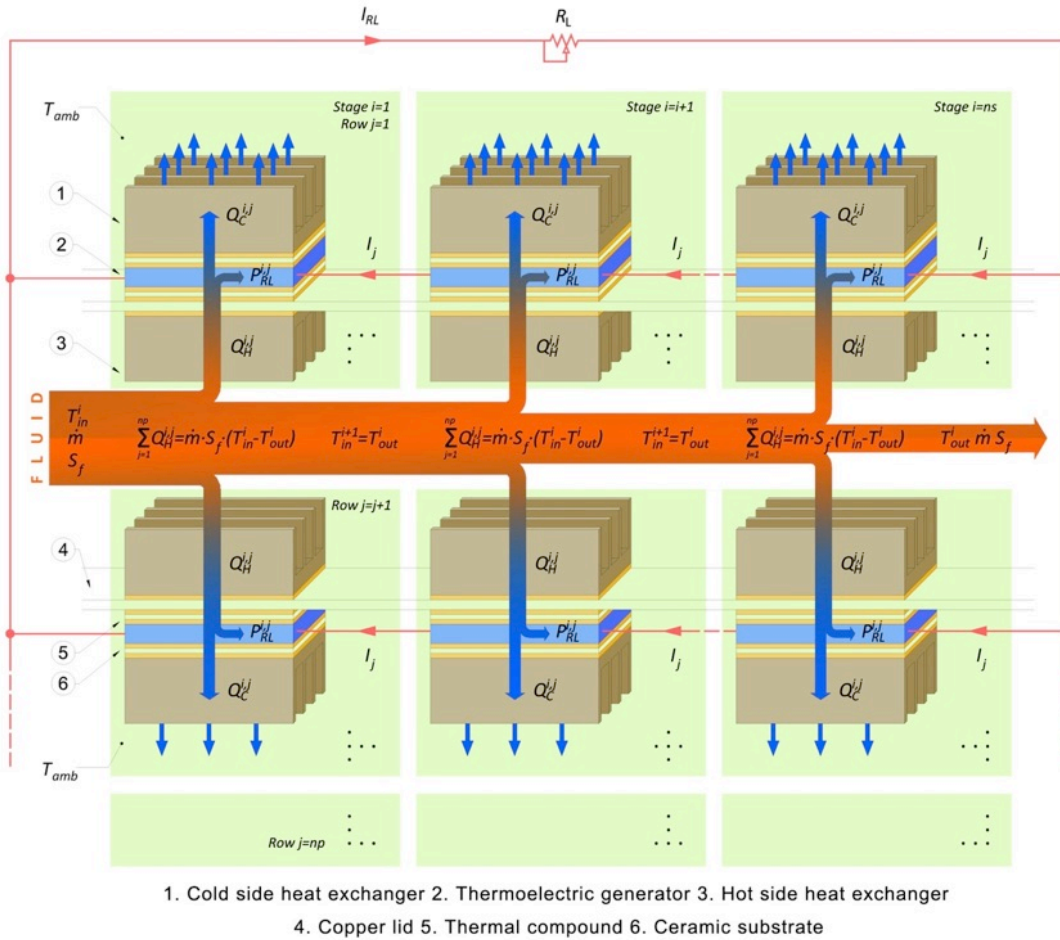
Figure 1.3. Basic scheme of a longitudinal thermoelectric energy harvester.

Figure 1.3 shows the basic scheme of the longitudinal model presented in this thesis, which allows the simulation of LTEHs composed of multiple *ns* stages and *np* rows. In fact, it is the same configuration used in the 1-D thermoelectric generator model explained above, which takes into account the heat extraction from fluid due the thermoelectric generation, resulting in a fluid temperature and power reduction at every stage: $T_{in}^i > T_{in}^{i+1}$ and $P_{RL}^{i,j} > P_{RL}^{i+1,j}$. When TEGs are interconnected, both heat transfer and electrical equations are dependents. It is important to note that current I_j flowing through a branch *j* is the same flowing through each TEG in the same branch, though they are not working at the same temperature difference: $T_{in}^i > T_{in}^{i+1}$. Consequently, the system of equations formed by heat transfer and electrical equations must be solved simultaneously at each time step.

8

Many models describing the electro-thermal behaviour of thermoelectric generators TEGs exist in literature. Gou et al. [17] and Meng et al. [18] presented a theoretic dynamic model of a general thermoelectric generator with finned heat exchangers. However, it does not take into account the electrical interconnection effect of the TEG array, neither the heat losses of the fluid at each stage. Hsiao et al. [19] also analyzed a model of a TE module applied on an automobile exhaust. They provided a scientific methodology with complicated equations on the field of thermoelectric simulations. However, the model cannot be used to simulate the behavior of a LTEH. It only solves the heat transfer and electrical equations of a single TEG module. Therefore, it does not consider the electrical and thermal losses due to the longitudinal and array configuration.

Wu [20] performed a theoretical analysis on waste-heat thermoelectric power generators. In this study, a real waste-heat thermoelectric generator model was presented based on accounting for both internal and external irreversibility to predict realistic specific power and efficiency. Therefore, this approach gave a much more realistic generator specific power and efficiency prediction than does the ideal TEG.

Crane and Jackson investigated thermoelectric waste heat recovery with regards to cross flow heat exchangers [21,22]. A cross flow heat exchanger model was validated against measured performance of advanced cross flow heat exchangers without thermoelectrics. The numerical simulations were compared to experimental data with good agreement between them.

Wang et al. [4] presented a mathematical model of a TEG device using the exhaust gas of vehicles as heat source. The model simulates the impact of relevant factors, including vehicles exhaust mass flow rate, temperature and mass flow rate of different types of cooling fluid, convection heat transfer coefficient, height of PN couple, the ratio of external resistance to internal resistance of the circuit on the output power and efficiency. However, just a few experimental results are provided.

Yu and Zhao [23] developed a numerical model for prediction of performance of a TEG with a parallel-plate heat exchanger. They assumed that the flat thermoelectric modules were held tightly between hot and cold fluids, which had multiple thermocouples with a single layer of p- and n-type semiconductors. The thermocouples along the fluid path were connected electrically in series. A typical energy balance was used to set up the model with the differential equations discretized along the axial direction of the hot fluid. The solution to the numerical model was provided using an iterative method. Simulations were performed to study the effects of the various parameters. An experimental study based on the Yu and Zhao model [23] was performed by Niu, Yu and Wang [24]. A comparison of the experimental results with the numerical model is presented in this work. A two fluid, multi-plate, multi-pass, counter/parallel flow heat exchanger with thermoelectric generators was created for the experimental phase. The data obtained through experimentation shows that the numerical model over-predicts performances of the TEGs over the entire range of data. At lower temperatures, the model displays better agreement with experimental results, but as hot fluid inlet temperatures are increased, the prediction diverges from the measured values. The discrepancy is associated to the lack of accounting for heat losses and the fact that thermoelectric properties are treated as constants.

Finally, Xiong et al. [25] developed a numerical model of two-stage thermoelectric energy harvesting system driven by waste heat from the slag water of a blast furnace. This model do consider the longitudinal heat losses of the fluid but do not consider a multiple TEG array, neither the electrical interconnection effect.

The above literatures provided some significant guidelines for the design of the thermoelectric energy harvesters in terms of the principle of thermodynamics. However, aforesaid models are only validated for stand-alone applications without taking into account the electrical interconnection effect of the TEG array.

The interconnection of TEGs can produce a global power production drop of 12% with respect to a not interconnected LTEH. That is because of the temperature mismatch between thermoelectric stages [26,27].

Module mismatch reduces performance of thermoelectric modules as they are connected together electrically. The degraded performance is suspected to be a result of the difference in key module parameters between modules including internal electrical resistance and Seebeck coefficient. Modules are producing less power than predicted by simple modeling means, so improved models need to be developed and employed. Experimental data must first be gathered by comparing thermoelectric modules with varying Seebeck coefficients and internal electrical resistances to test and validate the module mismatch models. Each module has these specific parameters that affect their voltage-current relationship thus affecting their maximum power produced. If the values of the maximum power points of the modules' power curves were simply added together, it could be significantly more than a maximum power point of the power curve that represents the modules linked electrically. A model for modules linked electrically in series as well as electrically in parallel is needed to accurately predict power recovered by modules with unequal material parameters.

Taking into account these phenomena, a complete LTEH model considering electrical interconnection effect is mandatory.

1.3 Motivation

Our world hungers for energy. As global population is growing and more and more people will increase their quality of life, this will also yield higher energy consumption. According to recent report the energy demand will continue to increase by 30-40% the next 20 years [28,29]. Today most of the energy, around 80%, comes from fossil fuels and will continue to do so in the near future. Because of the greenhouse gases these energy conversion technologies emits, along with its inherent non-sustainable usage of limited resources, others sources of energy will eventually need to take over a much higher portion of the energy production. Renewables, even though it accounts for very small portions of the energy production

today, is believed to take care of much of the growth in energy production in the last part of this century. But producing more clean and renewable energy is not the only solution. We also need to utilize the energy we already produce in a much more efficient way.

The utilisation of waste energy in industrial enterprises has enormous potential in terms of energy efficiency, the exploitation of which delivers both positive ecological and economic benefits.

In these days of mounting environmental awareness and more intensive discussions on the subject of sustainability and the concomitant conservation of fossil fuels, the energy industry is focusing increasingly on the topic of energy efficiency. Both of these topics are intimately entwined. In addition to renovation or modernisation of the plant and depending upon the specific circumstances, the utilisation of hitherto neglected energy potentials, such as waste heat, can contribute to a net increase in the energy yield from the primary energy carriers and therefore to increased energy efficiency.

The term 'waste heat' refers to any heat generated by a living organism, technical plant or process, which is dissipated into the surrounding environment without being used. It is created through inefficient facilities or process management as well as through thermodynamic constraints.

It is classified with reference to the prevailing temperature level in accordance with the following scheme:

- Low temperature waste heat: < 150 °C
- Medium temperature waste heat: 150 °C-500 °C
- High temperature waste heat: > 500 °C

The greatest untapped waste heat potential is to be found in the industrial sector. Extremely energy-intensive production processes are especially prone to the creation of heat loss sources, in which useful energy

generated from primary energy carriers is dissipated into the surrounding environment as industrial thermal waste.

It is estimated that mankind wastes ~20% of the 15 terawatts required annually for global power consumption as low level heat (<200ºC)[30]. This amounts to 10^{20} J/yr, which is greater than the total annual energy usage of all EU member states. Widespread availability of new low-cost thermoelectric devices would allow direct heat-to-electrical energy from this vast, essentially untapped, resource generating a new industrial sector based on local power generation from otherwise wasted energy sources (engines, boilers, heat pumps, etc.) amounting up to 50 billion €/yr[31].

From an ecological perspective, the generation of useful energy from waste heat is carbon neutral. No additional primary energy carriers are introduced for the conversion of waste heat into usable energy. Another ecological consideration is the fact that the useful energy gained through this technology substitute that which would have been consumed from other energy sources that do consume primary energy carriers during the conversion process. This substitution reduces the utilisation of primary energy sources, for example, in the production of process heating, electricity or heating.

In addition, this energy substitution has economic effects. By saving the thermal or electrical energy that would have to have been supplied through alternative energy production processes, the cost of fuel or electrical power can also be saved. Energy expenditure is often a significant cost factor, which directly influences the ability of production firms to compete in the market. By contrast with the consumption of energy from public sources, the costs associated with the conversion of waste heat to usable energy can be calculated over the long term. This reduced the dependency on the energy markets and the concomitant risk of unpredictable price increases.

Over and above this, the provision of process heating through waste heat exploitation can result in a lower CO2 certificate quantity requirement, which, in turn, results in cost savings.

Heat recovery has it theoretical foundation in thermodynamics. Waste heat has a lower energy value (a higher entropy) than other forms of energy such as electricity. The carnot efficiency is the highest theoretical efficiency a heat recovery system can obtain and is given by $\eta = T_H - T_C/T_H$ where T_H is the temperature of the waste heat, T_C the temperature of the cold side heat exchanger and η the ratio between the work done by the system (for example electricity generated) and the heat energy supplied. This equation shows how the higher the temperature of the waste heat is, the more efficient can this energy be exploited further.

Cases where the temperature is too low or the energy volume too small, are seldom considered usable with existing technology to encompass investment in energy recovery systems. Steam turbines, which are the most used technology for converting heat into electricity, takes up a lot of extra space, need extra maintenance and complicates the total process further while also having a much higher cost per watt produced at lower temperatures [32]. The same factors limit most of the existing waste heat recovery technologies.

Key advantages of TEGs for waste-heat recovery are their simplicity, minimal maintenance requirements, and reliability since there is no rotating machinery in the system. Thermoelectric devices are making gains in their efficiencies and power outputs for their most effective operating conditions. As these advances are made, applications for these devices need to be explored. Their implementation into industry could lead to a plethora of power recovered from waste heat in many different applications. Power utilities, turbine and compressor exhausts, manufacturing plants, automobile exhausts, and incinerator plants are prime examples of applications that could benefit from a thermoelectric system. Many of these systems, either directly or indirectly, use finite resources as their source of fuel.

For industry purposes, heat exchanger subsystem level needs to support the module level advancements to ensure proper design for the application of the thermoelectric modules. A modeling tool will allow for better development of thermoelectric subsystems for industry use and provide justification for implementation into the thermodynamic system.

A tool that is being developed by GREFEMA, consist of a computational platform that has the capability to simulate a thermodynamic system with a thermoelectric recovery system attached. Performance can be optimized by varying thermoelectric parameters as well as system design parameters. This allows the user to perform a direct analysis as well as obtain quantitative results. The results obtained span every point of the entire system and provide detail to the exact operation of the system. It also allows for optimization of design variables when proposing a thermoelectric heat recovery unit.

1.4 Objectives

The primary objective of this thesis is to develop a new computational model of a thermoelectric energy harvester capable to simulate the electro-thermal dynamics of a longitudinal thermoelectric energy harvester composed of an array of interconnected TEG modules, which, at the same time, can be disposed thermally and electrically in different series-parallel configurations. A secondary aim will be to develop a well optimized model running without interruptions or delays, so it can be used in design, performance optimization and further application of thermoelectric energy harvesters.

Although many models have been provided, most of them are only validated for stand-alone applications without taking into account the electrical interconnection effect of the TEG array. Therefore, the objectives of this work can be summarized as:

- Study and analyse the existing LTEH models.
- Propose a new model capable to simulate the transient electro-thermal dynamics of a LTEH.
- Develop a robust model that allows the optimization of the overall system by varying the module level design parameters.
- Consider that thermoelectric parameters are temperature-dependent.
- Reduce computation time.
- Test and validate the model with experimental data.
- Quantify the model mismatch.

Development and validation of a new TRNSYS type for the simulation of thermoelectric generators

This section is a transcription of the contents of the following paper (a copy of the published version can be found in Appendix A):

Abstract

Thermoelectric generators (TEGs) make use of the Seebeck effect in semiconductors for the direct conversion of heat into electrical energy, being of particular interest for high reliability systems or for waste heat recovery. Although several TEG models can be found in the literature, many of them not offer a theoretical solution because they are based on steady-state solutions or they are assuming fixed parameters as boundary conditions. Consequently, to assess and optimize thermoelectric generators in real applications a numerical transient simulation tool, which takes into account the whole energy system, is mandatory. For that purpose, a new TRNSYS type is developed. This TEG component, which can be used as a design tool, is presented in this paper and validated using experimental data.

The results show that the proposed component is able to cope with both thermal and electrical dynamics. The comparison between theoretic and experimental results has approved the reasonability of the new component. The normalized root mean square errors are 3.53% and 2.33% for temperature difference between hot and cold sides and electrical output power, respectively.

2.1 Introduction

A thermoelectric power generator is a solid-state device that provides direct energy conversion from thermal energy, due to a temperature gradient, into electrical energy based on Seebeck effect. Also, they can work in reverse and use electrical energy to create a temperature gradient for cooling or heating applications. The absence of moving parts, wide range of operating temperatures, scalability, and modular capabilities makes thermoelectricity attractive for a wide variety of applications, such as power for remote control and monitoring of oil or gas pipelines and production facilities, automotive waste heat recovery, power for navigational aids, spacecraft radioisotope power supply, telecommunications systems and cathodic protection, and other energy recovery processes [1–6]. Thermoelectric devices have relatively low efficiencies but there have been recent advances in thermoelectric materials potentially opening the door to new power applications [7,8]. As material advancements continue and a wider range of power generation applications will be considered, module and system level modelling becomes critical for the design of the next generation of thermoelectric systems.

Although several models for TEG modules can be found in the literature [17–19,33–37], many of them not offer a theoretical solution because their governing equations are based on steady-state solutions or they are assuming fixed temperatures as boundary conditions at both sides of the TEG. Moreover, almost none of them have studied the transient effects of load resistance. Complete transient analyses are seldom presented and just a few have already provided a complete mathematical solution of the heat conduction equation for TEG devices [35–37].

This study attempts to fill the existing gap in the simulation of thermoelectric generation through the development of a new component that can be used in TRNSYS software. TRNSYS [38], developed at the University of Wisconsin, is a transient systems simulation program with a

modular structure. It recognizes a system description language in which the user specifies the components that constitute the system and the manner in which they are connected. The TRNSYS library includes many of the components commonly found in thermal and electrical energy systems, as well as component routines to handle input of weather data or other time-dependent forcing functions and output of simulation results. The modular nature of TRNSYS gives the program flexibility, and facilitates the addition to the program of mathematical models not included in the standard TRNSYS library. TRNSYS is well suited to detailed analyses of any system whose behaviour is dependent on the passage of time. It has become reference software for researchers and engineers around the world. Main applications include: solar systems (solar thermal and photovoltaic systems), low energy buildings, HVAC systems, renewable energy systems, cogeneration, fuel cells and more.

Full integration of the new component within the TRNSYS simulation package is another advantage of this study, which makes it more applicable for designers in both the design and commissioning of waste energy harvesting systems. The incorporation of the TEG model into standard TRNSYS library will allow users to simulate TEGs coupled to many different thermal facilities and applications (e.g. solar thermal systems, geothermal systems and more). Because of the mentioned benefits, TRNSYS is chosen to implement the new component.

The objective of this work is to develop a computational model capable to simulate the electro-thermal dynamics of a TEG system into TRNSYS software. The new component is fully analysed and validated under steady and transient states with data obtained from the experimental setup.

2.2 TEG modelling

A TEG device in essence is a thermopile composed of a number of p- and n-type semiconductor pairs connected electrically in series. Heat carries the majority carriers from one junction to the other producing a current and voltage. By placing many PN couples in series electrically and in parallel thermally, a TEG module generates an open-circuit voltage proportional to the temperature differential across the elements.

According to Seebeck, Peltier and Thomson effects, the TEG power generation depends mainly on both temperature differential across the semiconductor elements and electrical load connected (i.e. changes of the temperature difference lead to changes of the open-circuit voltage, and the TEG output performance will change as well). Therefore, the unsteady-state heat transfer model is built to solve the TEG temperature distribution. Thereafter, the TEG power and performance outputs can be determined.

Similar with Gou [17,39], Kim [40], Nguyen [36] and Rodríguez [41], the basic configuration of the thermoelectric study follows the general design illustrated in Figure 2.1.
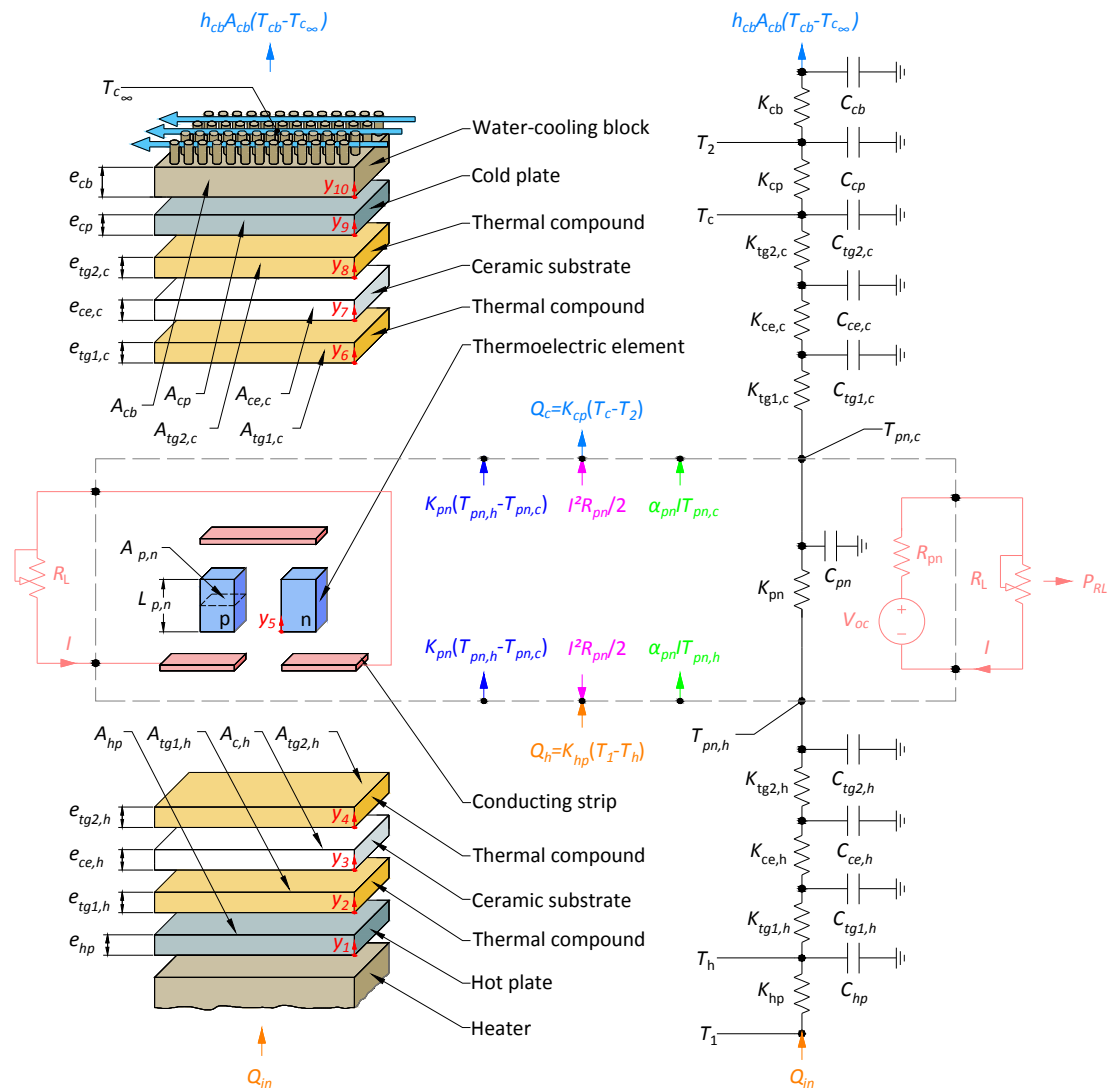
Figure 2.1. One-dimensional heat transfer model of thermoelectric generator.

A thermoelectric module is sandwiched between electrical heater and water-cooled heat exchanger that can be treated as a convective heat transfer system. The TEG consists of certain number of semiconductors, corresponding solder layers, conducting strips and thermal insulation material. In order to electrically isolate the module, a ceramic substrate is located both sides of the TEG. A thermal compound increases the thermal conductivity of the interfaces by filling microscopic air-gaps between ceramic substrates and aluminium plates and TEG and ceramic

substrates, respectively. At the same time, hot and cold plates allow to introduce temperature sensors on the experimental set up.

2.2.1 Assumptions and boundary conditions

In the analytical assessing, the thermal conductivity, electric conductivity, and Seebeck coefficient of semiconductors are all assumed to be temperature-independent, and adiabatic boundary conditions were supposed on the side surfaces of TEG element. Thermal conductivities, electrical resistivity, and specific heat capacities of non-thermoelectric materials are supposed constants within the operating temperature range.

Due to the fact that this study is focused on low-temperature system, the Thomson effect could be neglected [18]. Besides, initial temperature of the system is equal to ambience temperature, this means that temperatures at both sides of the TEG element are the same, and consequently initial output data is zero. Finally, an instantaneous response to electrical load transients is considered [35].

The heat leakage through the solder layer and conducting strips are neglected. The flow of heat and current in the system are assumed one-dimensional. All materials are assumed homogeneous and isotropic. Finally, heat losses due to radiation and transverse convection are neglected.

2.2.2 Governing equations

In thermoelectric devices, both refrigeration and generation applications, the internal and external nodal temperatures of TEG can not be determined analytically without knowing the heat flux due to the thermoelectric effects. The reasons are the nonlinearities of the thermoelectricity and heat transfer equations.

The model solves the nonlinearities using finite difference and Newton-Raphson methods, which calculates the temperature at different nodes separated in space by a discrete distance. In the transient state, the temperatures of these points are calculated at discrete periods of time and the temperatures for all the nodes are recalculated at the end of this time interval. Using the implicit finite difference method, the values of heat flux can be determined using the values of the temperatures of the time step before.

According to heat conduction theory, the one-dimensional unsteady heat conduction equation of non-thermoelectric elements can be shown as:

$$\rho_i S_i \frac{\partial T_i}{\partial t} = \lambda_i \frac{\partial^2 T_i}{\partial y_i^2} \tag{2.1}$$

where ρ, S and λ are density, specific heat capacity and thermal conductivity, respectively, t and y are time and axis coordinate, respectively. The subscript i determines the heat transfer related to node *i*. As found in the referenced literature [35,41], the thermal-electrical analogy is useful in the analysis of complicated unsteady heat transfer problems, which can be understood by creating an electric circuit like Figure 2.1 with following equations:

$$K_i = \frac{\lambda_i A_i}{e_i} \tag{2.2}$$

$$C_i = \rho_i S_i A_i e_i \tag{2.3}$$

where K_i and C_i are the thermal conductance and thermal capacity associated with each node *i.*

The governing equations for p- and n-type thermoelectric elements involve three basic effects, Seebeck effect, Peltier effect and Thomson effect. Besides, there are two accessorial effects, Joule effect and Fourier effect. Gou [17] explained that Peltier heat generates on the two sides of semiconductor and Joule heat can be regarded as flowing equally to the two sides of conductors, so they can be disposed as a boundary heat fluxes. Thomson heat is small enough to be neglected since it is a second-round effect. So the TEG inner unsteady-state heat transfer equation can be translated also as Eq. (2.1).

The boundary condition applied at the hot plate surface, $y_1 = 0$, corresponds to the applied heat from electrical heater Q_{in}. On the top surface, $y_{10} = e_{cb}$, the convection boundary equation is employed. The boundary conditions applied to solve the unsteady-state heat transfer Eq. (2.1) for the system shown in Figure 2.1 are listed below.

Between heater and hot plate surface

$$Q_{in} = -\lambda_{hp} A_{hp} \left. \frac{\partial T}{\partial y} \right|_{y_1=0} \tag{2.4}$$

Between hot plate and thermal compound

$$-\lambda_{hp} A_{hp} \left. \frac{\partial T}{\partial y} \right|_{y_1=e_{hp}} = -\lambda_{tc1,h} A_{tc1,h} \left. \frac{\partial T}{\partial y} \right|_{y_2=0} \tag{2.5}$$

Between thermal compound and ceramic plate

$$-\lambda_{tc1,h} A_{tc1,h} \left. \frac{\partial T}{\partial y} \right|_{y_2=e_{tc1,h}} = -\lambda_{ce,h} A_{ce,h} \left. \frac{\partial T}{\partial y} \right|_{y_3=0} \tag{2.6}$$

Between ceramic plate and thermal compound

$$-\lambda_{ce,h} A_{ce,h} \left. \frac{\partial T}{\partial y} \right|_{y_3=e_{ce,h}} = -\lambda_{tc2,h} A_{tc2,h} \left. \frac{\partial T}{\partial y} \right|_{y_4=0} \tag{2.7}$$

Between thermal compound and thermoelectric element

$$-\lambda_{tc2,h}A_{tc2,h}\left.\frac{\partial T}{\partial y}\right|_{y_4=e_{tc2,h}} = -\lambda_{pn}A_{pn}\left.\frac{\partial T}{\partial y}\right|_{y_5=0} + \alpha_{pn}IT_{pn,h} - \frac{1}{2}I^2R_{pn} \qquad (2.8)$$

Between thermoelectric element and thermal compound

$$-\lambda_{pn}A_{pn}\left.\frac{\partial T}{\partial y}\right|_{y_5=e_{pn}} + \alpha_{pn}IT_{pn,c} + \frac{1}{2}I^2R_{pn} = -\lambda_{tc1,c}A_{tc1,c}\left.\frac{\partial T}{\partial y}\right|_{y_6=0} \qquad (2.9)$$

Between thermal compound and ceramic plate

$$-\lambda_{tc1,c}A_{tc1,c}\left.\frac{\partial T}{\partial y}\right|_{y_6=e_{tc1,c}} = -\lambda_{ce,c}A_{ce,c}\left.\frac{\partial T}{\partial y}\right|_{y_7=0} \qquad (2.10)$$

Between ceramic plate and thermal compound

$$-\lambda_{ce,c}A_{ce,c}\left.\frac{\partial T}{\partial y}\right|_{y_7=e_{ce,c}} = -\lambda_{tc2,c}A_{tc2,c}\left.\frac{\partial T}{\partial y}\right|_{y_8=0} \qquad (2.11)$$

Between thermal compound and cold plate

$$-\lambda_{tc2,c}A_{tc2,c}\left.\frac{\partial T}{\partial y}\right|_{y_8=e_{tc2,c}} = -\lambda_{cp}A_{cp}\left.\frac{\partial T}{\partial y}\right|_{y_9=0} \qquad (2.12)$$

Between cold plate and water-cooling block

$$-\lambda_{cp}A_{cp}\left.\frac{\partial T}{\partial y}\right|_{y_9=e_{cp}} = -\lambda_{cb}A_{cb}\left.\frac{\partial T}{\partial y}\right|_{y_{10}=0} \qquad (2.13)$$

Between water-cooling block and cooling fluid

$$-\lambda_{cb}A_{cb}\left.\frac{\partial T}{\partial y}\right|_{y_{10}=e_{cb}} = h_{cb}A_{cb}(T_{cb} - T_{c\infty}) \qquad (2.14)$$

with

$$\alpha_{pn} = n(\alpha_p - \alpha_n) \tag{2.15}$$

$$\lambda_{pn} = n(\lambda_p + \lambda_n) \tag{2.16}$$

$$A_{pn} = n(A_p + A_n) \tag{2.17}$$

$$R_{pn} = n\left(\frac{\sigma_p e_p}{A_p} + \frac{\sigma_n e_n}{A_n}\right) \tag{2.18}$$

$$I = \frac{\alpha_{pn}(T_{pn,h} - T_{pn,c})}{R_{pn} + R_L} \tag{2.19}$$

where λ_{hp}, λ_{cp}, λ_{tc1}, λ_{ce}, λ_{tc2}, λ_{cb} and λ_{pn} are thermal conductivities of hot plate, cold plate, external thermal compound, ceramic plate, internal thermal compound, water-cooling block and thermoelectric generator, respectively; e_{hp}, e_{cp}, e_{tc1}, e_{ce}, e_{tc2}, e_{cb} and e_{pn} are lengths of hot plate, cold plate, external thermal compound, ceramic plate, internal thermal compound, water-cooling block and thermoelectric generator, respectively; A_{hp}, A_{cp}, A_{tc1}, A_{ce}, A_{tc2}, A_{cb} and A_{pn} are cross sectional areas of hot plate, cold plate, external thermal compound, ceramic plate, internal thermal compound, water-cooling block and thermoelectric generator, respectively; $T_{pn,h}$ and $T_{pn,c}$ are temperatures of hot and cold side of semiconductor, respectively; T_{cb} and $T_{c\infty}$ are cold side temperature of water-cooling block and cooling fluid temperature, respectively; h_{cb} is coefficient of convective heat transfer; I is electrical current flowing through the thermoelectric circuit; R_{pn} and α_{pn} are the electric resistance and Seebeck coefficient of TEG, respectively; n is the number of semiconductor thermocouples; α_n, α_p, λ_n, λ_p, A_n, A_p, e_n, e_p, σ_n, σ_p, are the Seebeck coefficients, thermal conductivities, cross sectional areas, lengths and electrical resisitivities of p- and n-type elements.

Once heat transfer equation system, Eq. (2.4) to (2.14) and additionally Eq. (2.15) to (2.19), is solved using implicit finite difference method, the nodal temperatures on hot and cold side of the semiconductor are found

for every time step. Consequently, the electrical and thermal outputs can be obtained every time step. According to Seebeck effect the open circuit electromotive force generated is expressed as follows

$$V_{oc}(t) = \alpha_{pn}\left(T_{pn,h}(t) - T_{pn,c}(t)\right) \tag{2.20}$$

The output current I and output voltage V_{RL} generated depends on the load resistance R_L and it can be calculated following Eq. (2.16) and (2.18), respectively.

$$V_{R_L}(t) = \frac{\alpha_{pn}\left(T_{pn,h}(t) - T_{pn,c}(t)\right)R_L}{R_{pn} + R_L} \tag{2.21}$$

Besides, short circuit current also can be obtained

$$I_{sc}(t) = \frac{\alpha_{pn}\left(T_{pn,h}(t) - T_{pn,c}(t)\right)}{R_{pn}} \tag{2.22}$$

So the output power when R_L is connected is given by

$$P_{R_L}(t) = V_{R_L}I = \frac{\alpha_{pn}{}^2\left(T_{pn,h}(t) - T_{pn,c}(t)\right)^2 R_L}{\left(R_{pn} + R_L\right)^2} \tag{2.23}$$

Deriving the Eq. (2.23) with respect to load resistance, $\partial P_{RL}/\partial R_L = 0$, it can be observed that maximum output power will be reached when load

electric resistance is equal to the internal electric resistance. Therefore, substituting $R_L = R_{pn}$ into Eq. (2.23) the maximal output power is

$$P_{max}(t) = \frac{\alpha_{pn}^2 \left(T_{pn,h}(t) - T_{pn,c}(t)\right)^2}{4R_{pn}}$$

(2.24)

The heat absorption on hot side and heat release on cold side of semiconductor are given by Q_h and Q_c, respectively.

$$Q_h(t) = K_{pn}\left(T_{pn,h}(t) - T_{pn,c}(t)\right) + \alpha_{pn}I(t)T_{pn,h}(t) - \frac{1}{2}I^2(t)R_{pn}$$

(2.25)

$$Q_c(t) = K_{pn}\left(T_{pn,h}(t) - T_{pn,c}(t)\right) + \alpha_{pn}I(t)T_{pn,c}(t) + \frac{1}{2}I^2(t)R_{pn}$$

(2.26)

Finally, the instantaneous and maximal system efficiency, η and η_{max}, are calculated by Eq. (2.27) and (2.28), respectively.

$$\eta(t) = \frac{P_{R_L}(t)}{Q_h(t)} =$$

$$\frac{\alpha_{pn}^2\left(T_{pn,h}(t) - T_{pn,c}(t)\right)^2 R_L}{\left(R_{pn} + R_L\right)^2 K_{pn}\left(T_{pn,h}(t) - T_{pn,c}(t)\right) + \left(R_{pn} + R_L\right)^2 \alpha_{pn} I(t) T_{pn,h}(t) - \frac{1}{2}\left(R_{pn} + R_L\right)^2 I^2(t) R_{pn}}$$

$$(2.27)$$

$$\eta_{max}(t) = \frac{P_{max}(t)}{Q_h(t)} = \frac{\alpha_{pn}^2\left(T_{pn,h}(t) - T_{pn,c}(t)\right)^2}{4 R_{pn} K_{pn}\left(T_{pn,h}(t) - T_{pn,c}(t)\right) + 4 R_{pn} \alpha_{pn} I(t) T_{pn,h}(t) - 2 R_{pn} I^2(t) R_{pn}}$$

$$(2.28)$$

2.2.3 Implementation in TRNSYS environment

The TRNSYS software package has been used extensively for thermal system analysis. It has a modular structure and consists of individual subroutines that represent real physical devices or utility components. The components can be connected together to form complex systems.

TRNSYS uses a modular approach to solve thermal energy systems. Basically, it is an equation-solving program based on standard numerical techniques, which provides different subroutines to find analytical solution to the set of equations. However, only a first-order linear differential equation solver is provided. Therefore, a subroutine for solving nonlinear differential equations of Section 2.2.2 using the finite difference and the Newton-Raphson methods is programmed in Fortran.
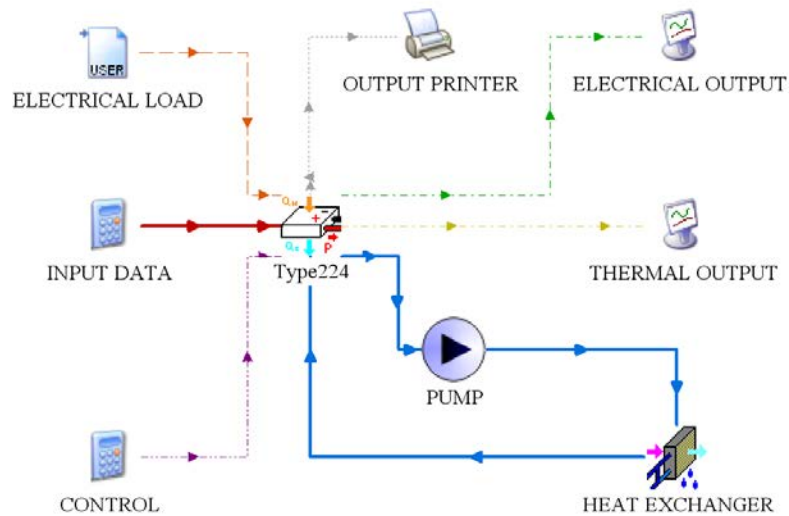
Figure 2.2. TRNSYS project created for TEG system behaviour simulation.

Figure 2.2 shows the TRNSYS project created to simulate the TEG model. To do so the following input connections has to be established:

- The applied heating rate Q_{in}, obtained from heater specifications.
- The cooling fluid temperature, extracted from experimental data measurements.
- The load resistance R_L, which is used to calculate the output data when specific resistance is connected between positive and negative connections. It may be assigned or leave as default if no load is considered.
- Simulation time step size, which is selected based on the required accuracy of the output data. It also affects to the required computational time.

Additionally, the geometric data and the material properties of the elements of the thermoelectric system studied have to be included into the TEG model as TRNSYS parameter data. All these parameters can be shown in Table 2.1 and Table 2.2. After the simulation, the output values

obtained from Eq. (2.20) to (2.28) are shown through built-in online plotter.

2.3 Experimental setup

To compare simulated results with experimental data, the simulation must have the same operating conditions as the experiment. The validation of the TRNSYS Type developed in this study uses experimental data from an especially designed equipment to perform this test. The experimental setup allows establishing parameters required for the simulation of the performance of the TEG, such thermal and electrical transients of different magnitudes.
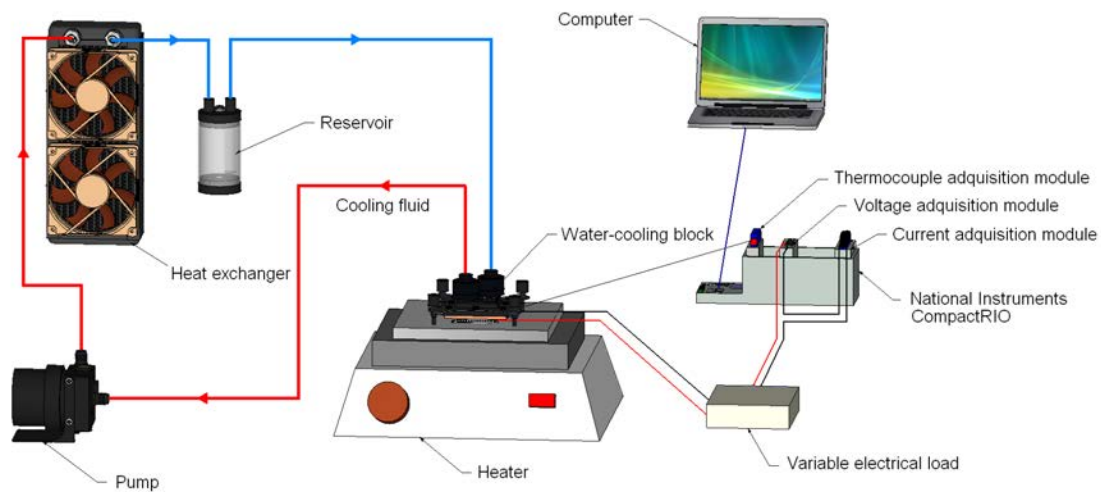
Figure 2.3. Experimental test scheme.

Figure 2.3 shows the schematic of the experiment with a TEG on top of a heat source. The source temperatures, T_1 and T_h, are measured by two K-type thermocouples with diameter of 2 mm placed, as shown in Figure 2.1, underneath the TEG and ceramic substrate, respectively. The thermocouple is sealed by conductive thermal compound to assure

uniform heat distribution on the TEG hot surface. A water-cooled block cools the top surface of the TEG through a pumped liquid cooling loop consisting of a pump, a heat exchanger and liquid lines. The pump circulates the fluid in the loop, which picks up the heat in the cold plate and dissipates it through the heat exchanger. Two ceramic plates made of alumina (Al_2O_3) are sandwiching the thermo-elements. The temperatures of the top surface (cold side) of the TEG, T_2 and T_c, are also measured by two K-type thermocouples of 2mm mounted above ceramic substrate and cold plate. The hot and cold plates are treated as heat spreaders to provide a uniform thermal field to both hot and cold sides of TEG module.

Initially, the system is at room temperature, measured as 16.17°C, and the electrical heater is switched on at its first heating level of Q_{in}=23.6W (Case 1). During temperature increase, an external switch intermittently connects and disconnects an electrical load of 2.5Ω (every 10 seconds). This allows us to obtain loaded and open-circuit outputs simultaneously. The transient temperatures at the hot and cold surfaces of the TEG, the output voltage and the output current are recorded simultaneously into a digital computer using a data acquisition system (National Instruments-cRIO). The data acquisition is set at a rate of 1s for about 3500s at which time the system attains the steady state. Once system reaches the steady state, the output voltage and current are recorded simultaneously while load resistance varied from 0Ω to 100Ω.

Table 2.1 shows the initial values of the test conducted. The experiment is repeated for two additional hot side heat fluxes Q_{in} of 33.5W (Case 2) and 53W (Case 3) in order to assess the model at three different temperature gradients.

To assess the TEG behaviour, several thermoelectric properties should be tabulated as a reference. The parameters are determined either according to direct measurement, from manufacturer's data or from the existing literature [17,42]. The geometric parameters and properties of

hot and cold plates and water-cooling block are estimated considering that materials used are aluminium and cooper, respectively.

Table 2.1 and Table 2.2 show the properties of materials used in the experimental setup. In Table 2.1, the Seebeck coefficient, thermal conductivity and electrical resistivity of the p- and n-type elements are listed at steady-state average temperatures of $\bar{T} = (T_h + T_c)/2$, which are extracted from experimental data. All these three parameters are obtained from manufacturer's datasheet.

Parameters	Case 1	Case 2	Case 3	Unit	Source
Q_{in}	23.60	33.50	53	W	Measured
$T_{C\infty}$	16.45	17.34	18.20	°C	Measured
R_L	2.5	2.5	2.5	Ω	Measured
a_n	163.546	167.273	171.659	µV/K	Manufacturer
a_p	-178.098	-188.726	-201.897	µV/K	Manufacturer
λ_n	1.510	1.453	1.415	W/mK	Manufacturer
λ_p	1.954	1.925	1.792	W/mK	Manufacturer
σ_n	10.896	12.001	13.767	µΩm	Manufacturer
σ_p	11.196	13.100	15.910	µΩm	Manufacturer

Table 2.1. Thermoelectric parameters for three different cases.

Parameters	Value	Unit	Source
n	98	-	Measured
e_n	2.54×10^{-3}	m	Measured
e_p	2.54×10^{-3}	m	Measured
e_{hp}	0.02	m	Measured
e_{tc1}	1×10^{-4}	m	Measured
e_{ce}	2.54×10^{-4}	m	Measured
e_{tc2}	1×10^{-4}	m	Measured
e_{cp}	0.02	m	Measured
e_{cb}	0.002	m	Measured
A_n	2.3×10^{-6}	m²	Measured
A_p	2.3×10^{-6}	m²	Measured
A_{hp}	7.22×10^{-3}	m²	Measured
A_{tc1}	8.41×10^{-4}	m²	Measured
A_{ce}	8.41×10^{-4}	m²	Measured
A_{tc2}	8.41×10^{-4}	m²	Measured
A_{cp}	8.41×10^{-4}	m²	Measured
A_{cb}	12.25×10^{-4}	m²	Measured
λ_{hp}	180	W/mK	Estimated
λ_{tc1}	2.5	W/mK	Manufacturer
λ_{ce}	36	W/mK	[35]
λ_{tc2}	2.5	W/mK	Manufacturer
λ_{cp}	180	W/mK	Estimated
λ_{cb}	380	W/mK	Estimated
ρ_n	7700	kg/m³	[42]
ρ_p	7700	kg/m³	[42]
ρ_{hp}	2700	kg/m³	Estimated
ρ_{tc1}	2040	kg/m³	Manufacturer
ρ_{ce}	3975	kg/m³	[35]
ρ_{tc2}	2040	kg/m³	Manufacturer
ρ_{cp}	2700	kg/m³	Estimated
ρ_{cb}	8930	kg/m³	Estimated

Parameters	Value	Unit	Source
S_n	200	J/kgK	[42]
S_p	200	J/kgK	[42]
S_{hp}	883	J/kgK	Estimated
S_{tc1}	200	J/kgK	Manufacturer
S_{ce}	765	J/kgK	[35]
S_{Ctc2}	200	J/kgK	Manufacturer
S_{cp}	883	J/kgK	Estimated
S_{cb}	385	J/kgK	Estimated
h_{cb}	23781	W/m²K	Manufacturer

Table 2.2. Properties of materials used in TEG tests.

Experiments are conducted under following conditions: the temperature of cooling fluid stays between 16.45°C and 18.20°C, the air temperature is 16.17°C and the flow rate of the cooling fluid is 72l/h.

2.4 Results and discussion

Based on transient and steady state experiments and TRNSYS simulations, the results and a discussion about their comparison are presented in this section.

2.4.1 Effects of step changes of supplied heat flow rates

The dynamic response characteristics of temperature difference between hot and cold sides $\Delta T = T_h - T_c$, hot side inlet heat flux Q_h, electric output power P_{RL} and closed-circuit voltage V_{RL} with step changes of supplied heat flow rate Q_{in} are described in Figure 2.4. Both the transitory experimental and simulation results are plotted versus the transient time

in the same plot. The conditions imposed in the experiment are listed in Table 2.1.
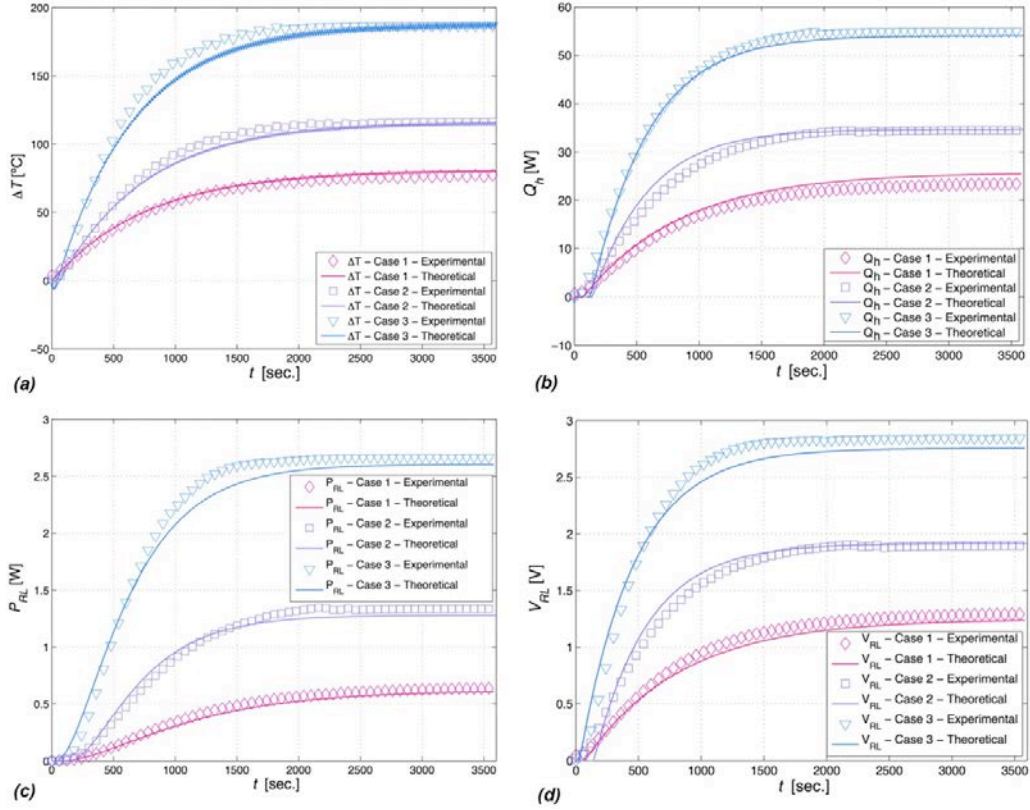
Figure 2.4. Correlation of experimental and simulated behaviours of the TEG system under step changes of heat flow rates. (a) Temperature difference between hot and cold sides $\Delta T = T_h - T_c$. (b) Hot side inlet heat flux. (c) Electric output power. (d) Closed-circuit voltage.

During the transient, the temperature difference across the TEG device increased until the steady state is achieved. It can be observed that the electric output characteristic is mostly dependent on the temperature difference. The hot side temperature T_h achieved is 99°C, 140°C and 216°C for cases 1, 2 and 3, respectively. Accordingly to experimental data obtained and Eq. (2.20) to (2.28), the higher the temperature difference across the TEG is, the more electrical power generated and the greater output system performance becomes.

2.4.2 Effects of step changes of load current at constant supplied heat flux

In Figure 2.5 to Figure 2.10, the step changes effects of load current under conditions of Table 2.1 can be observed. The system has been brought to steady-state temperatures of Figure 2.4 (a). It is very interesting to note the effect that the load current has on the temperature gradient across the device, which is the same obtained in Ref. [37]. The load currents imposed for cases 1 to 3 are 0.49 A, 0.71 A and 1.01 A, respectively.

Every increase in I leads to a decrease in temperature difference ΔT due to the greater value of the Peltier term of Eq. (2.8) and (2.9). This current increase also produces an increment of hot and cold side heat fluxes. However, as explained in Section 2.2.2, the maximum output power and efficiency happens only when load resistance is matched with internal resistance.
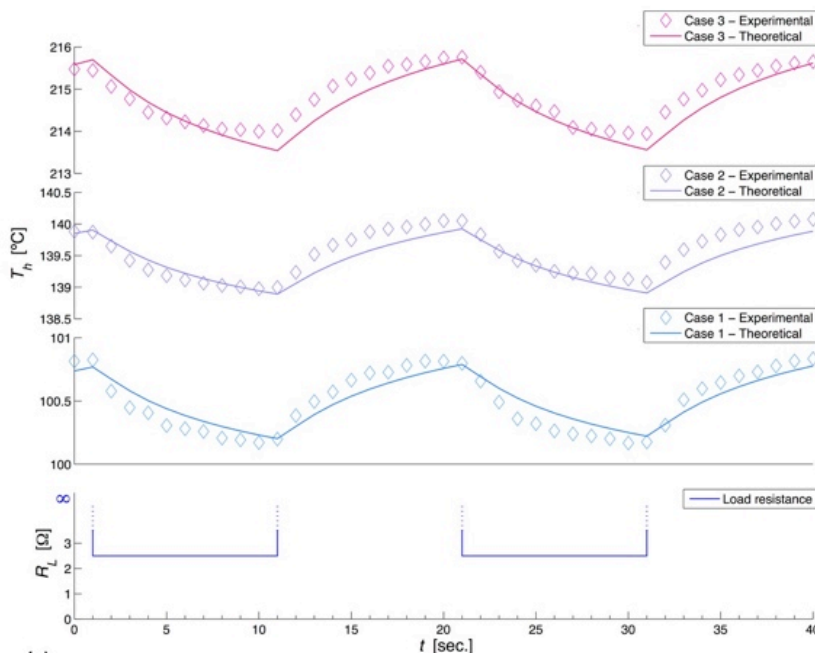
Figure 2.5. Correlation of experimental and simulated behaviours of the TEG system under step changes of load current. Hot side temperature.
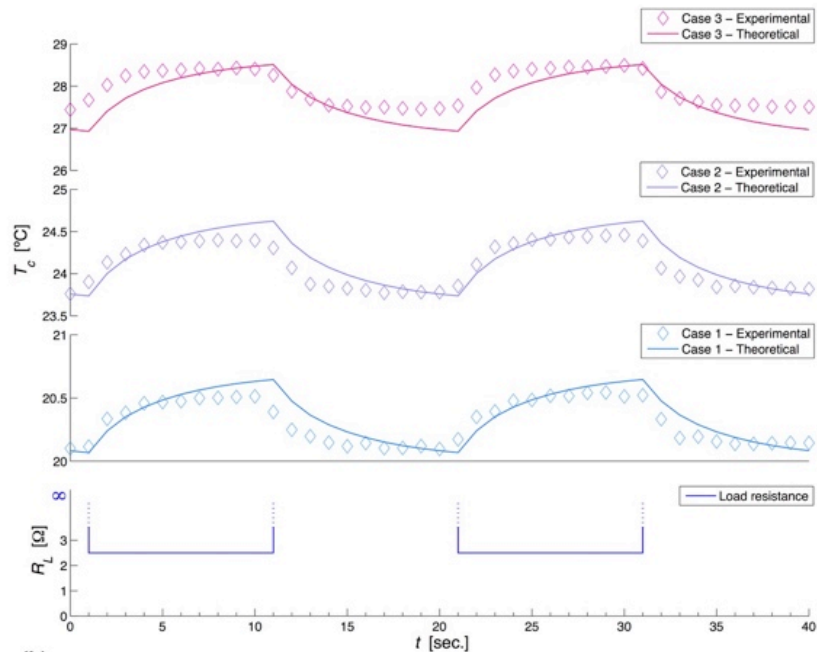
Figure 2.6. Correlation of experimental and simulated behaviours of the TEG system under step changes of load current. Cold side temperature.
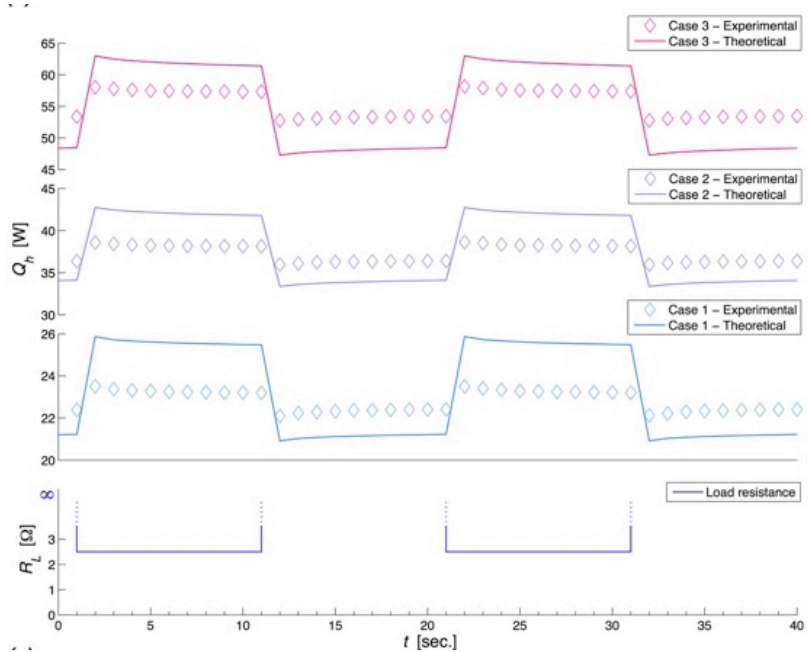
Figure 2.7. Correlation of experimental and simulated behaviours of the TEG system under step changes of load current. Hot side heat flux.
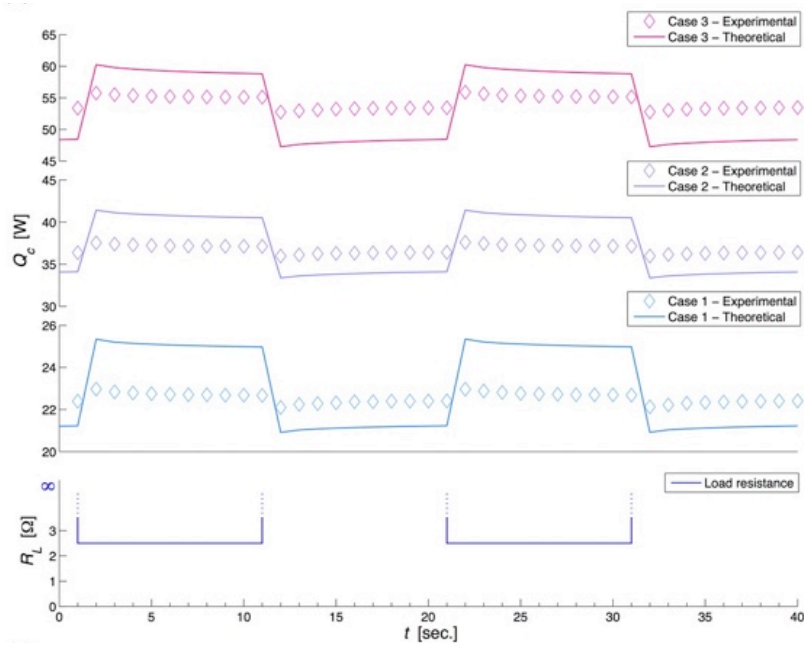
Figure 2.8. Correlation of experimental and simulated behaviours of the TEG system under step changes of load current. Cold side heat flux.
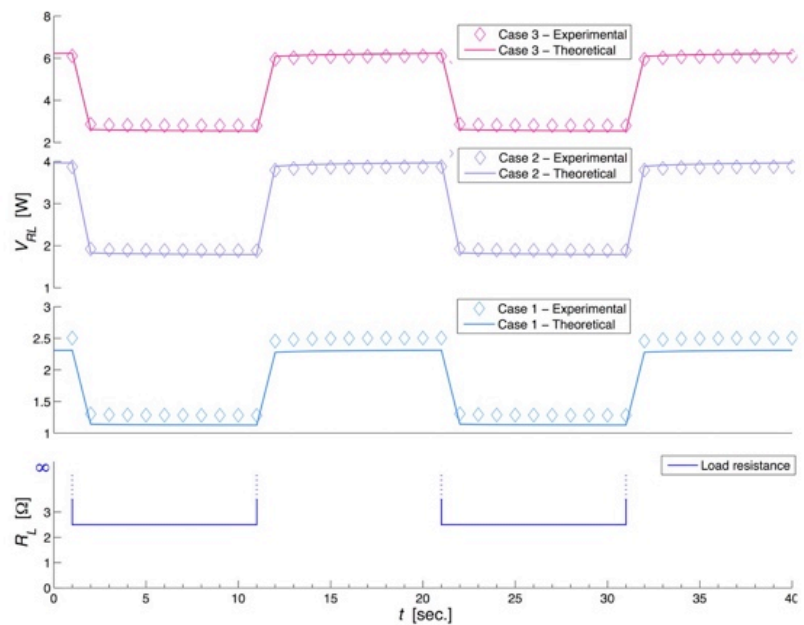
Figure 2.9. Correlation of experimental and simulated behaviours of the TEG system under step changes of load current. Closed-circuit voltage.
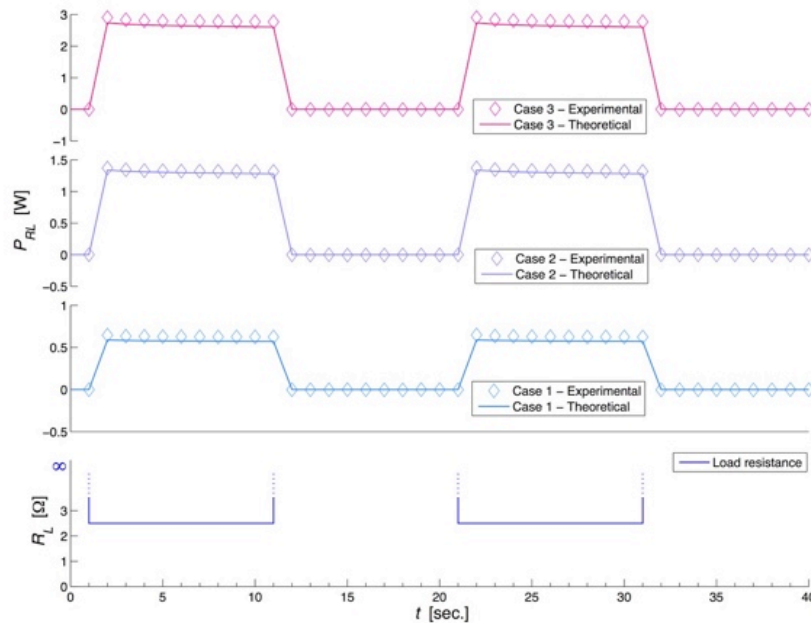
Figure 2.10. Correlation of experimental and simulated behaviours of the TEG system under step changes of load current. Electric output power.

As it can be appreciated from Figure 2.5 to Figure 2.10, the simulation results show good agreement with the experimental results, accurately tracking the electro-thermal coupled effects occurring in the TEG system. The plotted curves of T_h and T_c show that steady-state are not achieved with step changes of 10 seconds. It also can be shown that parameter variations with load current increase with higher values of supplied heat flux. The low accuracy observed in Figure 2.7 and Figure 2.8 may be caused by convection heat losses on hot and cold plates.

2.4.3 Effects of load resistance variation at steady-state

The variation of performance at steady-state with load resistance is shown in the following figures. Three different conditions corresponding to described cases in Table 2.1 are selected. The system has been brought to the same steady-state temperatures of Figure 2.4 (a).
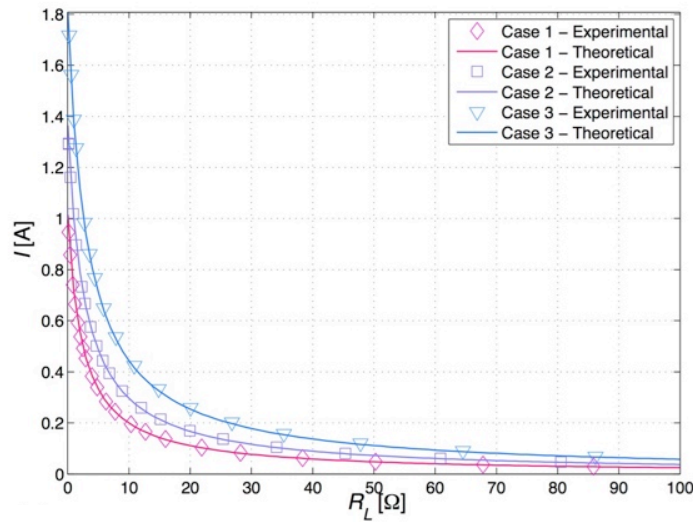
Figure 2.11. Correlation of experimental and simulated behaviours of the
TEG system under different load resistances. Load current.
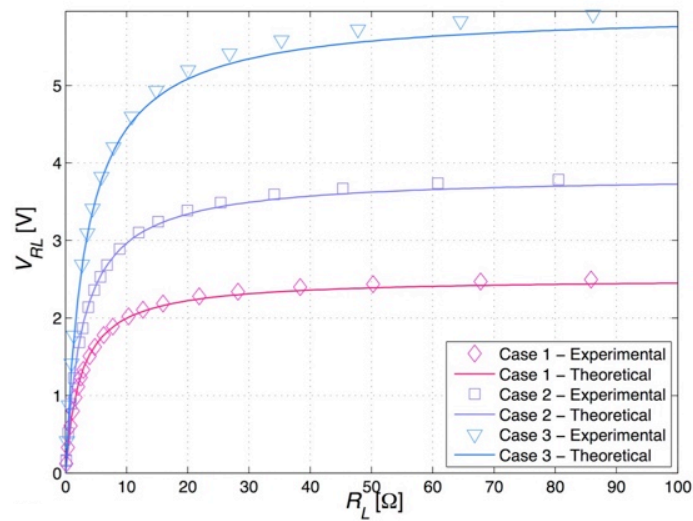
Figure 2.12. Correlation of experimental and simulated behaviours of the
TEG system under different load resistances. Closed-circuit voltage.
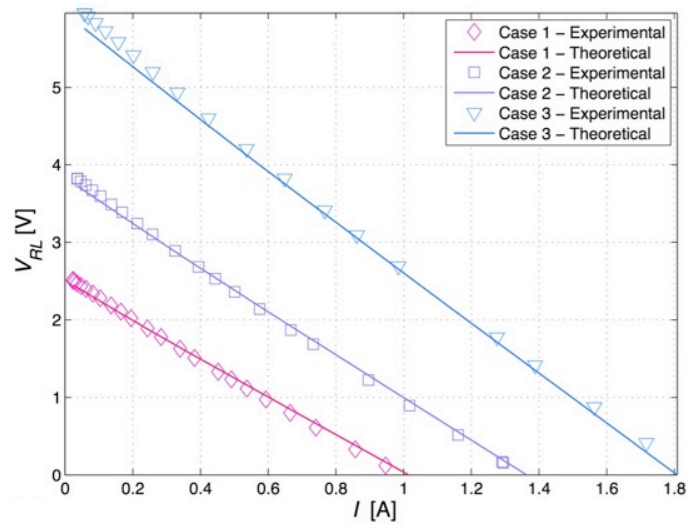
Figure 2.13. Correlation of experimental and simulated behaviours of the TEG system under different load resistances. Closed-circuit voltage versus load current.
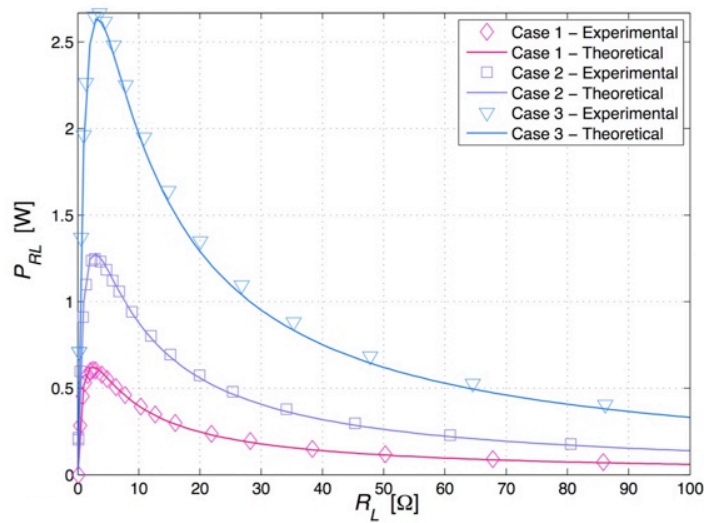
Figure 2.14. Correlation of experimental and simulated behaviours of the TEG system under different load resistances. Electric output power.
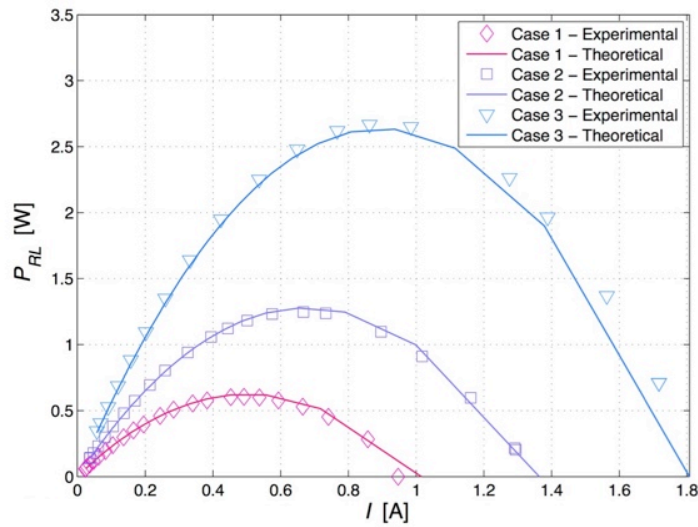
Figure 2.15. Correlation of experimental and simulated behaviours of the TEG system under different load resistances. Electric power generated versus load current.
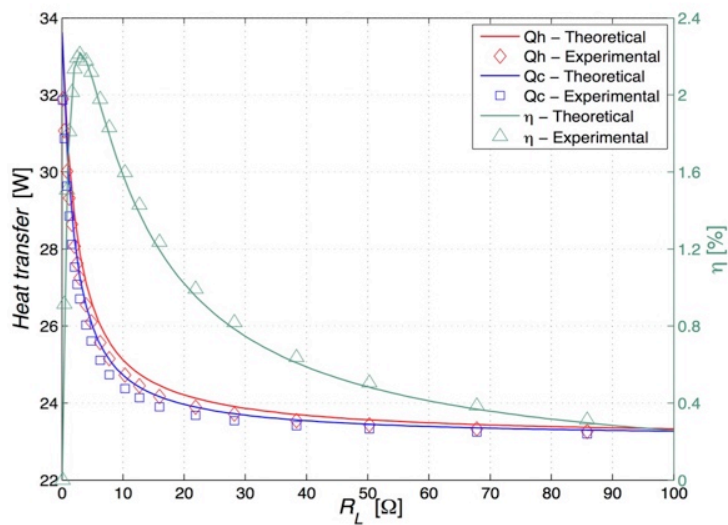
Figure 2.16. Correlation of experimental and simulated behaviours of the TEG system under different load resistances. Case 1 hot and cold side heat fluxes and system efficiency.
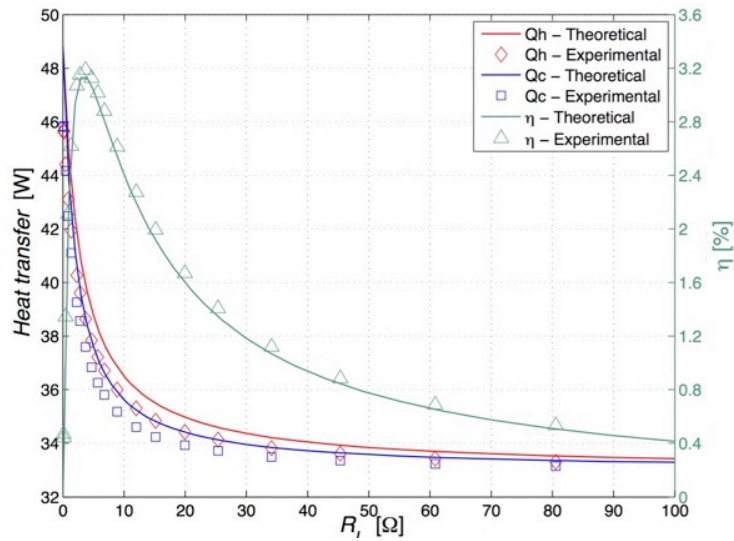
Figure 2.17. Correlation of experimental and simulated behaviours of the TEG system under different load resistances. Case 2 hot and cold side heat fluxes and system efficiency.
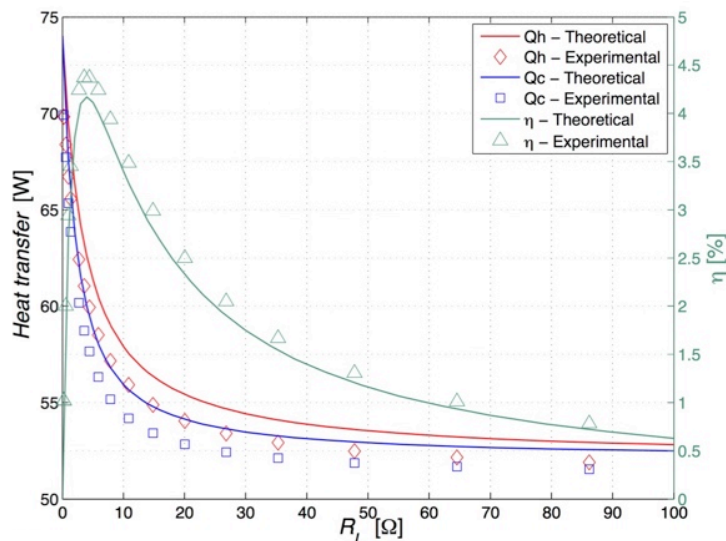
Figure 2.18. Correlation of experimental and simulated behaviours of the TEG system under different load resistances. Case 3 hot and cold side heat fluxes and system efficiency.

Figure 2.11 to Figure 2.18 demonstrate that the electrical output is strongly coupled to both the thermal behaviour and the load resistor value. The electric load resistance that produces the maximum electrical

power varies with the supplied heat flux. The power generation and system efficiency are the highest when the load resistance value is close to the internal resistance $R_L=R_{pn}$, which is measured to be about 2.5Ω. As can be shown in Figure 2.14, the generated power increases to a maximum but then decreases to reach a steady state. The electrical resistances at maximum power points are 2.4Ω (0.65W), 2.45Ω (1.28W) and 2.9Ω (2.6W) for cases 1 to 3, respectively. Those effects can be observed in the theoretical model as well.

Besides, in Figure 2.16, Figure 2.17 and Figure 2.18 it can be observed that both the hot and cold sides heat fluxes, Q_h and Q_c, decrease with resistance until steady state is achieved. It demonstrates that when load resistance R_L increase, the load current I falls to minimum, which reduces the Joule and Peltier effect of the Eq. (2.25) and (2.26). Consequently, when load current is very low, those effects are despicable and it's only the Fourier's law that governs the heat transfer equation.

2.4.4 Model uncertainty

The TEG model developed in this work is validated by comparing the experimental data with the numerical data predicted by our model at the same conditions. The calculus of the error is performed by the comparison of the temperature difference and the electrical output power of each point predicted by the model with the same point measured experimentally. The value of RMSE is 4.85°C and 0.0648W for temperature difference and electrical output power, respectively. The model presents a normalized root mean square error of 3.53% and 2.33% for temperature difference and electrical output power, respectively.

Although the model presented has slightly higher temperature difference RMSE and NRMSE than the model developed by Montecucco [37] (3.58°C and 2.76%, respectively), the output power prediction is significantly better (0.2W and 4.55%, respectively). It's important to note that the model accuracy is markedly affected by the thermoelectric

parameters introduced into the simulation model. Consequently, the more exact the thermoelectric parameters are, the more precise the outputs will be.

2.5 Conclusions

Although thermoelectric phenomena have been used for heating and cooling applications quite extensively, electricity generation has only seen very limited market in niche applications and it is only in recent years that interest has increased regarding new applications of energy generation through thermoelectric harvesting. The widespread use of TEGs depends on its optimization.

The TRNSYS component presented in this paper has been developed for this purpose and is described and validated using experimental data. The proposed component is able to cope with thermal and electrical dynamics. The comparison of results between theoretic analysis and experiment has approved the reasonability of the new component.

On the other hand, the TRNSYS simulation runs without interruptions or delays, therefore the numerical model, and consequently the new component, can be considered well optimized. Therefore, this system model can be used in performance optimization and further application of thermoelectric generation.

2.6 Acknowledgment

Modelling analysis of longitudinal thermoelectric energy harvester in low temperature waste heat recovery applications

This section is a transcription of the contents of the following paper (a copy of the published version can be found in Appendix B):

E Massaguer, A Massaguer, JR Gonzalez, L Montoro. Modelling analysis of longitudinal thermoelectric energy harvester in low temperature waste heat recovery applications. Applied Energy, 140, 184-195, 2015. ISSN 0306-2619 (Impact factor 5,613; Journal 8 of 89; 1st quartile; Energy and Fuels)

Abstract

The worldwide interest in thermoelectric waste heat recovery is constantly growing, with a wide range of applications ranging from small harvesters integrated into wireless sensor networks all the way to larger harvesters such as the ones that can potentially be integrated into cars. The wide range of applications makes a requirement for studying the dynamic response of TEGs. The aim of this work is to develop a mathematical model to accurately simulate the thermal and electrical behaviours of a longitudinal thermoelectric energy harvester (LTEH). In order to implement the theoretical analysis, a new TRNSYS component has been developed so this new model can also be used as a design tool.

The LTEH model presented in this paper is validated through the comparison of results between theoretical analysis and experimental data. Testing results and discussion show the reasonability of this new model and also their use as a simulation tool.

3.1 Introduction

Energy recovery techniques have become significantly demanding since it makes an important contribution towards reducing the greenhouse gases which cause global warming. Energy recovery includes any

technique or method that converts waste energy (i.e. thermal, chemical or mechanical energy) into another kind of energy which can be reused for other energy purposes (i.e. electrical energy).

Research activities in energy recovery from waste heat using thermoelectric effect have considerably increased since the 1990s. There are recently reported researches such as thermoelectric power generation from CPU waste heat [43], Si-Ge based TEGs applied to gasoline engine vehicles [44], bismuth telluride based TEGs applied to automotive exhaust systems (AETEG) [45,46], thermoelectric power generation systems applied to generate electricity from municipal waste heat [47], a thermoelectric power generator using solar heating [48] and so on.

At the same time, many mathematical models and approaches for simulating heat exchangers that utilizes thermoelectric modules for power generation has been designed. The majority of these models apply general heat transfer techniques in cohesion with thermoelectric module equations for a system level analysis.

Bohn developed one of the earliest models in 1981 [49]. It is an extension of the effectiveness-number of transfer units (ε-NTU) method for heat exchanger analysis. The model implements TEG model into the common ε-NTU equations by setting up a dimensionless ratio of actual power generated to the maximum possible power generation. An example case is provided for a parallel flow configuration with promising results; however, there is no experimental testing to validate the model. The Esarte et al. model [50] also uses ε-NTU method to simplify calculations. They set up an energy balance with a hot and cold side heat exchanger with a thermoelectric module in between and studied the influence of fluid flow rate, heat exchanger geometry, fluid properties and inlet temperatures on the power supplied by the TEG. The work could provide some guidelines for determining the optimum operating parameters of TEGs, however, limited experimental results are provided. Crane and Jackson investigated thermoelectric waste heat recovery with regards to

cross flow heat exchangers [21,23]. A cross flow heat exchanger model was validated against measured performance of advanced cross flow heat exchangers without thermoelectrics. The numerical simulations were compared to experimental data with good agreement between them. Yu and Zhao [23] developed a numerical model for prediction of performance of a TEG with a parallel-plate heat exchanger. They assumed that the flat thermoelectric modules were held tightly between hot and cold fluids, which had multiple thermocouples with a single layer of p- and n-type semiconductors. The thermocouples along the fluid path were connected electrically in series. A typical energy balance was used to set up the model with the differential equations discretized along the axial direction of the hot fluid. The solution to the numerical model was provided using an iterative method. Simulations were performed to study the effects of the various parameters. An experimental study based on the Yu and Zhao model [23] was performed by Niu, Yu and Wang [24]. A comparison of the experimental results with the numerical model is presented in this work. A two fluid, multi-plate, multi-pass, counter/parallel flow heat exchanger with thermoelectric generators was created for the experimental phase. The data obtained through experimentation shows that the numerical model over-predicts performances of the TEGs over the entire range of data. At lower temperatures, the model displays better agreement with experimental results, but as hot fluid inlet temperatures are increased, the prediction diverges from the measured values. The discrepancy is associated to the lack of accounting for heat losses and the fact that thermoelectric properties are treated as constants.

Wu [20] performed a theoretical analysis on waste-heat thermoelectric power generators. In this study, a real waste-heat thermoelectric generator model was presented based on accounting for both internal and external irreversibility to predict realistic specific power and efficiency. Therefore, this approach gave a much more realistic generator specific power and efficiency prediction than does the ideal TEG. Hsiao et al. [19] constructed a mathematical simulation model, based on the testing results of a TEG module, to predict the performance of a waste heat recovery system. They provided a scientific methodology with complicated equations on the field of thermoelectric simulations. Finally,

Wang et al. [4] presented a mathematical model of a TEG device using the exhaust gas of vehicles as heat source. The model simulates the impact of relevant factors, including vehicles exhaust mass flow rate, temperature and mass flow rate of different types of cooling fluid, convection heat transfer coefficient, height of PN couple, the ratio of external resistance to internal resistance of the circuit on the output power and efficiency. However, just a few experimental results are provided. Recently, Montecucco et al. [51] have studied the impact of thermal imbalance on the power produced at module and system level in a TEG array. Experimental results in series-parallel configurations clearly illustrate the issue and a theoretical model was presented to quantify the impact.

The above literatures have mainly been focused on the analytical analysis to a single or multiple thermoelectric elements for thermoelectric energy harvesting from gas exhaust waste heat. These analytical methods provided some significant guidelines for the design of the thermoelectric energy harvesters in terms of the principle of thermodynamics. However, aforesaid models are only validated for stand-alone applications without taking into account the electrical and thermal effects of TEG array configuration. A real thermoelectric energy harvester always comprises multiple thermoelectric modules placed with respect to the flow direction, and depending on the shape and the electrical output requirements of the harvester, TEGs can be wired in series/parallel configuration. Although series/parallel configuration has not been taken into account in this paper, it will be considered in future work. Moreover, there is no model in literature that uses liquid (e.g. water) as a heat source.

Thereafter, the objective of this work is to develop a new computational model capable to simulate the electro-thermal dynamics of a thermoelectric energy harvesting system. The new model incorporates to the 1D mathematical model developed in Ref. [52] the longitudinal thermal phenomena occurring in real LTEH systems. The model treats TEG modules as a whole block and takes into account the fluid heat and temperature reduction across the system due to thermoelectric energy harvesting. Following the base model [52], the new component is fully

analysed and validated under steady and transient states with data
obtained from the experimental setup and it is also created in TRNSYS.

3.2 Model description

A thermoelectric energy harvester is a device that converts some of the
waste heat of an element (i.e. liquid or gas) into electricity using the
Seebeck Effect. Although many different topologies and shapes have
been studied in literature (e.g. longitudinal, transverse, hexagonal,
circular, etc.) the longitudinal and rectangular box-like shape design is
termed as the baseline model [16]. Consequently, this is the type of the
thermoelectric harvester assessed in this paper. The name of the models
–longitudinal and transverse– are derived from the way the TEGs are
placed with respect to the fluid flow direction.

The LTEH follows the basic scheme shown in Figure 3.1. It consists of
four main elements:

- Hot-side heat exchanger used to capture and increase the heat
  extraction from the heat source to the TEG modules. It is directly
  exposed to the hot fluid.
- Cold-side heat exchanger to remove and transfer excess heat from
  outer side of the TEG modules to the ambient air.
- Multiple thermoelectric modules that convert the waste heat into
  useful electrical energy. The optimal number and configuration of
  TEG modules must be considered.
- Compression assembly system comprising a top and bottom lid, a
  support element that permits attachment of the lids and a sealing
  rubber.

TEGs are mounted along the exterior surfaces of the lids. The heat flows from hot side to cold side heat exchanger and through the TEG. The temperature difference between hot and cold sides of the TEG generates voltage and current by Seebeck effect. The thermoelectric generation also produces a heat extraction from fluid, resulting in a fluid temperature reduction at every stage. Consequently, both the fluid temperature and the electric power generation will be reduced as we incorporate new stages: $T_{in}^i > T_{in}^{i+1}$ and $P_{RL}^{i,j} > P_{RL}^{i+1,j}$, respectively. This effect is considered within the new model.

Figure 3.1. Heat transfer model of longitudinal thermoelectric energy harvester LTEH.

As can be seen in Figure 3.2, thermoelectric modules are sandwiched between hot side and cold side heat exchangers that can be treated as a convective heat transfer system. The TEG consists of certain number of semiconductors, corresponding solder layers, conducting strips and

thermal insulation material. In order to electrically isolate the module, a ceramic substrate made of alumina (Al$_2$O$_3$) is located both sides of the TEG. Moreover, a thermal compound increases the thermal conductivity of the interfaces by filling microscopic air-gaps between ceramic substrates and heat exchangers and also between TEG and ceramic substrate.
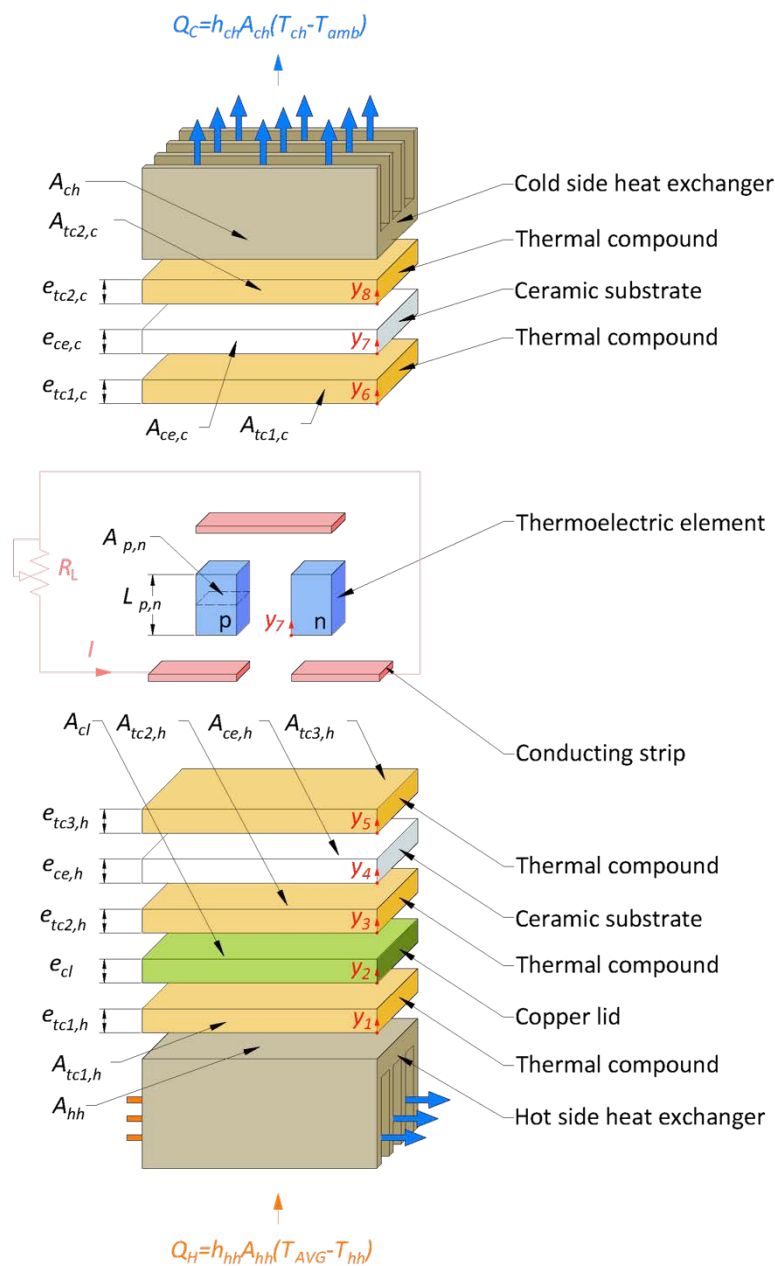
Figure 3.2. One dimensional heat transfer model of a single TEG module.

As already explained in Section 3.1, the new model developed in this paper is based on Massaguer et al. model [52]. It solves the system of equations using finite difference and Newton-Raphson methods and calculates the temperature at different nodes separated in space by a discrete distance. In the transient state, the temperatures of these points are calculated at discrete periods of time and the temperatures for all nodes are recalculated at the end of this time interval. Using the implicit finite difference method, the values of heat flux can be determined using the values of the temperatures of the time step before. Therefore, the unsteady-state heat transfer model solves the TEG temperature distribution first and then determines the TEG power and performance outputs.

However, the solution to the heat equations assumes one-dimensional heat transfer and treats the TEG module as a whole block (i.e. it considers the TEG as a real complete module). In order to obtain an accurately LTEH model, heat losses on the flow direction must be taken into account. Therefore, the longitudinal dimension must be attached to the Ref. [52] model. The fluid energy losses per stage due to the thermoelectric generation can be expressed as

$$\sum_{j=1}^{np} Q_H^{i,j}(t) \tag{3.1}$$

where i is the number of stage, j is the number of row, np is the number of parallel TEG modules placed in the same stage and Q_H is the heat extracted from the fluid and absorbed by a TEG module because of the thermoelectric generation. Q_H can be obtained applying convective heat transfer equations between fluid and hot side heat exchanger

$$Q_H^{i,j}(\mathrm{t}) = h_{hh}^{i,j} \cdot A_{hh}^{i,j} \cdot \left(\mathrm{T}_{AVG}^i(t) - T_{hh}^{i,j}(t) \right) \tag{3.2}$$

where h_{hh}, A_{hh} and T_{hh} are coefficients of convective heat transfer, cross sectional area and temperature of hot side heat exchanger, respectively. T_{AVG}^i is the average fluid temperature on hot side heat exchanger and it is the value used to solve the one-dimensional temperature distribution on each TE module, expressed as

$$T_{AVG}^i(t) = \frac{T_{in}^i(t) + T_{out}^i(t)}{2} \tag{3.3}$$

where T_{in}^i and T_{out}^i are the fluid inlet and outlet temperatures on stage i, respectively. Note that T_{AVG}^i is common for all rows j of a stage i.

Considering only heat losses due thermoelectric effect, the heat extracted from fluid in every stage can be found using the following equation

$$\sum_{j=1}^{np} Q_H^{i,j}(t) = \dot{m} \cdot S_f \cdot \left(T_{in}^i(t) - T_{out}^i(t) \right) \tag{3.4}$$

Consequently, T_{out}^i can be obtained from

$$T_{out}^i(t) = T_{in}^i(t) - \left(\frac{\sum_{j=1}^{np} Q_H^{i,j}(t)}{\dot{m} \cdot S_f} \right) \tag{3.5}$$

where $\dot{m}$ is the fluid mass flow rate and S_f is the fluid specific heat, both considered temperature independent.

Due to the fact that $Q_H^{i,j}$, T_{AVG}^i and T_{out}^i are reciprocally dependant, the
only way to obtain an accurate solution is using an iterative method. The
solution adopted consists of an iteration loop that runs Massaguer et al.
model coupled with above equations until T_{AVG}^i converges. The
convergence will be achieved when

$$\left| \mathrm{T}_{AVG_{k-1}}^i - \mathrm{T}_{AVG_k}^i \right| < \varepsilon \qquad (3.6)$$

where k is the iteration number and ε is the tolerance value set up to
$\varepsilon = 1e^{-4}$ °C. It must be noted that T_{AVG}^i is strictly necessary to be
calculated in order to obtain accurate temperature distribution and
electrical outputs on each module.

Once convergence has been attained, the inlet fluid temperature of next
stage will be temperature outlet in the stage before $T_{in}^{i+1} = T_{out}^i$.
Considering that the model solves consecutively the temperature
distribution at each stage, T_{out}^i must be obtained before starting next
stage. The same process is repeated until the last stage has been
reached, $i = ns$.

To better understand how the model is structured, the computer model
block is described in Figure 3.3.
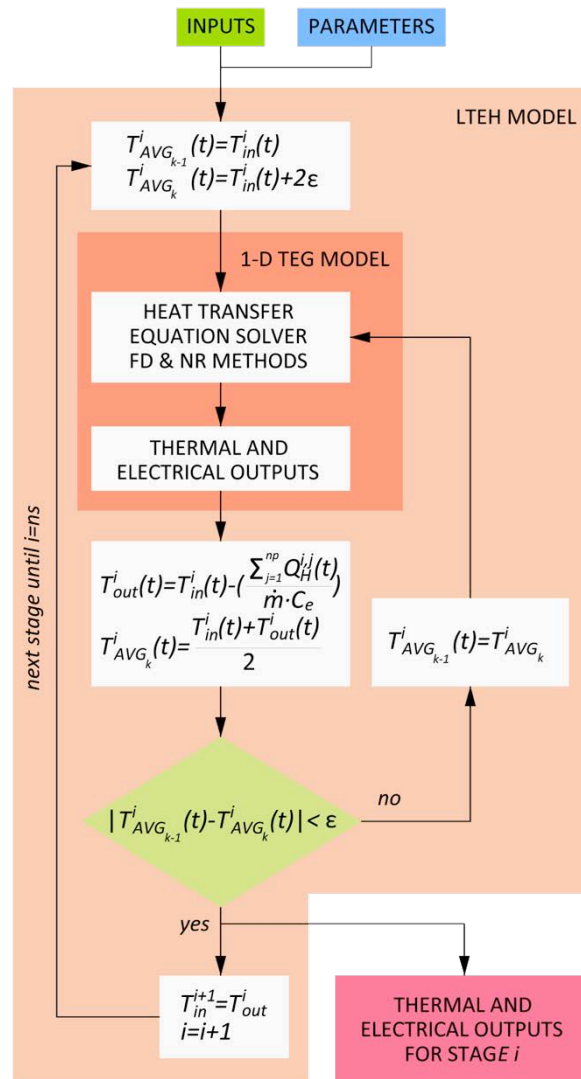
Figure 3.3. Block diagram representation of LTEH model.

Because of this new model is based on model presented in [52], the same assumptions have been inherited. On the other hand, new ones have been taken: thermal conductivity, electric conductivity and Seebeck coefficient of semiconductors are all assumed to be temperature-independent; adiabatic boundary conditions were supposed on the outside surfaces of TEG element; also thermal conductivity, electrical resistivity and specific heat capacities of non-thermoelectric materials are supposed constants within the operating temperature range; an instantaneous response to electrical load transients is considered; the heat leakage through solder layer and conducting strips are neglected

and, finally, heat losses due to radiation and transverse convection through remaining area and lateral walls are also neglected. All TEGs are considered equal and connected to an individual load resistance of the same value. Therefore, series-parallel configuration effects explained in Ref. [51] have not taken into account. In future work these effects will be incorporated.

3.3 Computer model

The model presented in Section 2 was programmed in Fortran due to the fact that TRNSYS software was chosen to develop the analysis. TRNSYS [38] is a flexible software tool used to simulate the performance of transient systems. At its heart, TRNSYS is a robust algebraic and differential equation solver that is able to read and process Fortran based components.

Each component is represented by a number of parameters and time-dependent inputs, and produces a number of time-dependent outputs. A given output of a specific component can be used as input to itself or to any number of other components. This is mainly how the system components can be interconnected.

The basic configuration of the LTEH dynamic study follows the general design illustrated in Figure 3.4.
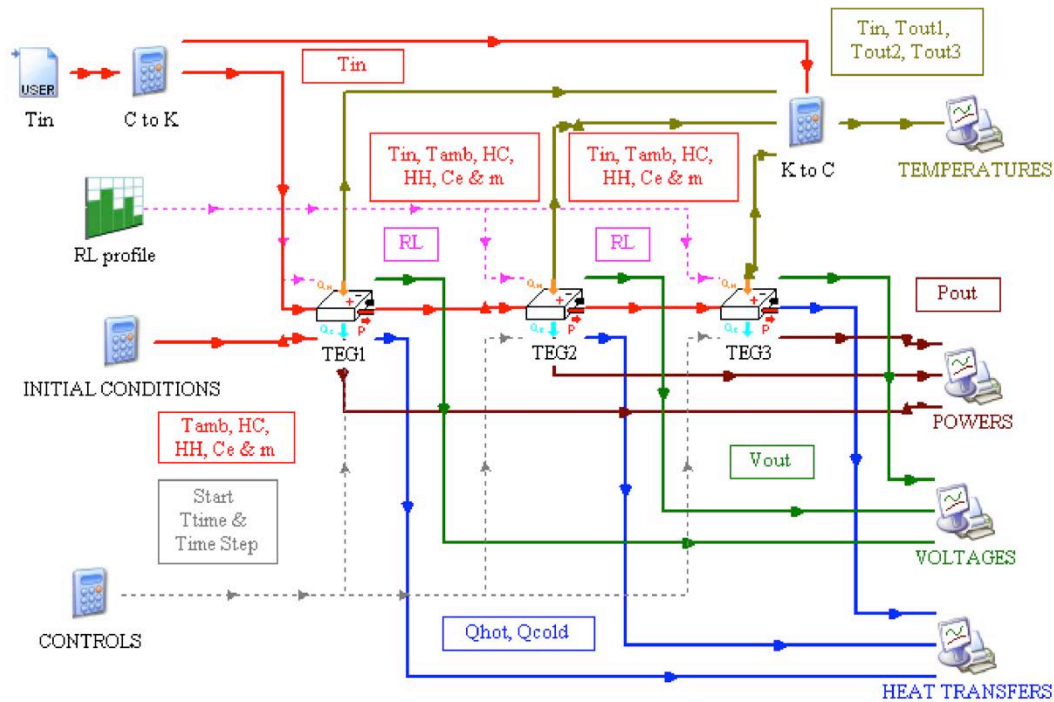
Figure 3.4. TRNSYS project created for LTEH system behaviour
simulation. The connection parameters are indicated within boxes.

As it can be appreciated from Figure 3.4, the TRNSYS project developed is composed of several components. The initial conditions block contains the ambient temperature, convective heat transfer coefficients of hot and cold side heat exchangers, fluid specific heat and mass flow rate. Besides, the T_{in} and R_L components contain the temperature and load resistance profiles, respectively. Both T_{in} and R_L profiles are treated as system inputs and can be shown in Figure 3.7. The three equal components called TEG1 to 3 correspond to the three stages that form the complete LTEH tested in Section 3.4. Each TEG component contains the thermal and electrical characteristics of a single row and the number of rows per stage. Control component allows selecting the start and stop time for a simulation. Additionally, the simulation time step can also be selected. Finally, the geometric data and the material properties have to be included into the LTEH model as TRNSYS parameter data. All these parameters can be shown in Table 3.1.

3.4 Experimental setup

In order to validate the new LTEH model, an experimental setup has been build. This new equipment allowed us to obtain real data to be compared with simulation results. The experimental setup allows establishing thermal and electrical transients of different magnitudes.

1. Cold side heat exchanger 2. Thermoelectric generator 3. Copper lid 4. Sealing rubber
5. Hot side heat exchanger 6. Support element 7. Thermal insulation
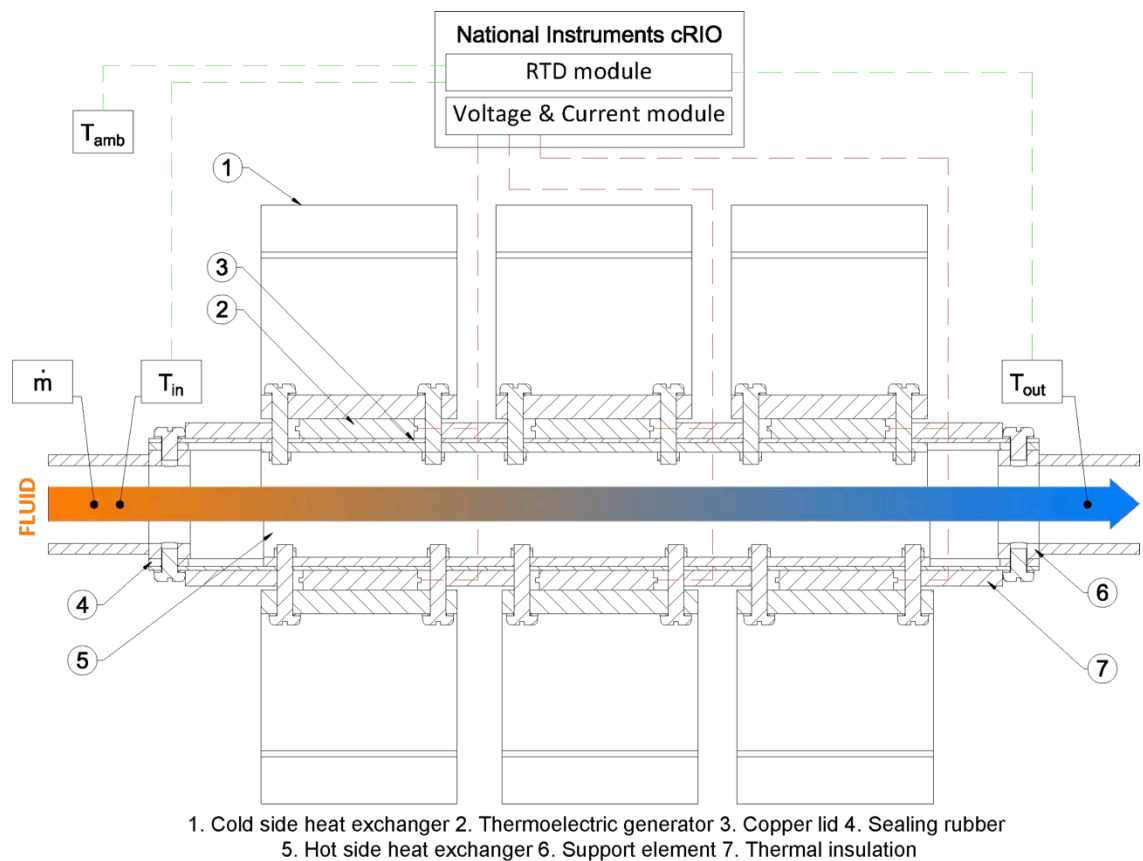
Figure 3.5. Transversal section of the experimental LTEH with data acquisition modules.

Figure 3.5 shows the schematic of the experiment. A closed loop water system was designed to supply hot water at different temperatures. The heat source is an electric accumulator that produces hot water up to 80°C. A recirculating pump moves hot water through the water loop. It

picks up the heat in the accumulator and exchanges it through the LTEH
system. An ultrasonic flow meter was used to measure the fluid mass flow
rate $\dot{m}$. The temperatures T_{in} and T_{out} were measured by two RTD
sensors placed, as shown in Figure 3.4, on the inlet and outlet of the
LTEH system, respectively.

1. Cold side heat exchanger 2. Thermoelectric generator 3. Copper lid 4. Sealing rubber
5. Hot side heat exchanger 6. Support element
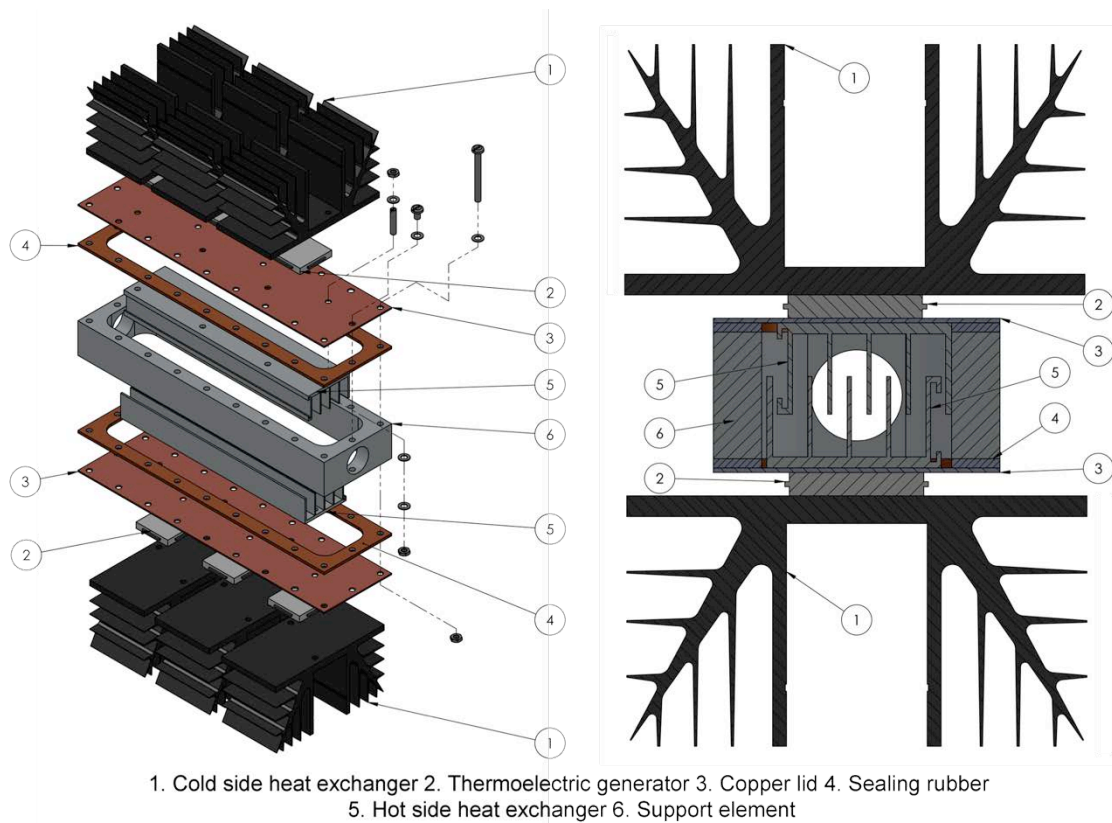
Figure 3.6. Exploded and cross sectional view of the experimental setup.

As can be seen in Figure 3.6, the LTEH experimental setup is composed
of six elements: two hot-side heat exchangers, six cold-side heat
exchangers, six thermoelectric modules that convert the waste heat into
useful electrical energy, a compression assembly system comprising a
top and bottom lid, a support element that permits attachment of the lids
and a sealing rubber. All heat exchangers and external lids are made
from aluminium and copper, respectively. TEGs are mounted on the top
and at the bottom surface, and arranged uniformly over the available
surface. They are sandwiched between assembly system and cold side

heat exchangers; therefore, the model can be treated as a natural convective heat transfer system. The remaining area and the lateral walls are thermally insulated to minimize heat leakage.

In order to validate the model under thermal and electrical dynamics, three temperature steps were established combining steady and transient states. Initially, the fluid temperature was 29.35°C while the room temperature was measured as 20.10°C. The mass flow rate of the fluid $\dot{m}$ was 54 kg/h. On the first step, the electrical accumulator was switched on and the pump started moving fluid through the water loop. While T_{in} started increasing, the R_L was set to 2.2Ω. When temperature achieved 50°C, T_{in} was maintained while load resistance changed to 1Ω and to open circuit after. As can be shown in Figure 3.7, the same process was repeated for two additional inlet temperatures T_{in} of 65°C and 80°C.
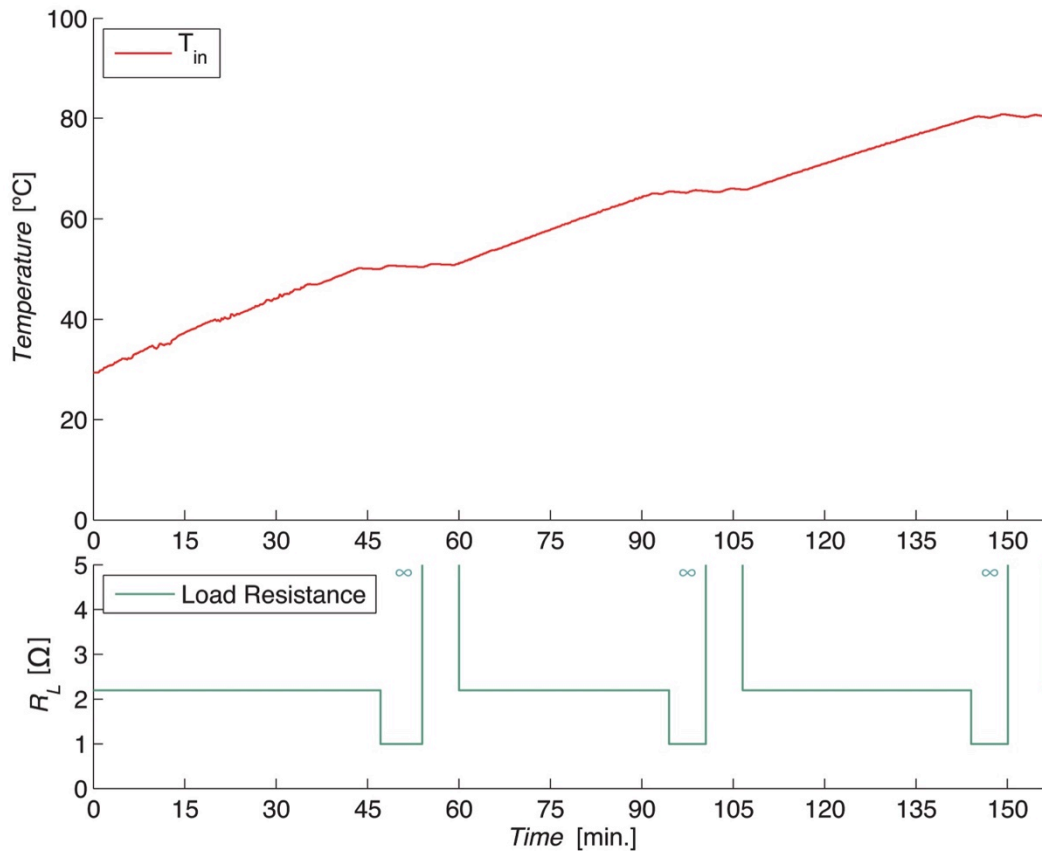
Figure 3.7. T_{in} and R_L profiles.

During experimental data acquisition, the transient temperatures at the inlet and outlet of the LTEH and the output voltage and current of each TEG were recorded simultaneously into a digital computer using a data acquisition system (National Instruments-cRIO). The data acquisition was set at a rate of 1 s for about 10400 s.

Finally, the properties of materials used in the experiment are tabulated in Table 3.1. The parameters were determined either according to direct measurement, from manufacturer's data or from existing literature [52]. Estimated values are extracted from ideal material properties (i.e. thermal conductivity, density and specific heat of aluminium and copper, respectively) and from theoretical calculations (i.e. convective heat transfer coefficient of hot side heat exchanger). The Seebeck coefficient, thermal conductivity and electrical resistivity of the p- and n-type elements are listed at steady-state average temperature of $\bar{T} = (T_{f,max} + T_{amb})/2$, which was 50.05°C.

Parameters	Case 1	Unit	Source
T_{amb}	20.10	°C	Measured
np	2	-	Experiment
ns	3	-	Experiment
$\dot{m}$	54	kg/h	Measured
S_f	4180	J/kgK	Estimated
a_n	141.587	µV/K	Manufacturer
a_p	-146.550	µV/K	Manufacturer
λ_n	1.615	W/mK	Manufacturer
λ_p	1.872	W/mK	Manufacturer
σ_n	9.604	µΩm	Manufacturer
σ_p	8.881	µΩm	Manufacturer
ρ_n	7700	kg/m³	[52]
ρ_p	7700	kg/m³	[52]
e_n	2.54×10^{-3}	m	Manufacturer

Parameters	Case 1	Unit	Source
e_p	2.54×10^{-3}	m	Manufacturer
A_n	2.3×10^{-6}	m^2	Manufacturer
A_p	2.3×10^{-6}	m^2	Manufacturer
S_n	200	J/kgK	[52]
S_p	200	J/kgK	[52]
N	98	-	Manufacturer
e_{tg1}	1×10^{-4}	m	Measured
e_{cl}	2×10^{-3}	m	Measured
e_{tg2}	1×10^{-4}	m	Measured
e_{ce}	2.54×10^{-4}	m	Measured
e_{tg3}	1×10^{-4}	m	Measured
A_{hh}	1.5×10^{-3}	m^2	Measured
A_{tg1}	8.41×10^{-4}	m^2	Measured
A_{ce}	8.41×10^{-4}	m^2	Measured
A_{tg2}	8.41×10^{-4}	m^2	Measured
A_{cl}	8.41×10^{-4}	m^2	Measured
A_{ch}	8.41×10^{-4}	m^2	Measured
λ_{tg1}	2.5	W/mK	Manufacturer
λ_{ce}	36	W/mK	[52]
λ_{tg2}	2.5	W/mK	Manufacturer
λ_{cl}	380	W/mK	Estimated
λ_{tg3}	2.5	W/mK	Estimated
ρ_{hh}	2700	kg/m^3	Estimated
ρ_{tg1}	2040	kg/m^3	Manufacturer
ρ_{ce}	3975	kg/m^3	[52]
ρ_{tg2}	2040	kg/m^3	Manufacturer
ρ_{cl}	8930	kg/m^3	Estimated
ρ_{tg3}	2040	kg/m^3	Manufacturer
ρ_{ch}	2700	kg/m^3	Estimated
S_{hp}	883	J/kgK	Estimated
S_{tg1}	200	J/kgK	Manufacturer
S_{ce}	765	J/kgK	[52]

Parameters	Case 1	Unit	Source
S_{tg2}	200	J/kgK	Manufacturer
S_{cl}	385	J/kgK	Estimated
S_{tg3}	200	J/kgK	Manufacturer
S_{ch}	883	J/kgK	Estimated
h_{ch}	200	W/m^{2}K	Manufacturer
h_{hh}	5000	W/m^{2}K	Estimated

Table 3.1. Thermoelectric parameters and material properties.

3.5 Results and discussion

Based on the transient and steady state experiments explained in Section
3.4 and TRNSYS simulations, the results and a discussion about their
comparison are presented in this section. Due to the fact that TEGs are
placed in the same stage and they produce the same output values, only
one TEG per stage has been presented. Both the transitory experimental
and simulation results are plotted versus the transient time in the same
plot. The conditions imposed in the experiment are listed in Table 3.1.
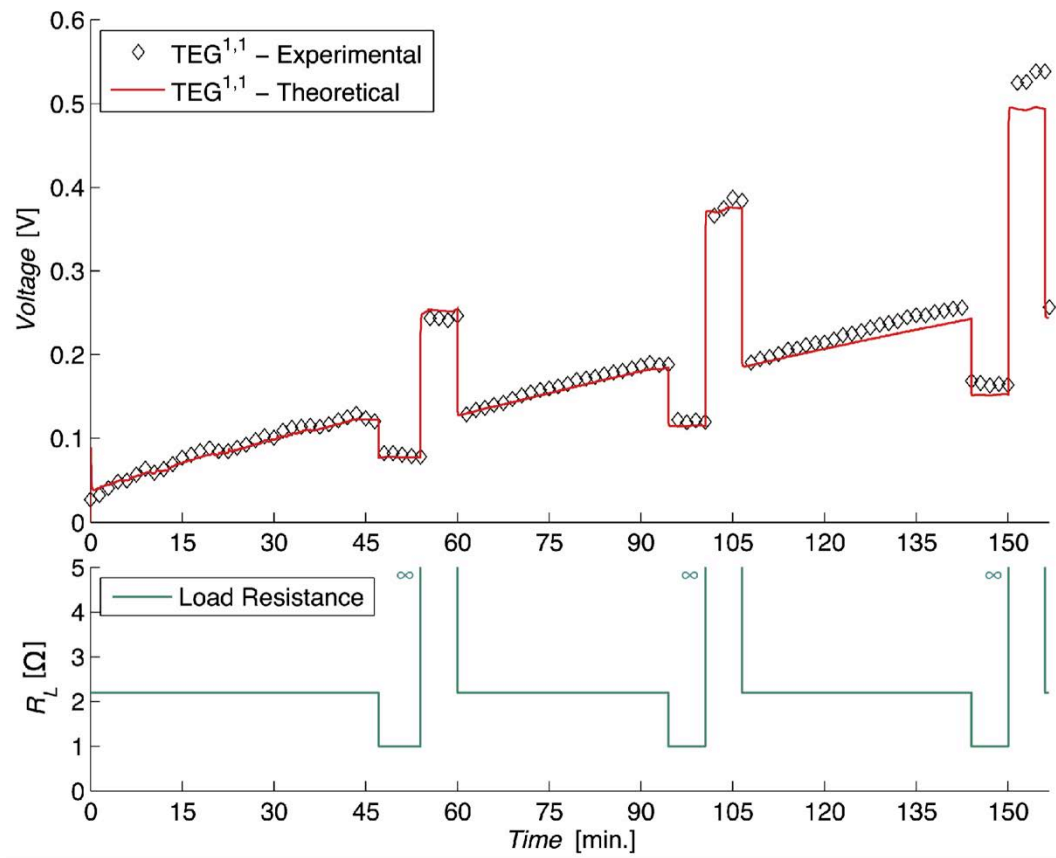
Figure 3.8. Correlation of experimental and simulated output voltage of a
TEG located in stage 1.
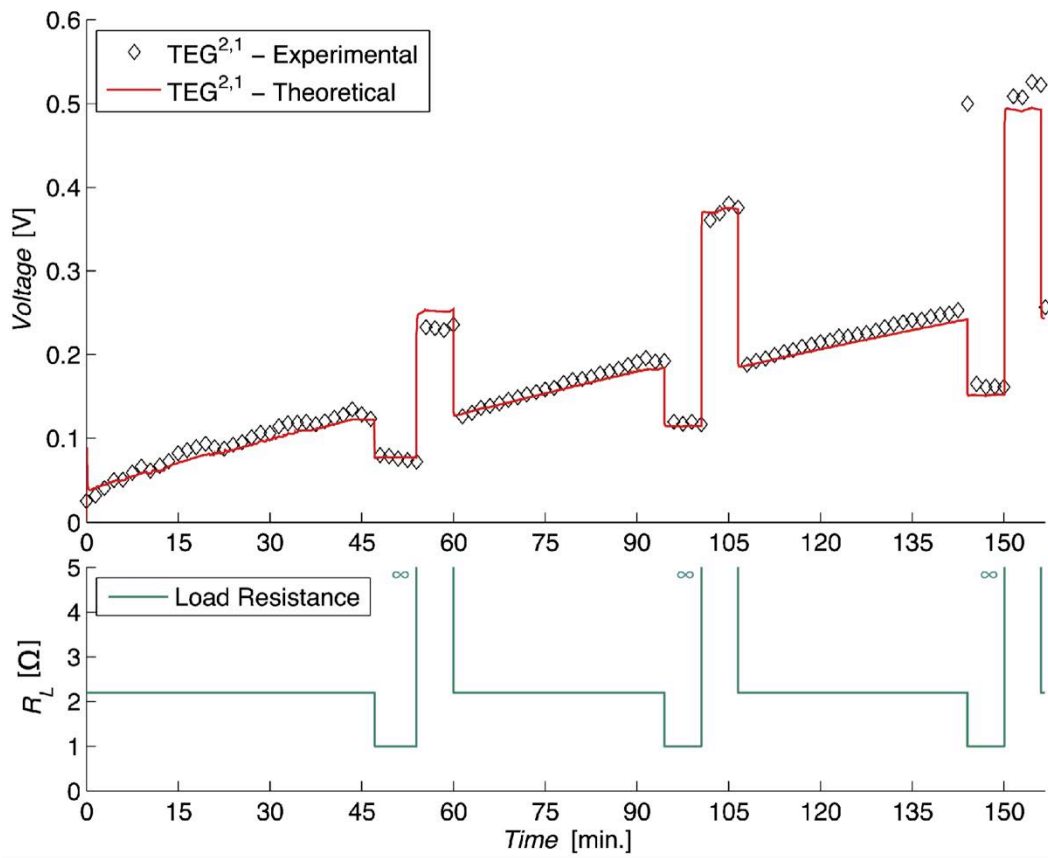
Figure 3.9. Correlation of experimental and simulated output voltage of a
TEG located in stage 2.
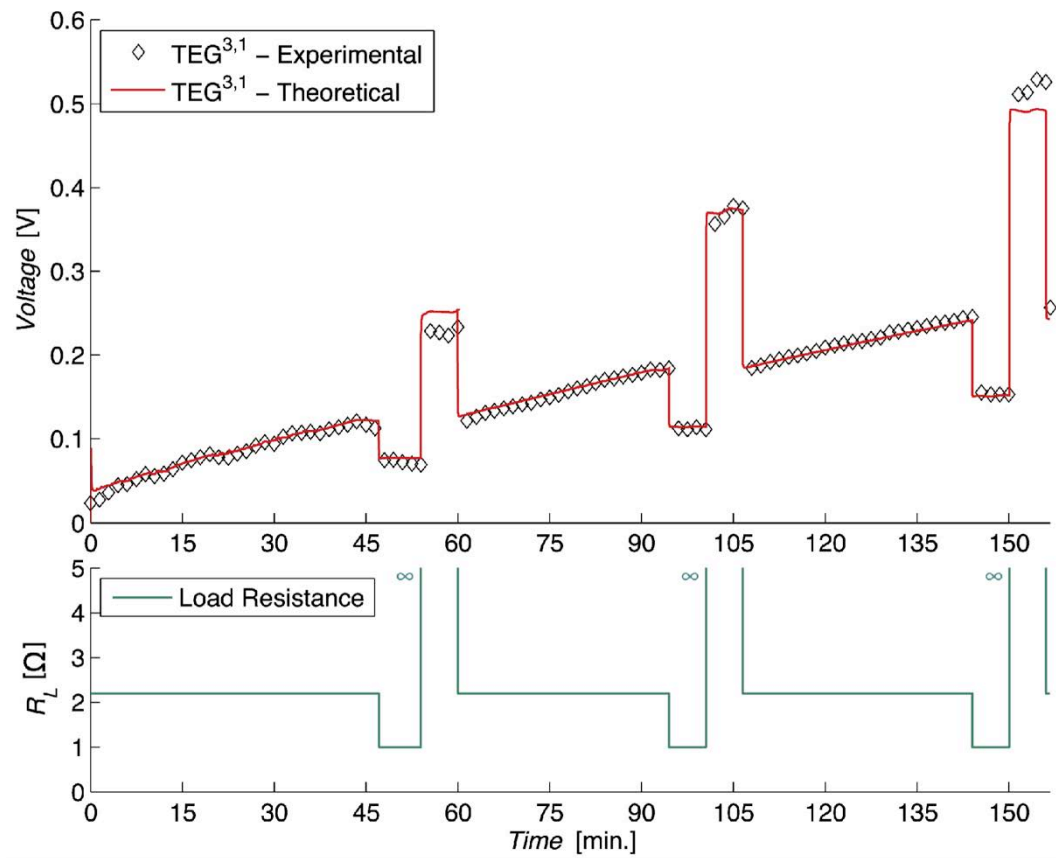
Figure 3.10. Correlation of experimental and simulated output voltage of a
TEG located in stage 3.

In Figure 3.8 to Figure 3.10, the effects of inlet temperature and step changes of load resistance under conditions of Section 3.4 can be observed. Although there is not appreciable difference between above voltages, an accurately analysis shown that as the stage increase, the output voltage decreases. The voltage difference between each stage is strongly affected by the quantity of heat extracted from the fluid. The more inlet temperature, the more heat transfers through TEGs and the more difference of voltages between each stage. Unlike theoretical model, experimental results show a progressive increase of open-circuit voltage when no load resistance is connected due to the disappearance of the Peltier therm. That is because of the instantaneous response of the model to electrical variations.
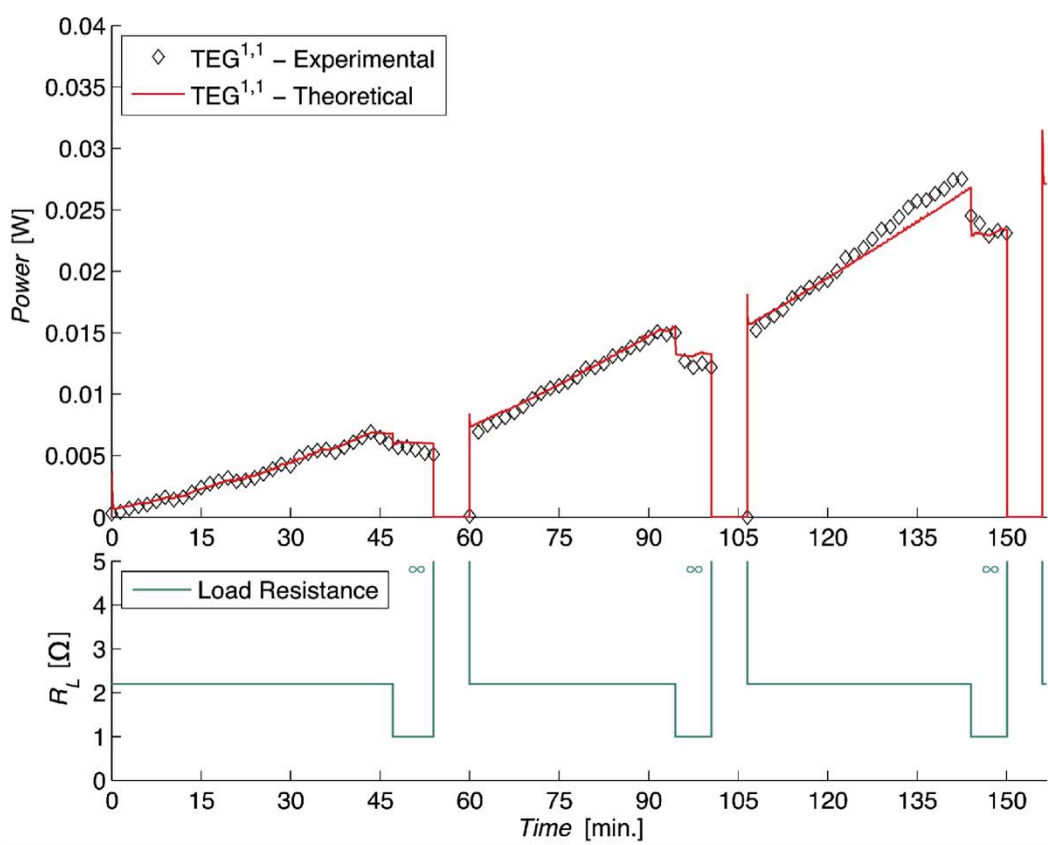
Figure 3.11. Correlation of experimental and simulated output electrical
power of a TEG located in stage 1.
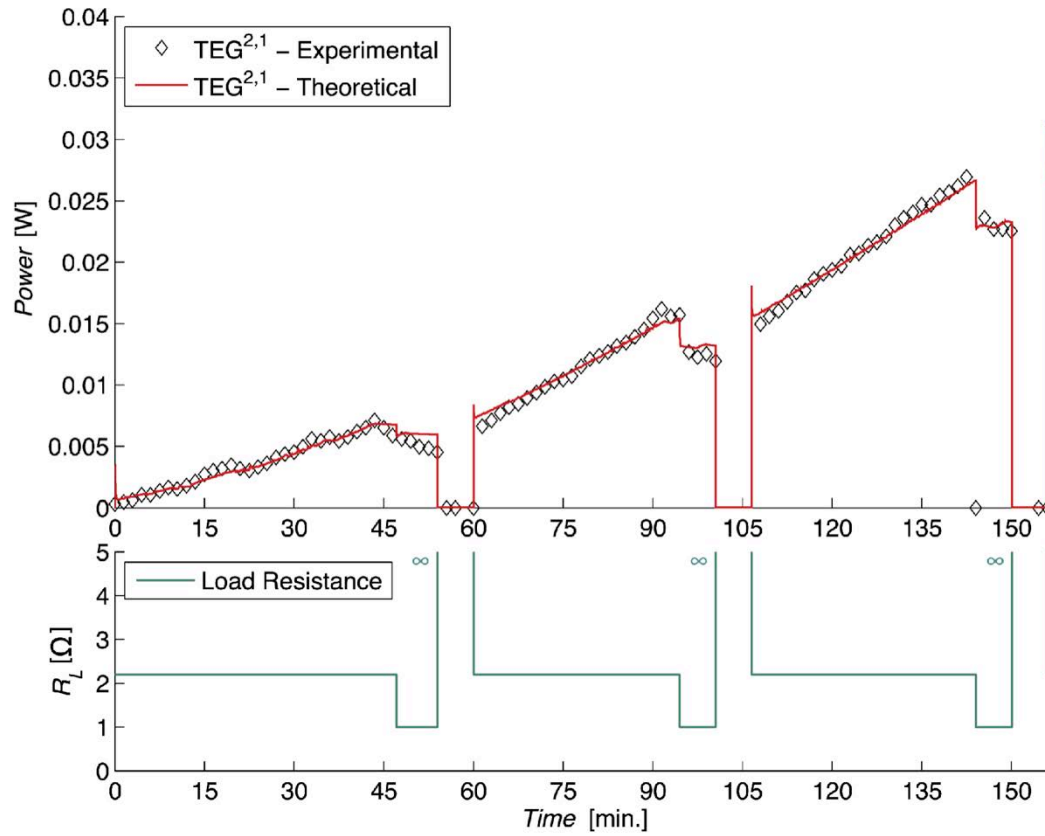
Figure 3.12. Correlation of experimental and simulated output electrical
power of a TEG located in stage 2.
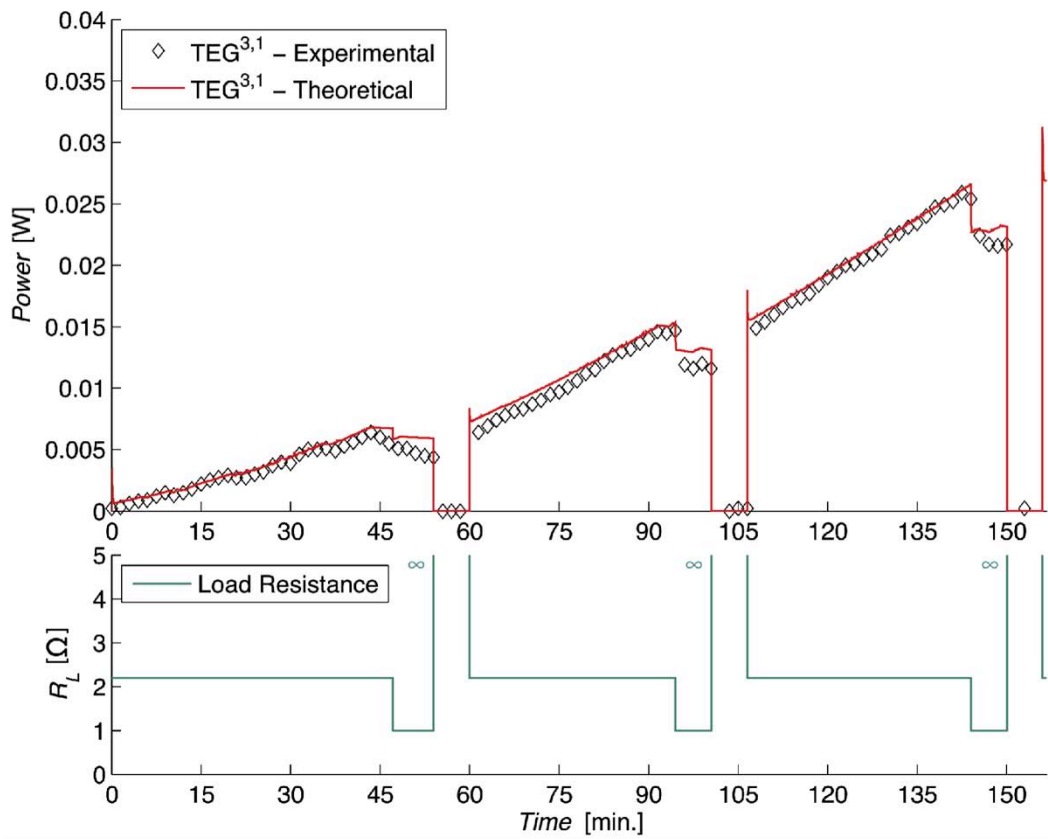
Figure 3.13. Correlation of experimental and simulated output electrical
power of a TEG located in stage 3.

Simultaneously to the voltage measurements, the electrical output power P_{RL} was obtained. As can be observed from Figure 3.11 to Figure 3.13, P_{RL} tend to increase as inlet temperature T_{in} increases. Moreover, as the stage increase, the output electrical power decreases. However, electrical power does not only depend on the temperature difference between hot and cold sides of the TEG, but also on the load resistance connected. As explained in Ref. [52], the power generation is highest when the load resistance value is close to the internal resistance $R_L=R_{pn}$, which is measured to be about 2.2Ω. Consequently, different values of R_L will produce lower electrical powers. This effect can be observed in above figures.

For the purpose of assessing the model, the temperature difference
between inlet T_{in} and outlet T_{out} was also measured. Due to the fact that
T_{out} differences between experimental and theoretical data were too
small, the $\Delta T = T_{in}(t) - T_{out}(t)$ was plotted instead. The comparison
between experimental and theoretical data is shown in Figure 3.14.
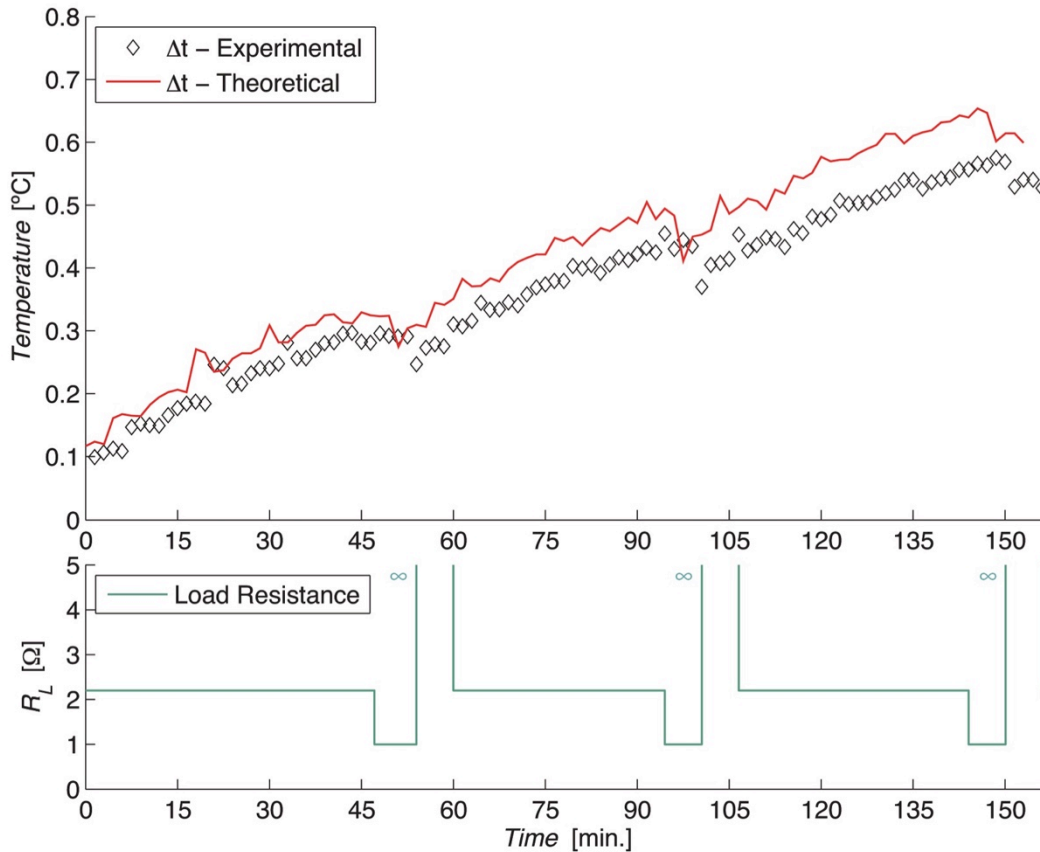
Figure 3.14. Correlation of experimental and simulated temperature
difference between inlet and outlet of LTEH.

Figure 3.14 demonstrates that T_{out} is strongly affected by load resistance.
Every increase in I leads to an increase of temperature difference
between hot and cold side of TEGs due to the greater value of the Peltier
effect. This current increment also produces an increment of hot and cold
side heat fluxes. Consequently, every decrease in R_L leads to a reduction
in fluid outlet temperature.

The same effect occurs with heat extracted from LTEH, Eq. (3.1). As can be shown in Figure 3.15, the total amount of heat extracted from fluid by TEGs can be calculated considering the Eq. (3.4) and experimental ΔT from Figure 3.14. It is interesting to note that heat transfer decrease with load resistance due to the greater value of Peltier therm. Higher heat transfer can be observed when lowest values of load resistance are selected, and conversely. Besides, the LTEH efficiency η also is affected by load resistance but not in the same way. In Figure 3.15, it can be observed that R_L values close to internal resistance produces the maximum system efficiencies η. This not only occurs to power generation but also to system efficiency which is highest when load resistance value is close to the internal resistance $R_L = R_{pn}$.
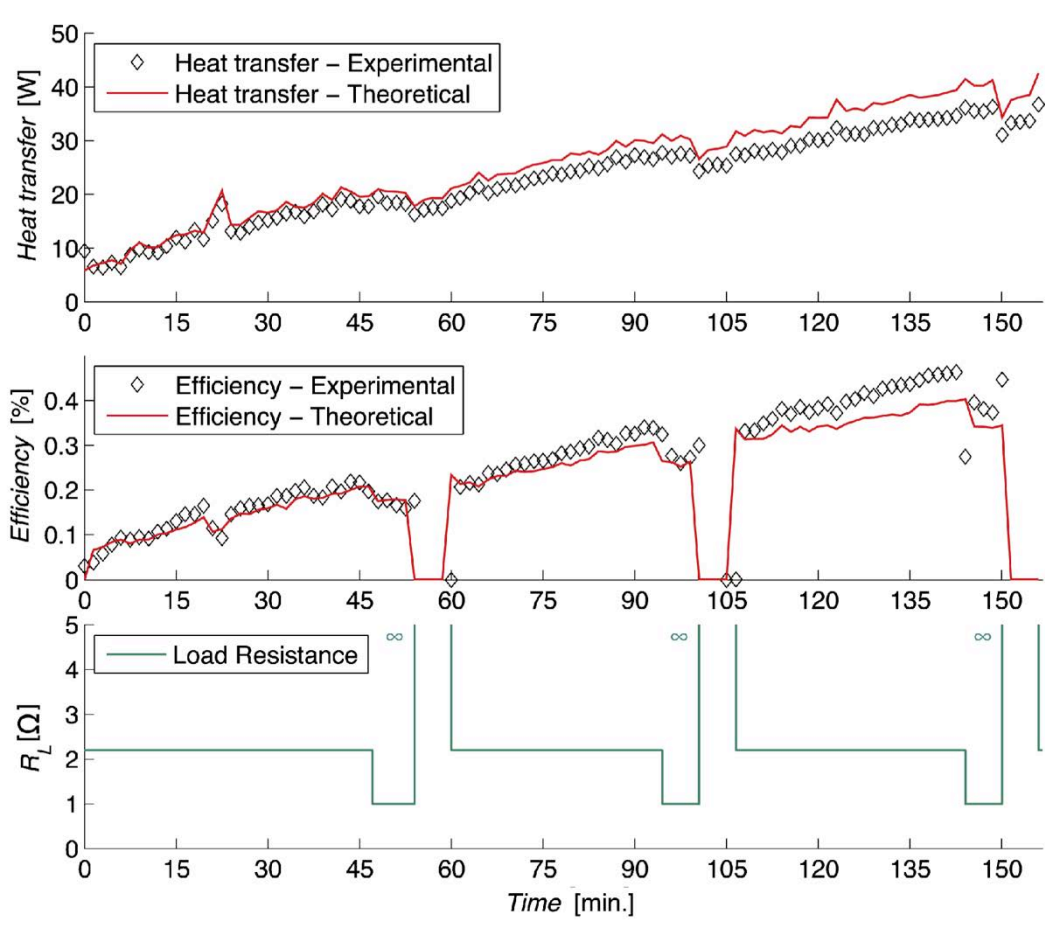
Figure 3.15. Correlation of experimental and simulated heat transfer and system efficiency of the LTEH.

As it can be appreciated from all figures, the simulation results show good agreement with the experimental results, accurately tracking the electro-thermal coupled effects occurring in the LTEH system. However, the plotted curves show highest correlation when inlet temperatures are near to average range. This is due to the fact that thermoelectric parameters (i.e. Seebeck coefficient, thermal conductivity and electrical resistance of TEGs) are constant and obtained from steady-state average temperature $\bar{T} = \left(T_{f,max} + T_{amb}\right)/2$. The maximum error derived from this assumption is estimated to be 2.35% for the temperature range of this experiment. In future work, equations that relate above parameters with temperature will be considered in the model.

3.6 Conclusions

In this paper, a new computational model capable to simulate the electro-thermal dynamics of a LTEH is presented, and a thermoelectric energy harvester has been constructed to validate it. The new component, developed in TRNSYS software, had been analysed and validated under low temperature conditions and under steady and transient states with data obtained from the experimental setup.

The comparison of results between theoretic analysis and experiment has approved the reasonability of the new component. The root mean square errors RMSE for heat extracted, electrical power generated and temperature difference between inlet and outlet are 0.566W, 3.9×10^{-3} W and 7.4×10^{-3} °C, respectively. Additionally, the normalized root mean square errors NRMSE are 0.67%, 0.5% and 0.894%, respectively.

Although global maximum output electrical power and efficiency is quite low: 0.162W and 0.46%, respectively; these values could be improved by optimizing the arrangement of TEGs, increasing its clamping force, reducing the number of layers or increasing the convective heat transfer with better geometries of hot and cold side heat exchangers.

Besides, the TRNSYS simulation runs without interruptions or delays, consequently the numerical model and the new component can be considered well optimized. Therefore, this new model can be used in design, performance optimization and further application of thermoelectric energy harvesters.

3.7 Acknowledgment

Advances in modelling and analysis of longitudinal thermoelectric energy harvesters

This section is a transcription of the contents of the following paper:

Abstract

A thermoelectric energy harvesting system takes advantage of any temperature difference between inner and outer surfaces to produce electricity by Seebeck effect. They are often used as waste heat recovery systems from exhaust gases on internal combustion engines. To boost the output power, energy harvesters are often composed of multiple arrays of TEGs electrically arranged in series-parallel configuration. The way that TEGs are connected strongly affects the electro-thermal outputs of each TEG and the whole harvester as well. Although many TE models co-exist in literature, there is no thermoelectric energy harvester model considering this effect. Therefore, the purpose of this work is to improve the accuracy of longitudinal thermoelectric energy harvester (LTEH) models introducing the prediction of the interconnection effects. The comparison of results between theoretical and experimental data shows great accuracy and the possibility to be used as a simulation tool.

p. 81-114 EMBARGOED UNTIL PUBLICATION

Chapter 5

Discussion and conclusions

Although thermoelectric phenomena have been used for heating and cooling applications quite extensively, electricity generation has only seen very limited market in niche applications and it is only in recent years that interest has increased regarding new applications of energy generation through thermoelectric harvesting. The widespread use of TEGs depends on its optimization.

In order to meet the main objectives of this thesis, which are described in Chapter 1, initially a new TRNSYS type modelling the transient behaviour of a single thermoelectric generator has been described and validated. The proposed component, which is explained in Chapter 2, is able to cope with thermal and electrical dynamics. It has been used as a base model of the LTEH model explained in Chapter 3. The new component, which has also been programmed into TRNSYS environment, modelizes an array of TEGs placed with respect to the fluid flow direction.

However, the model is only adequate for the simulation of LTEHs when independent load resistances are connected to each TEG. Ideally each TEG should be independently electronically controlled but this would greatly increase the number and complexity of the MPPT power electronic converters needed and adversely affect the cost of implementing the system. A real LTEH is always formed by an array of multiple interconnected TEGs. Consequently, a complete LTEH model that takes into account the electrical interconnection of the TEG array has been developed in Chapter 4.

The comparisons of results between theoretic models and experiments have approved the reasonability of them. Therefore, they can be used in design, performance optimization and further application of thermoelectric energy harvesters.

Taking into account the maximum error of voltage, current and temperature measurements presents in Table 4.2, which are the same for all papers, the worst scenarios of power generation and efficiency can be deduced from law of error propagation. Under the worst-scenario

accuracy of measurements, uncertainties stays inside a low deviation range: ±0.57% for power generation measurement and ±0.67% for efficiency. Those uncertainties are smaller than the accuracy obtained from the theoretical model. In fact, they are so small that can not be appreciated in a chart.

In order to avoid experimental measurement errors such bias in the instrument relative to the defined unit of measurement, all instruments and equipment used are send out for calibration before any measurements requiring highly accurate data.

Errors between theoretical and experimental data may be due to the measuring instrument, the lack of accuracy of the material parameters introduced into the model, the neglection of Thomson effect, the ignorance of the contact resistances and the non-temperature dependence of non-thermoelectric material parameters. Accuracy could be improved by: enabling variations on the number of nodes, considering heat losses due to convection in lateral faces or introducing temperature-dependent parameters. In fact, the plotted curves of Chapter 2 and 3 show highest correlation when inlet temperatures are near to average range. That is because thermoelectric parameters (i.e. Seebeck coefficient, thermal conductivity and electrical resistance of TEGs) are constant, that is to say, non-temperature dependent, and obtained from steady-state average temperature.

The obtained LTEH efficiencies are somewhat lower than expected, mainly because of the low hot side temperatures used. In the same manner, low heat transfers on the cold side heat exchanger due to the natural convection contributes to this reduced power generated and efficiency. Contact resistances has not been considered but could also adversely affect the heat flow.

As it can be observed in Chapter 4, the comparison between a LTEH with independent resistances loaded to each TEG and when TEG array are loaded to unique load resistance shows a significant difference. Such

problem can impact the performance of a thermoelectric system, and a theoretical analysis is presented to justify the results and to calculate expected performance. The experimental results show that the power lost by mismatched conditions (temperature, mechanical load, manufacturing tolerances, aging) can be significant. Not taking into account interconnection and temperature mismatch effects lead to an overestimation of the total power production in large LTEHs.

The first two models have been programmed in Fortran to be able to be used into TRNSYS platform, because it is one of the most flexible energy simulation software packages. These new components allow users to simulate thermoelectric energy harvesters in infinite thermodynamic systems.

However, the last model presents higher complexity and computational requirements than the first two models. We have thus chosen MATLAB instead of TRNSYS. This has allowed us to implement and debug the complex above equations easier than any other low-level code. Matlab programs are often much shorter and easier to read than programs written for instance in C or Fortran. However, it requires additional time, e.g. for checking the syntax every time a program is started. Consequently, Matlab code uses more memory and processing time than Fortran code does.

Finally, a number of improvement actions must be performed to allow the development of a truly general-purpose LTEH model. These actions suggest a variety of research works that need to be pursued to make such a tool feasible:

- Consider non-thermoelectric material parameters temperature dependent.
- Introduce the procedure to internally calculate the convection coefficients of the hot and cold side heat exchangers at each stage.
- Take into account the contact resistances.

- Enable variations in the number of nodes.

- Analyse different electrical interconnections to determine which is the most efficient way to connect the TEG array.

Appendixes

Published paper: Development and validation of a new TRNSYS type for the simulation of thermoelectric generators

Development and validation of a new TRNSYS type for the simulation of thermoelectric generators

E. Massaguer *, A. Massaguer, L. Montoro, J.R. Gonzalez

Department of Mechanical Engineering and Industrial Construction, University of Girona, C. de Maria Aurèlia Capmany, 61, 17071 Girona, Spain

HIGHLIGHTS

- A new TRNSYS component for simulation of thermoelectric generators is developed.
- A TEG model is proposed and validated under transient and steady-state conditions.
- The results have approved the reasonability of the new component.

ABSTRACT

Thermoelectric generators (TEGs) make use of the Seebeck effect in semiconductors for the direct conversion of heat into electrical energy, being of particular interest for high reliability systems or for waste heat recovery. Although several TEG models can be found in the literature, many of them not offer a theoretical solution because they are based on steady-state solutions or they are assuming fixed parameters as boundary conditions. Consequently, to assess and optimize thermoelectric generators in real applications a numerical transient simulation tool, which takes into account the whole energy system, is mandatory. For that purpose, a new TRNSYS type is developed. This TEG component, which can be used as a design tool, is presented in this paper and validated using experimental data.

The results show that the proposed component is able to cope with both thermal and electrical dynamics. The comparison between theoretic and experimental results has approved the reasonability of the new component. The normalized root mean square errors are 3.53% and 2.33% for temperature difference between hot and cold sides and electrical output power, respectively.

© 2014 Elsevier Ltd. All rights reserved.

1. Introduction

A thermoelectric power generator is a solid-state device that provides direct energy conversion from thermal energy, due to a temperature gradient, into electrical energy based on Seebeck effect. Also, they can work in reverse and use electrical energy to create a temperature gradient for cooling or heating applications. The absence of moving parts, wide range of operating temperatures, scalability, and modular capabilities makes thermoelectricity attractive for a wide variety of applications, such as power for remote control and monitoring of oil or gas pipelines and production facilities, automotive waste heat recovery, power for navigational aids, spacecraft radioisotope power supply, telecommunications systems and cathodic protection, and other energy recovery processes [1–6]. Thermoelectric devices have relatively low efficiencies but there have been recent advances in thermoelectric materials potentially opening the door to new power applications [7,8]. As material advancements continue and a wider range of power generation applications will be considered, module and system level modelling becomes critical for the design of the next generation of thermoelectric systems.

Although several models for TEG modules can be found in the literature [9–16], many of them not offer a theoretical solution because their governing equations are based on steady-state solutions or they are assuming fixed temperatures as boundary conditions at both sides of the TEG. Moreover, almost none of them have studied the transient effects of load resistance. Complete transient analyses are seldom presented and just a few have already provided a complete mathematical solution of the heat conduction equation for TEG devices [13–15].

This study attempts to fill the existing gap in the simulation of thermoelectric generation through the development of a new component that can be used in TRNSYS software. TRNSYS [17],

---
* Corresponding author. Tel.: +34 972 418 489; fax: +34 972 418 098.
E-mail address: Eduard.massaguer@udg.edu (E. Massaguer).

Nomenclature

Abbreviation		T	temperature (K)
		y	axis coordinate (m)
TEG	thermoelectric generator	t	time (s)
Symbols		*Subscript*	
n	number of thermocouples	hp	hot plate
α	Seebeck coefficient (V/K)	$tc_{1,2}$	thermal compound
σ	electrical resistivity (Ω m)	ce	ceramic substrate
e	length (m)	cp	cold plate
A	cross sectional area (m^2)	cb	water-cooling block
ρ	material density (kg(m^3))	h	hot side
S	specific heat capacity (J/kg K)	c	cold side
λ	thermal conductivity (W/m K)	p	p-type semiconductor
K	thermal conductance (W/K)	n	n-type semiconductor
C	thermal capacity (J/K))	in	input
h	convective heat transfer coefficient (W/m^2 K)	L	load resistance
Q	heat rate (W)	C_∞	cooling water
V	electric voltage (V)	oc	open circuit
I	electric current (A)	max	maximum
P	electric power (W)	ss	steady-state
η	efficiency (%)		
R	electric resistance (Ω)		

developed at the University of Wisconsin, is a transient systems simulation program with a modular structure. It recognizes a system description language in which the user specifies the components that constitute the system and the manner in which they are connected. The TRNSYS library includes many of the components commonly found in thermal and electrical energy systems, as well as component routines to handle input of weather data or other time-dependent forcing functions and output of simulation results. The modular nature of TRNSYS gives the program flexibility, and facilitates the addition to the program of mathematical models not included in the standard TRNSYS library. TRNSYS is well suited to detailed analyses of any system whose behaviour is dependent on the passage of time. It has become reference software for researchers and engineers around the world. Main applications include: solar systems (solar thermal and photovoltaic systems), low energy buildings, HVAC systems, renewable energy systems, cogeneration, fuel cells and more.

Full integration of the new component within the TRNSYS simulation package is another advantage of this study, which makes it more applicable for designers in both the design and commissioning of waste energy harvesting systems. The incorporation of the TEG model into standard TRNSYS library will allow users to simulate TEGs coupled to many different thermal facilities and applications (e.g. solar thermal systems, geothermal systems and more). Because of the mentioned benefits, TRNSYS is chosen to implement the new component.

The objective of this work is to develop a computational model capable to simulate the electro-thermal dynamics of a TEG system into TRNSYS software. The new component is fully analysed and validated under steady and transient states with data obtained from the experimental setup.

2. TEG modelling

A TEG device in essence is a thermopile composed of a number of p- and n-type semiconductor pairs connected electrically in series. Heat carries the majority carriers from one junction to the other producing a current and voltage. By placing many PN couples in series electrically and in parallel thermally, a TEG module

generates an open-circuit voltage proportional to the temperature differential across the elements.

According to Seebeck, Peltier and Thomson effects, the TEG power generation depends mainly on both temperature differential across the semiconductor elements and electrical load connected (i.e. changes of the temperature difference lead to changes of the open-circuit voltage, and the TEG output performance will change as well). Therefore, the unsteady-state heat transfer model is built to solve the TEG temperature distribution. Thereafter, the TEG power and performance outputs can be determined.

Similar with Gou [12,21], Kim [20], Nguyen [14] and Rodríguez [19], the basic configuration of the thermoelectric study follows the general design illustrated in Fig. 1.

A thermoelectric module is sandwiched between electrical heater and water-cooled heat exchanger that can be treated as a convective heat transfer system. The TEG consists of certain number of semiconductors, corresponding solder layers, conducting strips and thermal insulation material. In order to electrically isolate the module, a ceramic substrate is located both sides of the TEG. A thermal compound increases the thermal conductivity of the interfaces by filling microscopic air-gaps between ceramic substrates and aluminium plates and TEG and ceramic substrates, respectively. At the same time, hot and cold plates allow to introduce temperature sensors on the experimental set up.

2.1. Assumptions and boundary conditions

In the analytical assessing, the thermal conductivity, electric conductivity, and Seebeck coefficient of semiconductors are all assumed to be temperature-independent, and adiabatic boundary conditions were supposed on the side surfaces of TEG element. Thermal conductivities, electrical resistivity, and specific heat capacities of non-thermoelectric materials are supposed constants within the operating temperature range.

Due to the fact that this study is focused on low-temperature system, the Thomson effect could be neglected [17]. Besides, initial temperature of the system is equal to ambience temperature, this means that temperatures at both sides of the TEG element are the
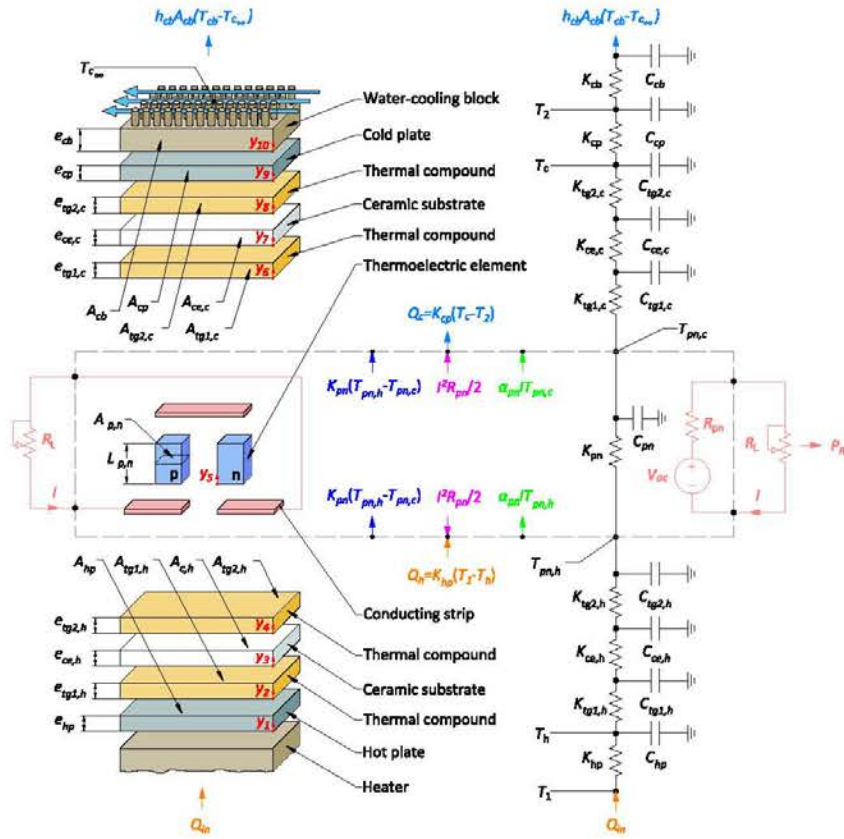
Fig. 1. One-dimensional heat transfer model of thermoelectric generator.

same, and consequently initial output data is zero. Finally, an instantaneous response to electrical load transients is considered [13].

The heat leakage through the solder layer and conducting strips are neglected. The flow of heat and current in the system are assumed one-dimensional. All materials are assumed homogeneous and isotropic. Finally, heat losses due to radiation and transverse convection are neglected.

2.2. Governing equations

In thermoelectric devices, both refrigeration and generation applications, the internal and external nodal temperatures of TEG cannot be determined analytically without knowing the heat flux due to the thermoelectric effects. The reasons are the nonlinearities of the thermoelectricity and heat transfer equations.

The model solves the nonlinearities using finite difference and Newton–Raphson methods, which calculates the temperature at different nodes separated in space by a discrete distance. In the transient state, the temperatures of these points are calculated at discrete periods of time and the temperatures for all the nodes are recalculated at the end of this time interval. Using the implicit finite difference method, the values of heat flux can be determined using the values of the temperatures of the time step before.

According to heat conduction theory, the one-dimensional unsteady heat conduction equation of non-thermoelectric elements can be shown as:

$$\rho_i S_i \frac{\partial T_i}{\partial t} = \lambda_i \frac{\partial^2 T_i}{\partial y_i^2} \tag{1}$$

where ρ, S and λ are density, specific heat capacity and thermal conductivity, respectively, t and y are time and axis coordinate, respectively. The subscript i determines the heat transfer related to node i. As found in the referenced literature [13,19], the thermal–electrical analogy is useful in the analysis of complicated unsteady heat transfer problems, which can be understood by creating an electric circuit like Fig. 1 with following equations:

$$K_i = \frac{\lambda_i A_i}{e_i} \tag{2}$$

$$C_i = \rho_i S_i A_i e_i \tag{3}$$

where K_i and C_i are the thermal conductance and thermal capacity associated with each node i.

The governing equations for p- and n-type thermoelectric elements involve three basic effects, Seebeck effect, Peltier effect and Thomson effect. Besides, there are two accessorial effects, Joule effect and Fourier effect. Gou [12] explained that Peltier heat generates on the two sides of semiconductor and Joule heat can be regarded as flowing equally to the two sides of conductors, so they can be disposed as a boundary heat fluxes. Thomson heat is small enough to be neglected since it is a second-round effect. So the TEG inner unsteady-state heat transfer equation can be translated also as Eq. (1).

The boundary condition applied at the hot plate surface, $y_1 = 0$, corresponds to the applied heat from electrical heater Q_{in}. On the top surface, $y_{10} = e_{cb}$, the convection boundary equation is employed. The boundary conditions applied to solve the unsteady-state heat transfer Eq. (1) for the system shown in Fig. 1 are listed below.

Between heater and hot plate surface

$$Q_{in} = -\lambda_{hp} A_{hp} \frac{\partial T}{\partial y}\Big|_{y_1 = 0} \tag{4}$$

Between hot plate and thermal compound

$$-\lambda_{hp} A_{hp} \frac{\partial T}{\partial y}\Big|_{y_1 = e_{hp}} = -\lambda_{tc1,h} A_{tc1,h} \frac{\partial T}{\partial y}\Big|_{y_2 = 0} \tag{5}$$

Between thermal compound and ceramic plate

$$-\lambda_{tc1,h} A_{tc1,h} \frac{\partial T}{\partial y}\Big|_{y_2 = e_{tc1,h}} = -\lambda_{ce,h} A_{ce,h} \frac{\partial T}{\partial y}\Big|_{y_3 = 0} \tag{6}$$

Between ceramic plate and thermal compound

$$-\lambda_{ce,h} A_{ce,h} \frac{\partial T}{\partial y}\Big|_{y_3 = e_{ce,h}} = -\lambda_{tc2,h} A_{tc2,h} \frac{\partial T}{\partial y}\Big|_{y_4 = 0} \tag{7}$$

Between thermal compound and thermoelectric element

$$-\lambda_{tc2,h} A_{tc2,h} \frac{\partial T}{\partial y}\Big|_{y_4 = e_{tc2,h}} = -\lambda_{pn} A_{pn} \frac{\partial T}{\partial y}\Big|_{y_5 = 0} + \alpha_{pn} I T_{pn,h} - \frac{1}{2} I^2 R_{pn} \tag{8}$$

Between thermoelectric element and thermal compound

$$-\lambda_{pn} A_{pn} \frac{\partial T}{\partial y}\Big|_{y_5 = e_{pn}} + \alpha_{pn} I T_{pn,c} + \frac{1}{2} I^2 R_{pn} = -\lambda_{tc1,c} A_{tc1,c} \frac{\partial T}{\partial y}\Big|_{y_6 = 0} \tag{9}$$

Between thermal compound and ceramic plate

$$-\lambda_{tc1,c} A_{tc1,c} \frac{\partial T}{\partial y}\Big|_{y_6 = e_{tc1,c}} = -\lambda_{ce,c} A_{ce,c} \frac{\partial T}{\partial y}\Big|_{y_7 = 0} \tag{10}$$

Between ceramic plate and thermal compound

$$-\lambda_{ce,c} A_{ce,c} \frac{\partial T}{\partial y}\Big|_{y_7 = e_{ce,c}} = -\lambda_{tc2,c} A_{tc2,c} \frac{\partial T}{\partial y}\Big|_{y_8 = 0} \tag{11}$$

Between thermal compound and cold plate

$$-\lambda_{tc2,c} A_{tc2,c} \frac{\partial T}{\partial y}\Big|_{y_8 = e_{tc2,c}} = -\lambda_{cp} A_{cp} \frac{\partial T}{\partial y}\Big|_{y_9 = 0} \tag{12}$$

Between cold plate and water-cooling block

$$-\lambda_{cp} A_{cp} \frac{\partial T}{\partial y}\Big|_{y_9 = e_{cp}} = -\lambda_{cb} A_{cb} \frac{\partial T}{\partial y}\Big|_{y_{10} = 0} \tag{13}$$

Between water-cooling block and cooling fluid

$$-\lambda_{cb} A_{cb} \frac{\partial T}{\partial y}\Big|_{y_{10} = e_{cb}} = h_{cb} A_{cb} (T_{cb} - T_{c\infty}) \tag{14}$$

With

$$\alpha_{pn} = n(\alpha_p - \alpha_n) \tag{15}$$

$$\lambda_{pn} = n(\lambda_p + \lambda_n) \tag{16}$$

$$A_{pn} = n(A_p + A_n) \tag{17}$$

$$R_{pn} = n\left(\frac{\sigma_p e_p}{A_p} + \frac{\sigma_n e_n}{A_n}\right) \tag{18}$$

$$I = \frac{\alpha_{pn}(T_{pn,h} - T_{pn,c})}{R_{pn} + R_L} \tag{19}$$

where λ_{hp}, λ_{cp}, λ_{tc1}, λ_{ce}, λ_{tc2}, λ_{cb} and λ_{pn} are thermal conductivities of hot plate, cold plate, external thermal compound, ceramic plate, internal thermal compound, water-cooling block and thermoelectric generator, respectively; e_{hp}, e_{cp}, e_{tc1}, e_{ce}, e_{tc2}, e_{cb} and e_{pn} are lengths of hot plate, cold plate, external thermal compound, ceramic plate, internal thermal compound, water-cooling block and thermoelectric generator, respectively; A_{hp}, A_{cp}, A_{tc1}, A_{ce}, A_{tc2}, A_{cb} and A_{pn} are cross sectional areas of hot plate, cold plate, external thermal compound, ceramic plate, internal thermal compound, water-cooling block and thermoelectric generator, respectively; $T_{pn,h}$ and $T_{pn,c}$ are temperatures of hot and cold side of semiconductor, respectively; T_{cb} and $T_{c\infty}$ are cold side temperature of water-cooling block and cooling fluid temperature, respectively; h_{cb} is coefficient of convective heat transfer; I is electrical current flowing through the thermoelectric circuit; R_{pn} and α_{pn} are the electric resistance and Seebeck coefficient of TEG, respectively; n is the number of semiconductor thermocouples; α_n, α_p, λ_n, λ_p, A_n, A_p, e_n, e_p, σ_n, σ_p, are the Seebeck coefficients, thermal conductivities, cross sectional areas, lengths and electrical resistivities of p- and n-type elements.

Once heat transfer equation system, Eqs. (4)–(14) and additionally Eqs. (15)–(19), is solved using implicit finite difference method, the nodal temperatures on hot and cold side of the semiconductor are found for every time step. Consequently, the electrical and thermal outputs can be obtained every time step. According to Seebeck effect the open circuit electromotive force generated is expressed as follows

$$V_{oc}(t) = \alpha_{pn}(T_{pn,h}(t) - T_{pn,c}(t)) \tag{20}$$

The output current I and output voltage V_{RL} generated depends on the load resistance R_L and it can be calculated following Eqs. (16) and (18), respectively.

$$V_{R_L}(t) = \frac{\alpha_{pn}(T_{pn,h}(t) - T_{pn,c}(t))R_L}{R_{pn} + R_L} \tag{21}$$

Besides, short circuit current also can be obtained

$$I_{sc}(t) = \frac{\alpha_{pn}(T_{pn,h}(t) - T_{pn,c}(t))}{R_{pn}} \tag{22}$$

So the output power when R_L is connected is given by

$$P_{R_L}(t) = V_{R_L} I = \frac{\alpha_{pn}^2(T_{pn,h}(t) - T_{pn,c}(t))^2 R_L}{(R_{pn} + R_L)^2} \tag{23}$$

Deriving the Eq. (23) with respect to load resistance, $P_{RL}/R_L = 0$, it can be observed that maximum output power will be reached when load electric resistance is equal to the internal electric resistance. Therefore, substituting $R_L = R_{pn}$ into Eq. (23) the maximal output power is

$$P_{max}(t) = \frac{\alpha_{pn}^2(T_{pn,h}(t) - T_{pn,c}(t))^2}{4R_{pn}} \tag{24}$$

The heat absorption on hot side and heat release on cold side of semiconductor are given by Q_h and Q_c, respectively.

$$Q_h(t) = K_{pn}(T_{pn,h}(t) - T_{pn,c}(t)) + \alpha_{pn} I(t) T_{pn,h}(t) - \frac{1}{2} I^2(t) R_{pn} \tag{25}$$

$$Q_c(t) = K_{pn}(T_{pn,h}(t) - T_{pn,c}(t)) + \alpha_{pn} I(t) T_{pn,c}(t) + \frac{1}{2} I^2(t) R_{pn} \tag{26}$$

Finally, the instantaneous and maximal system efficiency, η and η_{max}, are calculated by Eqs. (27) and (28), respectively.

$$\eta(t) = \frac{P_{R_L}(t)}{Q_h(t)}$$

$$= \frac{\alpha_{pn}^2(T_{pn,h}(t) - T_{pn,c}(t))^2 R_L}{(R_{pn} + R_L)^2 K_{pn}(T_{pn,h}(t) - T_{pn,c}(t)) + (R_{pn} + R_L)^2 \alpha_{pn} I(t) T_{pn,h}(t) - \frac{1}{2}(R_{pn} + R_L)^2 I^2(t) R_{pn}} \tag{27}$$

$$\eta_{max}(t) = \frac{P_{max}(t)}{Q_h(t)}$$

$$= \frac{\alpha_{pn}^2 (T_{pn,h}(t) - T_{pn,c}(t))^2}{4R_{pn}K_{pn}(T_{pn,h}(t) - T_{pn,c}(t)) + 4R_{pn}\alpha_{pn}I(t)T_{pn,h}(t) - 2R_{pn}I^2(t)R_{pn}}$$

$$(28)$$

2.3. Implementation in TRNSYS environment

The TRNSYS software package has been used extensively for thermal system analysis. It has a modular structure and consists of individual subroutines that represent real physical devices or utility components. The components can be connected together to form complex systems.

TRNSYS uses a modular approach to solve thermal energy systems. Basically, it is an equation-solving program based on standard numerical techniques, which provides different subroutines to find analytical solution to the set of equations. However, only a first-order linear differential equation solver is provided. Therefore, a subroutine for solving nonlinear differential equations of Section 2.2 using the finite difference and the Newton–Raphson methods is programmed in Fortran.

Fig. 2 shows the TRNSYS project created to simulate the TEG model. To do so the following input connections has to be established:

- The applied heating rate Q_{in}, obtained from heater specifications.
- The cooling fluid temperature, extracted from experimental data measurements.
- The load resistance R_L, which is used to calculate the output data when specific resistance is connected between positive and negative connections. It may be assigned or leave as default if no load is considered.
- Simulation time step size, which is selected based on the required accuracy of the output data. It also affects to the required computational time.

Additionally, the geometric data and the material properties of the elements of the thermoelectric system studied have to be included into the TEG model as TRNSYS parameter data. All these parameters can be shown in Tables 1 and 2.

After the simulation, the output values obtained from Eqs. (20)–(28) are shown through built-in online plotter.

3. Experimental setup

To compare simulated results with experimental data, the simulation must have the same operating conditions as the experiment. The validation of the TRNSYS Type developed in this study uses experimental data from an especially designed equipment to perform this test. The experimental setup allows establishing parameters required for the simulation of the performance of the TEG, such thermal and electrical transients of different magnitudes.

Fig. 3 shows the schematic of the experiment with a TEG on top of a heat source. The source temperatures, T_1 and T_h, are measured by two K-type thermocouples with diameter of 2 mm placed, as shown in Fig. 1, underneath the TEG and ceramic substrate, respectively. The thermocouple is sealed by conductive thermal compound to assure uniform heat distribution on the TEG hot surface. A water-cooled block cools the top surface of the TEG through a pumped liquid cooling loop consisting of a pump, a heat exchanger and liquid lines. The pump circulates the fluid in the loop, which picks up the heat in the cold plate and dissipates it through the heat exchanger. Two ceramic plates made of alumina (Al_2O_3) are sandwiching the thermo-elements. The temperatures of the top surface (cold side) of the TEG, T_2 and T_c, are also measured by two K-type thermocouples of 2 mm mounted above ceramic substrate and cold plate. The hot and cold plates are treated as heat spreaders to provide a uniform thermal field to both hot and cold sides of TEG module.

Initially, the system is at room temperature, measured as 16.17 °C, and the electrical heater is switched on at its first heating level of Q_{in} = 23.6 W (Case 1). During temperature increase, an external switch intermittently connects and disconnects an electrical load of 2.5 Ω (every 10 s). This allows us to obtain loaded and open-circuit outputs simultaneously. The transient temperatures at the hot and cold surfaces of the TEG, the output voltage and the output current are recorded simultaneously into a digital computer using a data acquisition system (National Instruments-cRIO). The data acquisition is set at a rate of 1 s for about 3500 s at which time the system attains the steady state. Once system reaches the
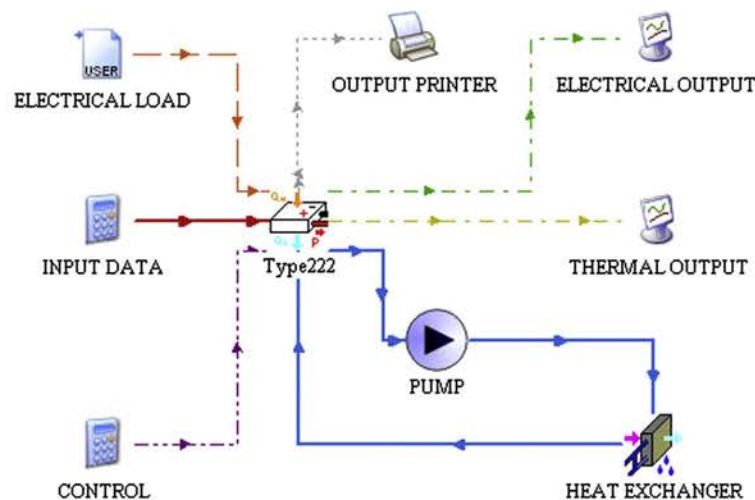

Fig. 2. TRNSYS project created for TEG system behaviour simulation.

Table 1
Thermoelectric parameters for three different cases.

Parameters	Case 1	Case 2	Case 3	Unit	Source
Q_{in}	23.60	33.50	53	W	Measured
T_{coo}	16.45	17.34	18.20	°C	Measured
R_L	2.5	2.5	2.5	Ω	Measured
α_n	163.546	167.273	171.659	µV/K	Manufacturer
α_p	−178.098	−188.726	−201.897	µV/K	Manufacturer
λ_n	1.510	1.453	1.415	W/m K	Manufacturer
λ_p	1.954	1.925	1.792	W/m K	Manufacturer
σ_n	10.896	12.001	13.767	µΩ m	Manufacturer
σ_p	11.196	13.100	15.910	µΩ m	Manufacturer

Table 2
Properties of materials used in TEG tests.

Parameters	Value	Unit	Source
n	98	–	Measured
e_n	2.54×10^{3}	m	Measured
e_p	2.54×10^{3}	m	Measured
e_{hp}	0.02	m	Measured
e_{tc1}	1×10^{4}	m	Measured
e_{ce}	2.54×10^{4}	m	Measured
e_{tc2}	1×10^{4}	m	Measured
e_{cp}	0.02	m	Measured
e_{cb}	0.002	m	Measured
A_n	2.3×10^{6}	m²	Measured
A_p	2.3×10^{6}	m²	Measured
A_{hp}	7.22×10^{3}	m²	Measured
A_{tc1}	8.41×10^{4}	m²	Measured
A_{ce}	8.41×10^{4}	m²	Measured
A_{tc2}	8.41×10^{4}	m²	Measured
A_{cp}	8.41×10^{4}	m²	Measured
A_{cb}	12.25×10^{4}	m²	Measured
λ_{hp}	180	W/m K	Estimated
λ_{tc1}	2.5	W/m K	Manufacturer
λ_{ce}	36	W/m K	[13]
λ_{tc2}	2.5	W/m K	Manufacturer
λ_{cp}	180	W/m K	Estimated
λ_{cb}	380	W/m K	Estimated
ρ_n	7700	kg/m³	[18]
ρ_p	7700	kg/m³	[18]
ρ_{hp}	2700	kg/m³	Estimated
ρ_{tc1}	2040	kg/m³	Manufacturer
ρ_{ce}	3975	kg/m³	[13]
ρ_{tc2}	2040	kg/m³	Manufacturer
ρ_{cp}	2700	kg/m³	Estimated
ρ_{cb}	8930	kg/m³	Estimated
S_n	200	J/kg K	[18]
S_p	200	J/kg K	[18]
S_{hp}	883	J/kg K	Estimated
S_{tc1}	200	J/kg K	Manufacturer
S_{ce}	765	J/kg K	[13]
S_{tc2}	200	J/kg K	Manufacturer
S_{cp}	883	J/kgK	Estimated
S_{cb}	385	J/kg K	Estimated
h_{cb}	23781	W/m² K	Manufacturer

steady state, the output voltage and current are recorded simultaneously while load resistance varied from 0 Ω to 100 Ω. Table 1 shows the initial values of the test conducted. The experiment is repeated for two additional hot side heat fluxes Q_{in} of 33.5 W (Case 2) and 53 W (Case 3) in order to assess the model at three different temperature gradients.

To assess the TEG behaviour, several thermoelectric properties should be tabulated as a reference. The parameters are determined either according to direct measurement, from manufacturer's data or from the existing literature [12,18]. The geometric parameters and properties of hot and cold plates and water-cooling block are estimated considering that materials used are aluminium and cooper, respectively. Tables 1 and 2 show the properties of materials used in the experimental setup.

In Table 1, the Seebeck coefficient, thermal conductivity and electrical resistivity of the p- and n-type elements are listed at steady-state average temperatures of $\overline{T} = (T_h + T_c)/2$, which are extracted from experimental data. All these three parameters are obtained from manufacturer's datasheet.

Experiments are conducted under following conditions: the temperature of cooling fluid stays between 16.45 °C and 18.20 °C, the air temperature is 16.17 °C and the flow rate of the cooling fluid is 72 l/h.

4. Results and discussion

Based on transient and steady state experiments and TRNSYS simulations, the results and a discussion about their comparison is presented in this section.

4.1. Effects of step changes of supplied heat flow rates

The dynamic response characteristics of temperature difference between hot and cold sides $\Delta T = T_h - T_c$, hot side inlet heat flux Q_h, electric output power P_{RL} and closed-circuit voltage V_{RL} with step changes of supplied heat flow rate Q_{in} are described in Fig. 4. Both the transitory experimental and simulation results are plotted versus the transient time in the same plot. The conditions imposed in the experiment are listed in Table 1.

During the transient, the temperature difference across the TEG device increased until the steady state is achieved. It can be observed that the electric output characteristic is mostly dependent on the temperature difference. The hot side temperature T_h achieved is 99 °C, 140 °C and 216 °C for cases 1, 2 and 3, respectively. Accordingly to experimental data obtained and Eqs. (20)–(28), the higher the temperature difference across the TEG is, the more electrical power generated and the greater output system performance becomes.

4.2. Effects of step changes of load current at constant supplied heat flux

In Fig. 5, the step changes effects of load current under conditions of Table 1 can be observed. The system has been brought to steady-state temperatures of Fig. 4(a). It is very interesting to note the effect that the load current has on the temperature gradient across the device, which is the same obtained in Ref. [15]. The load currents imposed for cases 1–3 are 0.49 A, 0.71 A and 1.01 A, respectively.

Every increase in I leads to a decrease in temperature difference ΔT due to the greater value of the Peltier term of Eqs. (8) and (9). This current increase also produces an increment of hot and cold side heat fluxes. However, as explained in Section 2.2, the maximum output power and efficiency happens only when load resistance is matched with internal resistance.

As it can be appreciated from Fig. 5, the simulation results show good agreement with the experimental results, accurately tracking the electro-thermal coupled effects occurring in the TEG system. The plotted curves of T_h and T_c show that steady-state are not achieved with step changes of 10 s. It also can be shown that parameter variations with load current increase with higher values of supplied heat flux. The low accuracy observed in Fig. 5(c) and (d) may be caused by convection heat losses on hot and cold plates.

4.3. Effects of load resistance variation at steady-state

The variation of performance at steady-state with load resistance is shown in Fig. 6. Three different conditions corresponding
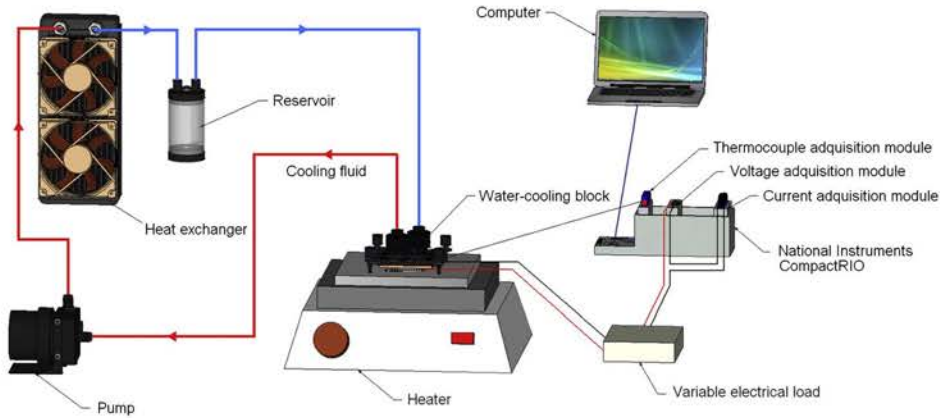
Fig. 3. Experimental test scheme.
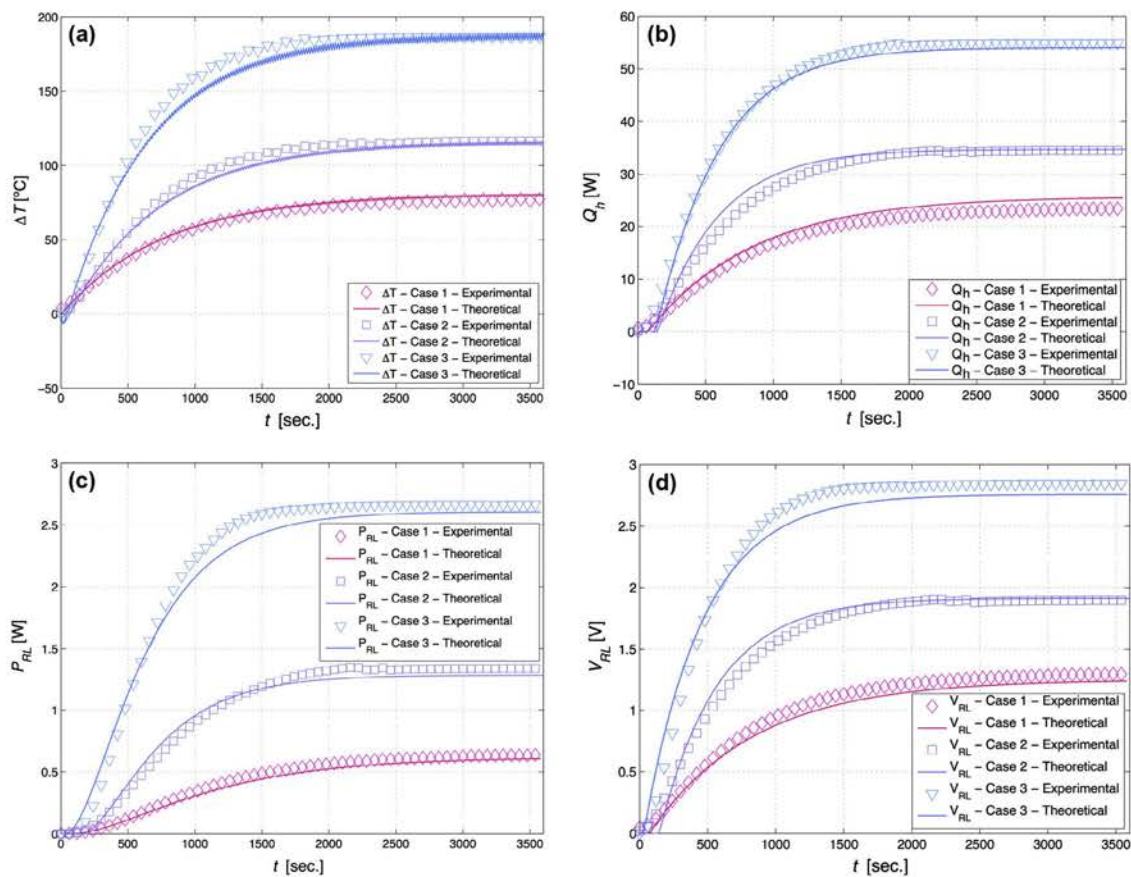
Fig. 4. Correlation of experimental and simulated behaviours of the TEG system under step changes of heat flow rates. (a) Temperature difference between hot and cold sides $\Delta T = T_h - T_c$. (b) Hot side inlet heat flux. (c) Electric output power. (d) Closed-circuit voltage.

to described cases in Table 1 are selected. The system has been brought to the same steady-state temperatures of Fig. 4(a).

Fig. 6 demonstrates that the electrical output is strongly coupled to both the thermal behaviour and the load resistor value.

The electric load resistance that produces the maximum electrical power varies with the supplied heat flux. The power generation and system efficiency are the highest when the load resistance value is close to the internal resistance $R_L = R_{pn}$, which is measured

       E. Massaguer et al./Applied Energy 134 (2014) 65–74
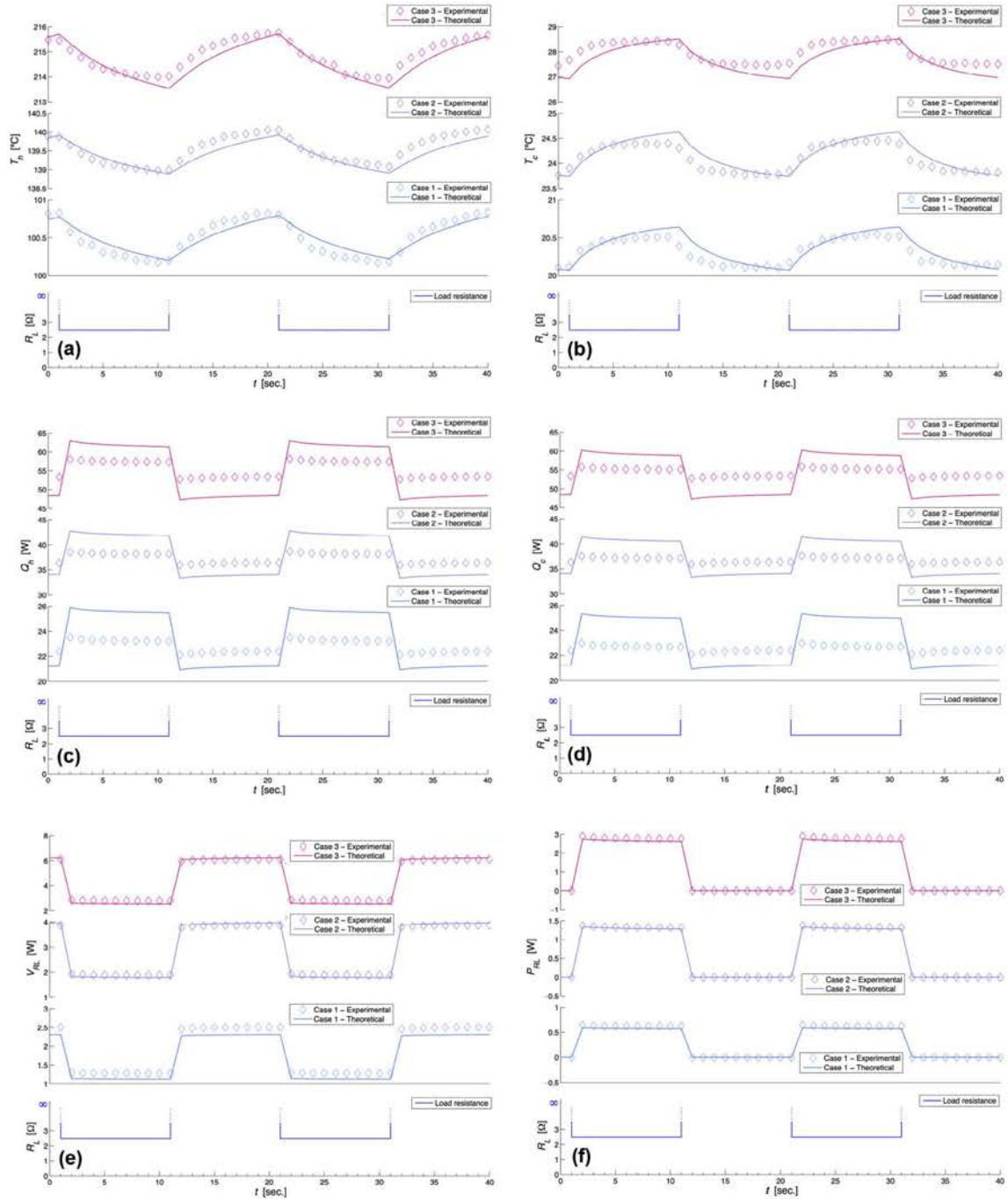
Fig. 5. Correlation of experimental and simulated behaviours of the TEG system under step changes of load current. (a) Hot side temperature. (b) Cold side temperature. (c) Hot side heat flux. (d) Cold side heat flux. (e) Closed-circuit voltage. (f) Electric output power.

to be about 2.5 Ω. As can be shown in Fig. 6(d), the generated power increases to a maximum but then decreases to reach a steady state. The electrical resistances at maximum power points are 2.4 Ω (0.65 W), 2.45 Ω (1.28 W) and 2.9 Ω (2.6 W) for cases

1–3, respectively. Those effects can be observed in the theoretical model as well.

Besides, in Fig. 6(f)–(h) it can be observed that both the hot and cold sides heat fluxes, Q_h and Q_c, decrease with resistance until

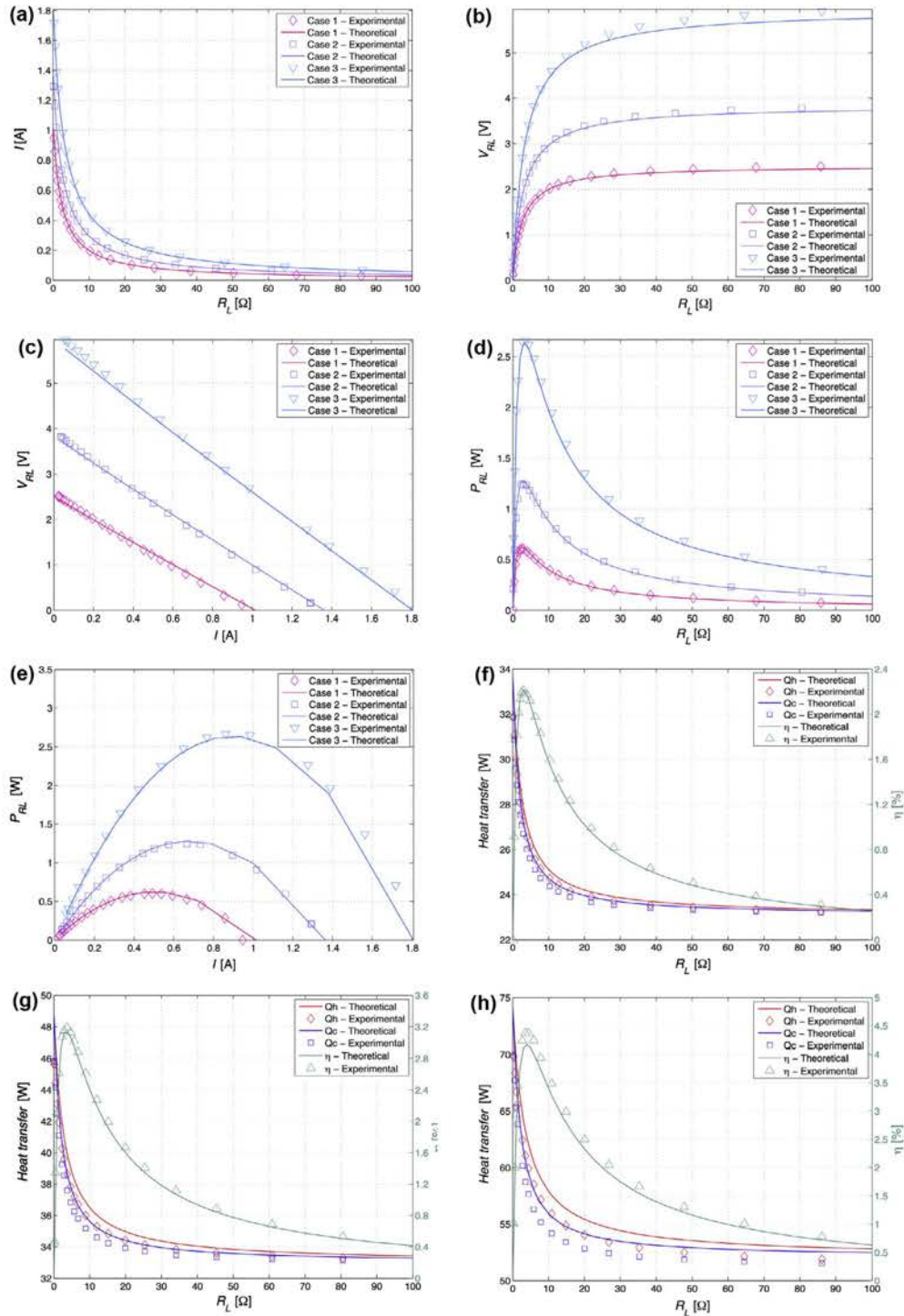**Fig. 6.** Correlation of experimental and simulated behaviours of the TEG system under different load resistances. (a) Load current. (b) Closed-circuit voltage. (c) Closed-circuit voltage versus load current. (d) Electric output power. (e) Electric power generated versus load current. (f)–(h) Hot and cold side heat fluxes and system efficiency.

steady state is achieved. It demonstrates that when load resistance R_L increase, the load current I falls to minimum, which reduces the Joule and Peltier effect of the Eqs. (25) and (26). Consequently, when load current is very low, those effects are despicable and it is only the Fourier's law that governs the heat transfer equation.

4.4. Model uncertainty

The TEG model developed in this work is validated by comparing the experimental data with the numerical data predicted by our model at the same conditions. The calculus of the error is performed by the comparison of the temperature difference and the electrical output power of each point predicted by the model with the same point measured experimentally. The value of RMSE is 4.85 °C and 0.0648 W for temperature difference and electrical output power, respectively. The model presents a normalized root mean square error of 3.53% and 2.33% for temperature difference and electrical output power, respectively.

Although the model presented has slightly higher temperature difference RMSE and NRMSE than the model developed by Montecucco [15] (3.58 °C and 2.76%, respectively), the output power prediction is significantly better (0.2 W and 4.55%, respectively). It is important to note that the model accuracy is markedly affected by the thermoelectric parameters introduced into the simulation model. Consequently, the more exact the thermoelectric parameters are, the more precise the outputs will be.

5. Conclusions

Although thermoelectric phenomena have been used for heating and cooling applications quite extensively, electricity generation has only seen very limited market in niche applications and it is only in recent years that interest has increased regarding new applications of energy generation through thermoelectric harvesting. The widespread use of TEGs depends on its optimization.

The TRNSYS component presented in this paper has been developed for this purpose and is described and validated using experimental data. The proposed component is able to cope with thermal and electrical dynamics. The comparison of results between theoretic analysis and experiment has approved the reasonability of the new component.

On the other hand, the TRNSYS simulation runs without interruptions or delays, therefore the numerical model, and consequently the new component, can be considered well optimized. Therefore, this system model can be used in performance optimization and further application of thermoelectric generation.

References

[1] Riffat SB, Ma X. Thermoelectrics: a review of present and potential applications. Appl Therm Eng 2003;23:913–35.
[2] Omer SA, Infield DG. Design and thermal analysis of two stage solar concentrator for combined heat and thermoelectric power generation. Energy Convers Manage 2000;41:737–56.
[3] Risse S, Zellbeck H. Close-coupled exhaust gas energy recovery in a gasoline engine. Res Therm Manage 2013;74:54–61.
[4] Wang Y, Dai C, Wang S. Theoretical analysis of a thermoelectric generator using exhaust gas of vehicles as heat source. Appl Energy 2013;112:1171–80.
[5] Weng Chien-Chou, Huang Mei-Jiau. A simulation study of automotive waste heat recovery using a thermoelectric power generator. Int J Therm Sci 2013;71:302–9.
[6] Champier D, Bédécarrats J, Kousksou T, Rivaletto M, Strub F, Pignolet P. Study of a TE (thermoelectric) generator incorporated in a multifunction wood stove. Energy 2011;36:1518–26.
[7] Venkatasubramanian R, Siivola E, Colpitts T, O'Quinn B. Thin-film thermoelectric devices with high room-temperature figures of merit. Nature 2001;413:597–602.
[8] Boukai AI, Bunimovich Y, Tahir-Kheli J, et al. Silicon nanowires as efficient thermoelectric materials. Nature 2008;451:168–71.
[9] Hsiao YY, Chang WC, Chen SL. A mathematic model of thermoelectric module with applications on waste heat recovery from automobile engine. Energy 2010;35:1447–54.
[10] Chen L et al. Effect of heat transfer on the performance of thermoelectric generators. Int J Therm Sci 2002;41:95–9.
[11] Ebling D et al. Multiphysics simulation of thermoelectric systems for comparison with experimental device performance. J Electron Mater 2009;38(7):1456–61.
[12] Gou X, Yang S, Xiao H, Ou Q. A dynamic model for thermoelectric generator applied in waste heat recovery. Energy 2013;52:201–9.
[13] Montecucco A, Buckle JR, Knox AR. Solution to the 1-D unsteady heat conduction equation with internal Joule heat generation for thermoelectric devices. Appl Therm Eng 2012;35:177–84.
[14] Nguyen NQ, Pochiraju KV. Behaviour of thermoelectric generators exposed to transient heat sources. Appl Therm Eng 2013;51:1–9.
[15] Montecucco A, Knox AR. Accurate simulation of thermoelectric power generating systems. Appl Energy 2014;118:166–72.
[16] Meng FK, Chen LG, Sun FR. A numerical model and comparative investigation of a thermoelectric generator with multi-irreversibilities. Energy 2011;36:3513–22.
[17] Klein SA et al. TRNSYS 16: A Transient System Simulation Program. USA: University of Wisconsin; 2006.
[18] Cheng CH, Huang SY, Cheng TC. A three-dimensional theoretical model for predicting transient thermal behavior of thermoelectric coolers. Int J Heat Mass Transf 2010;53:2001–11.
[19] Rodríguez A, Vián JG, Astrain D, Martínez A. Study of thermoelectric systems applied to electric power generation. Energy Convers Manage 2009;50:1236–43.
[20] Kim S. Analysis and modeling of effective temperature differences and electrical parameters of thermoelectric generators. Appl Energy 2013;102:1458–63.
[21] Gou X, Xiao H, Yang S. Modeling, experimental study and optimization on low-temperature waste heat thermoelectric generator system. Appl Energy 2010;87:3131–6.

Appendix B

Published paper: Modelling analysis of longitudinal thermoelectric energy harvester in low temperature waste heat recovery applications

ELSEVIER

AppliedEnergy

Modeling analysis of longitudinal thermoelectric energy harvester in low temperature waste heat recovery applications

CrossMark

Eduard Massaguer *, Albert Massaguer, Lino Montoro, J.R. Gonzalez

Department of Mechanical Engineering and Industrial Construction, University of Girona, C. de Maria Aurèlia Capmany, 61, 17071 Girona, Spain

HIGHLIGHTS

- A new LTEH model is proposed and validated under transient and steady-state conditions.
- The thermoelectric energy harvester model is developed in TRNSYS.
- Comparison of simulation and experimental results shows great accuracy.
- The new TRNSYS component can be used as a design tool.

ARTICLE INFO

ABSTRACT

The worldwide interest in thermoelectric waste heat recovery is constantly growing, with a wide range of applications ranging from small harvesters integrated into wireless sensor networks all the way to larger harvesters such as the ones that can potentially be integrated into cars. The wide range of applications makes a requirement for studying the dynamic response of TEGs. The aim of this work is to develop a mathematical model to accurately simulate the thermal and electrical behaviours of a longitudinal thermoelectric energy harvester (LTEH). In order to implement the theoretical analysis, a new TRNSYS component has been developed so this new model can also be used as a design tool.

The LTEH model presented in this paper is validated through the comparison of results between theoretical analysis and experimental data. Testing results and discussion show the reasonability of this new model and also their use as a simulation tool.

© 2014 Elsevier Ltd. All rights reserved.

1. Introduction

Energy recovery techniques have become significantly demanding since it makes an important contribution towards reducing the greenhouse gases which cause global warming. Energy recovery includes any technique or method that converts waste energy (i.e. thermal, chemical or mechanical energy) into another kind of energy which can be reused for other energy purposes (i.e. electrical energy).

Research activities in energy recovery from waste heat using thermoelectric effect have considerably increased since the 1990s. There are recently reported researches such as thermoelectric power generation from CPU waste heat [1], Si–Ge based TEGs applied to gasoline engine vehicles [2], bismuth telluride based TEGs applied to automotive exhaust systems (AETEG) [3,4],

thermoelectric power generation systems applied to generate electricity from municipal waste heat [5], a thermoelectric power generator using solar heating [6] and so on.

At the same time, many mathematical models and approaches for simulating a heat exchanger that utilizes thermoelectric modules for power generation has been designed. The majority of these models apply general heat transfer techniques in cohesion with thermoelectric module equations for a system level analysis.

Bohn developed one of the earliest models in 1981 [7]. It is an extension of the effectiveness-number of transfer units (ε-NTU) method for heat exchanger analysis. The model implements thermoelectric generator equations into the common ε-NTU equations by setting up a dimensionless ratio of actual power generated to the maximum possible power generation. An example case is provided for a parallel flow configuration with promising results; however, there is no experimental testing to validate the model. The Esarte et al. model [8] also uses ε-NTU method to simplify calculations. They set up an energy balance with a hot and cold side heat exchanger with a thermoelectric module in between

* Corresponding author. Tel.: +34 972 418 489; fax: +34 972 418 098.
  E-mail address: eduard.massaguer@udg.edu (E. Massaguer).

185

Nomenclature

Abbreviation		np	number of TEGs in parallel
TEG	thermoelectric generator	ns	number of TEGs in series
LTEH	longitudinal thermoelectric energy harvester	t	time (s)

Symbols		*Subscript*	
N	number of thermocouples	hh	hot side heat exchanger
α	Seebeck coefficient (V/K)	$tc1,2,3$	thermal compound
σ	electrical resistivity (Ωm)	ce	ceramic substrate
e	length (m)	ch	cold side heat exchanger
A	cross sectional area (m^2)	cl	copper lid
ρ	material density (kg(m^3))	H	hot side
S	specific heat capacity (J/kg K)	C	cold side
λ	thermal conductivity (W/m K)	p	p-type semiconductor
$\dot{m}$	mass flow rate (kg/h)	n	n-type semiconductor
h	convective heat transfer coefficient (W/m^2 K)	in	input
Q	heat rate (W)	out	output
V	electric voltage (V)	L	load resistance
I	electric current (A)	amb	ambient air
P	electric power (W)	AVG	average
η	efficiency (%)	i	stage number
R	electric resistance (Ω)	j	row number
T	temperature (K)	f	fluid
y	axis coordinate (m)	k	iteration number

and studied the influence of fluid flow rate, heat exchanger geometry, fluid properties and inlet temperatures on the power supplied by the thermoelectric generator. The Work could provide some guidelines for determining the optimum operating parameters of thermoelectric generator, however, limited experimental results are provided. Crane and Jackson investigated thermoelectric waste heat recovery with regards to cross flow heat exchangers [9,10]. A cross flow heat exchanger model was validated against measured performance of advanced cross flow heat exchangers without thermoelectrics. The numerical simulations were compared to experimental data with good agreement between them. Yu and Zhao [11] developed a numerical model for prediction of performance
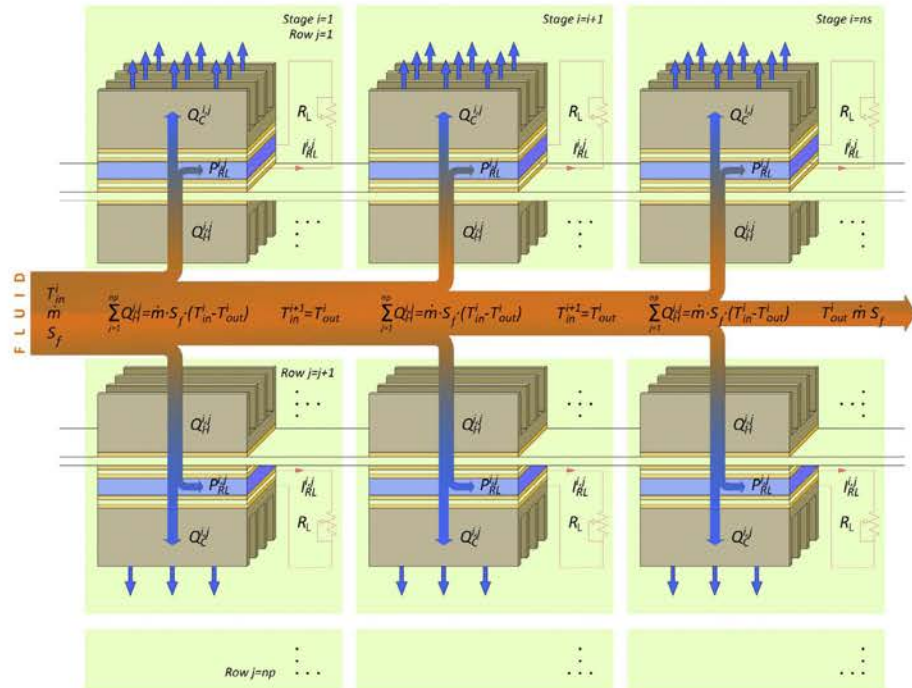
Fig. 1. Heat transfer model of longitudinal thermoelectric energy harvester LTEH.

137

of a thermoelectric generator with a parallel-plate heat exchanger. They assumed that the flat thermoelectric modules were held tightly between hot and cold fluids, which had multiple thermocouples with a single layer of P-type and N-type semiconductors. The thermocouples along the fluid path were connected electrically in series. A typical energy balance was used to set up the model with the differential equations discretized along the axial direction of the hot fluid. The solution to the numerical model was provided using an iterative method. Simulations were performed to study the effects of the various parameters. An experimental study based on the Yu and Zhao model [11] was performed by Niu, Yu and Wang [12]. A comparison of the experimental results with the numerical model is presented in this work. A two fluid, multi-plate, multi-pass, counter/parallel flow heat exchanger with thermoelectric generators was created for the experimental phase. The data obtained through experimentation shows that the numerical model over predicts performances of the TEGs over the entire range of data. At lower temperatures, the model displays better agreement with experimental results, but as hot fluid inlet temperatures are increased, the prediction diverges from the measured values. The discrepancy is associated to the lack of accounting for heat losses and the fact that the thermoelectric properties are treated as constants.

Wu [13] performed a theoretical analysis on waste-heat thermoelectric power generators. In this study, a real waste-heat thermoelectric generator model was presented based on accounting for both internal and external irreversibility to predict realistic specific power and efficiency. Therefore, this approach gave a much more realistic generator specific power and efficiency prediction than does the ideal thermoelectric generator. Hsiao et al. [14] constructed a mathematical simulation model, based on the testing results of a TEG module, to predict the performance of a waste heat recovery system. They provided a scientific methodology with complicated equations on the field of thermoelectric simulations. Finally, Wang et al. [15] presented a mathematical model of a TEG device using the exhaust gas of vehicles as heat source. The model simulates the impact of relevant factors, including vehicles exhaust mass flow rate, temperature and mass flow rate of different types of cooling fluid, convection heat transfer coefficient, height of PN couple, the ratio of external resistance to internal resistance of the circuit on the output power and efficiency. However, just a few experimental results are provided. Recently, Montecucco et al. [16] have studied the impact of thermal imbalance on the power produced at module and system level in a TEG array. Experimental results in series–parallel

Fig. 2. One dimensional heat transfer model of a single TEG module.

Fig. 3. Block diagram representation of LTEH model.

configurations clearly illustrate the issue and a theoretical model was presented to quantify the impact.

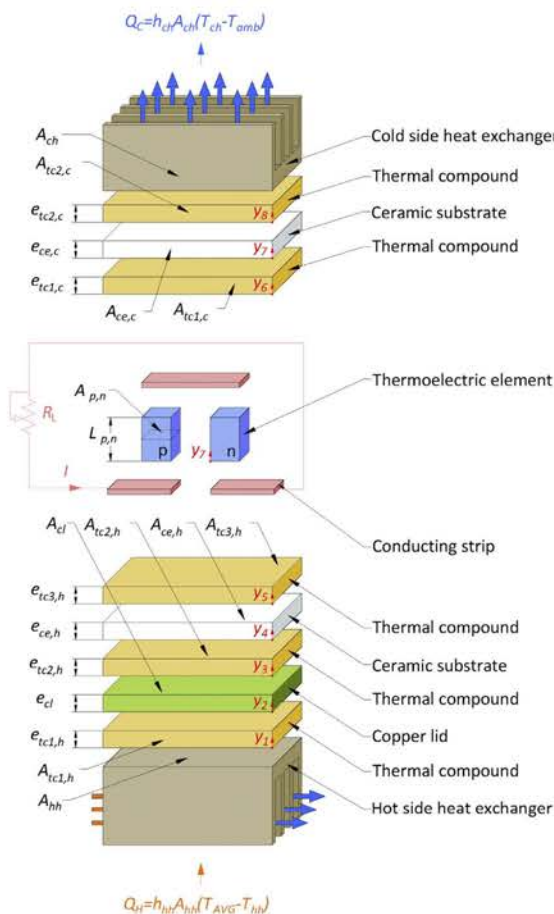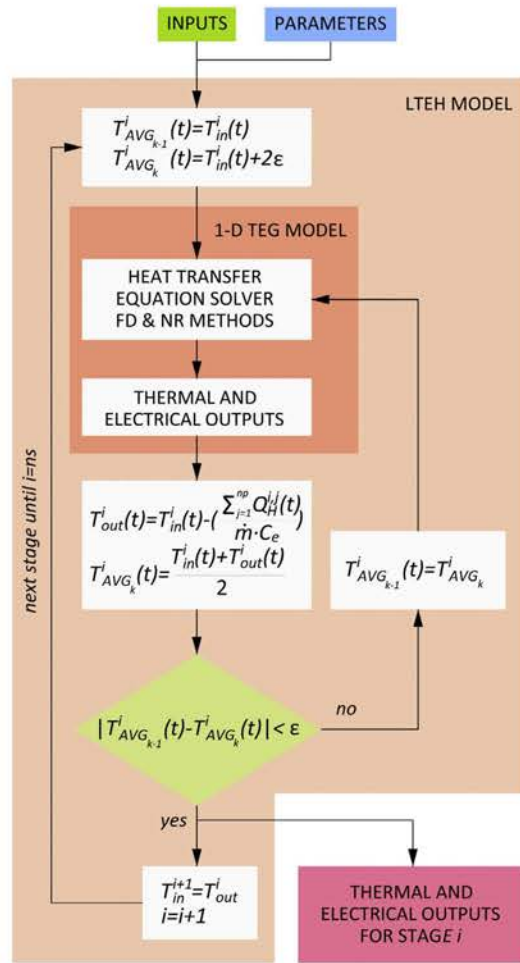In the above literatures, those research works have mainly been focused on the analytical analysis to a single or multiple thermoelectric elements for thermoelectric energy harvesting from gas exhaust waste heat. These analytical methods provided some significant guidelines for the design of the thermoelectric energy harvesters in terms of the principle of thermodynamics. However, aforesaid models are only validated for stand-alone applications without taking into account the electrical and thermal effects of TEG array configuration. A real thermoelectric energy harvester always comprises multiple thermoelectric modules placed with respect to the flow direction, and depending on the shape and the electrical output requirements of the harvester, TEGs can be wired in series/parallel configuration. Although series/parallel configuration has not been taken into account in this paper, it will be considered in future work. Moreover, there is no model in literature that uses liquid (e.g. water) as a heat source.

Thereafter, the objective of this work is to develop a new computational model capable to simulate the electro-thermal dynamics of a thermoelectric energy harvesting system. The new model incorporates to the 1D mathematical model developed in Ref. [17] the longitudinal thermal phenomena occurring in real LTEH systems. The model treats TEG modules as a whole block and takes into account the fluid heat and temperature reduction across the system due to thermoelectric energy harvesting. Following the base model [17], the new component is fully analysed and validated under steady and transient states with data obtained from the experimental setup and it is also created in TRNSYS.

2. Model description

A thermoelectric energy harvester is a device that converts some of the waste heat of an element (i.e. liquid or gas) into electricity using the Seebeck effect. Although many different topologies and shapes have been studied in literature (e.g. longitudinal,

transverse, hexagonal, circular, etc.) the longitudinal and rectangular box-like shape design is termed as the baseline model [18]. Consequently, this is the type of the thermoelectric harvester assessed in this paper. The name of the models – longitudinal and transverse – are derived from the way the TEGs are placed with respect to the fluid flow direction.

The LTEH follows the basic scheme shown in Fig. 1. It consists of four main elements:

- Hot-side heat exchanger used to capture and increment the heat extraction from the heat source to the TEG modules. It is directly exposed to the hot fluid.
- Cold-side heat exchanger to remove and transfer excess heat from outer side of the TEG modules to the ambient air.
- Multiple thermoelectric modules that convert the waste heat into useful electrical energy. The optimal number and configuration of TEG modules must be considered.
- Compression assembly system comprising a top and bottom lid, a support element that permits attachment of the lids and a sealing rubber.

TEGs are mounted along the exterior surfaces of the lids. The heat flows from hot side to cold side heat exchanger and through the TEG. The temperature difference between hot and cold sides of the TEG generates voltage and current by Seebeck effect. The thermoelectric generation also produces a heat extraction from fluid, resulting in a fluid temperature reduction at every stage. Consequently, both the fluid temperature and the electric power generation will be reduced as we incorporate new stages: $T_{in}^i > T_{in}^{i+1}$ and $P_{RL}^{i,j} > P_{RL}^{i+1,j}$, respectively. This effect is considered within the new model.

As can be seen in Fig. 2, a thermoelectric module is sandwiched between hot side and cold side heat exchanger that can be treated as a convective heat transfer system. The TEG consists of certain number of semiconductors, corresponding solder layers, conducting strips and thermal insulation material. In order to electrically
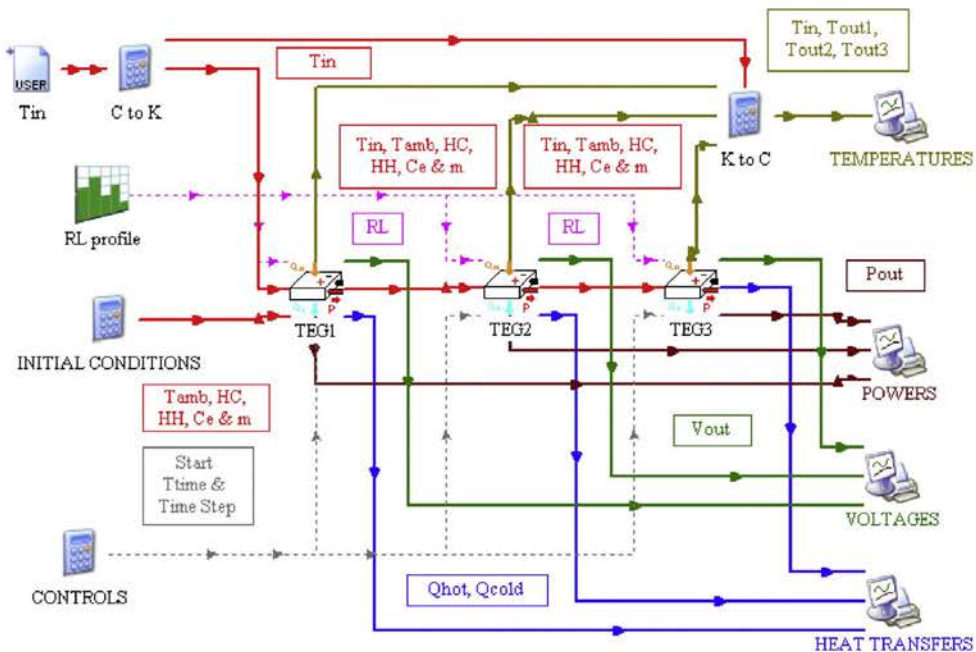

Fig. 4. TRNSYS project created for LTEH system behaviour simulation. The connection parameters are indicated within boxes.

isolate the module, a ceramic substrate made of alumina (Al_2O_3) is located both sides of the TEG. Moreover, a thermal compound increases the thermal conductivity of the interfaces by filling microscopic air–gaps between ceramic substrates and heat exchangers and also between TEG and ceramic substrate.

As already explained in Section 1, the new model developed in this paper is based on Massaguer et al. model [17]. It solves the system of equations using finite difference and Newton–Raphson methods and calculates the temperature at different nodes separated in space by a discrete distance. In the transient state, the temperatures of these points are calculated at discrete periods of time and the temperatures for all nodes are recalculated at the end of this time interval. Using the implicit finite difference method, the values of heat flux can be determined using the values of the temperatures of the time step before. Therefore, the unsteady-state heat transfer model solves the TEG temperature distribution first and then determines the TEG power and performance outputs.

However, the solution to the heat equations assumes one-dimensional heat transfer and treats the TEG module as a whole block (i.e. it considers the TEG as a real complete module). In order to obtain an accurately LTEH model, heat losses on the flow direction must be taken into account. Therefore, the longitudinal dimension must be attached to the Ref. [17] model. The fluid energy losses per stage due to the thermoelectric generation can be expressed as

$$\sum_{j=1}^{np} Q_H^{i,j}(t) \tag{1}$$

where i is the number of stage, j is the number of row, np is the number of parallel TEG modules placed in the same stage and Q_H is the heat extracted from the fluid and absorbed by a TEG module because of the thermoelectric generation. Q_H can be obtained applying convective heat transfer equations between fluid and hot side heat exchanger

$$Q_H^{i,j}(t) = h_{hh}^{i,j} \cdot A_{hh}^{i,j} \cdot (T_{AVG}^i(t) - T_{hh}^{i,j}(t)) \tag{2}$$

where h_{hh}, A_{hh} and T_{hh} are coefficients of convective heat transfer, cross sectional area and temperature of hot side heat exchanger, respectively. T_{AVG}^i is the average fluid temperature on hot side heat exchanger and it is the value used to solve the one-dimensional temperature distribution on each TE module, expressed as

$$T_{AVG}^i(t) = \frac{T_{in}^i(t) + T_{out}^i(t)}{2} \tag{3}$$

where T_{in}^i and T_{out}^i are the fluid inlet and outlet temperature on stage i, respectively. Note that T_{AVG}^i is common for all rows j of a stage i.

Considering only heat losses due thermoelectric effect, the heat extracted from fluid in every stage can be found using next equation

$$\sum_{j=1}^{np} Q_H^{i,j}(t) = \dot{m} \cdot S_f \cdot (T_{in}^i(t) - T_{out}^i(t)) \tag{4}$$

Consequently, T_{out}^i can be obtained from

$$T_{out}^i(t) = T_{in}^i(t) - \left(\frac{\sum_{j=1}^{np} Q_H^{i,j}(t)}{\dot{m} \cdot S_f} \right) \tag{5}$$

where $\dot{m}$ is the fluid mass flow rate and S_f is the fluid specific heat, both considered temperature independent.

Due to the fact that $Q_H^{i,j}$, T_{AVG}^i and T_{out}^i are reciprocally dependant, the only way to obtain an accurate solution is using an iterative method. The solution adopted consists of an iteration loop that runs Massaguer et al. model coupled with above equations until T_{AVG}^i converges. The convergence will be achieved when

$$\left| T_{AVG_{k-1}}^i - T_{AVG_k}^i \right| < \varepsilon \tag{6}$$

where k is the iteration number and ε is the tolerance value set up to $\varepsilon = 1e^{-4}\,°C$. It must be noted that T_{AVG}^i is strictly necessary to obtain an accurate temperature distribution and, consequently, the electrical outputs on each module.

Once convergence has been attained, the inlet fluid temperature next stage will be temperature outlet in the stage before $T_{in}^{i+1} = T_{out}^i$. Considering that the model solves consecutively the temperature distribution at each stage, T_{out}^i must be obtained before starting next stage. The same process is repeated until the last stage has been reached $i = ns$.

To better understand how the model is structured, the computer model block is described in Fig. 3.

Table 1
Thermoelectric parameters and material properties.

Parameters	Value	Unit	Source
T_{amb}	20:10	°C	Measured
Time step	1	s	Experiment
np	2	–	Experiment
ns	3	–	Experiment
$\dot{m}$	54	kg/h	Measured
S_f	4180	J/kg K	Estimated
α_n	$-141,587$	μV/K	Manufacturer
α_p	146,550	μV/K	Manufacturer
λ_n	1615	W/m K	Manufacturer
λ_p	1872	W/m K	Manufacturer
σ_n	9604	μΩm	Manufacturer
σ_p	8881	μΩm	Manufacturer
ρ_n	7700	kg/m^3	[17]
ρ_p	7700	kg/m^3	[17]
e_n	2.54×10^{-3}	m	Manufacturer
e_p	2.54×10^{-3}	m	Manufacturer
A_n	2.3×10^{-6}	m^2	Manufacturer
A_p	2.3×10^{-6}	m^2	Manufacturer
S_n	200	J/kg K	[17]
S_p	200	J/kg K	[17]
N	98	–	Manufacturer
$e_{tc1,2,3}$	1×10^{-4}	m	Measured
e_{cl}	2×10^{-3}	m	Measured
e_{ce}	2.54×10^{-4}	m	Measured
e_{hh}	2×10^{-3}	m	Measured
e_{ch}	2×10^{-3}	m	Measured
$A_{tc1,2,3}$	8.41×10^{-4}	m^2	Measured
A_{cl}	8.41×10^{-4}	m^2	Measured
A_{ce}	8.41×10^{-4}	m^2	Measured
A_{hh}	1.5×10^{-3}	m^2	Measured
A_{ch}	8.41×10^{-4}	m^2	Measured
$\lambda_{tc1,2,3}$	2:05	W/m K	Manufacturer
λ_{cl}	380	W/m K	Estimated
λ_{ce}	36	W/m K	[17]
λ_{hh}	210	W/m K	Estimated
λ_{ch}	210	W/m K	Estimated
$\rho_{tc1,2,3}$	2040	kg/m^3	Manufacturer
ρ_{cl}	8930	kg/m^3	Estimated
ρ_{ce}	3975	kg/m^3	[17]
ρ_{hh}	2700	kg/m^3	Estimated
ρ_{ch}	2700	kg/m^3	Estimated
$S_{tc1,2,3}$	200	J/kg K	Manufacturer
S_{cl}	385	J/kg K	Estimated
S_{ce}	765	J/kg K	[17]
S_{hh}	883	J/kg K	Estimated
S_{ch}	883	J/kg K	Estimated
h_{ch}	200	W/m^2 K	Manufacturer
h_{hh}	5000	W/m^2 K	Estimated
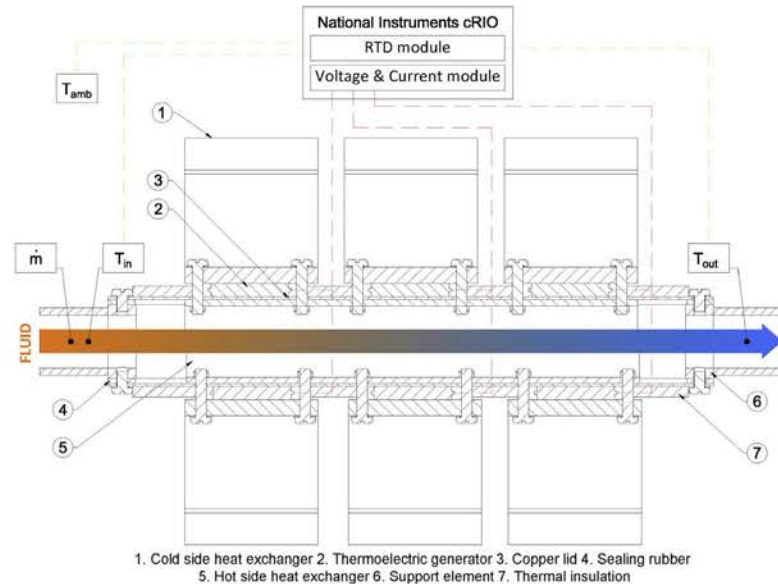
1. Cold side heat exchanger 2. Thermoelectric generator 3. Copper lid 4. Sealing rubber
5. Hot side heat exchanger 6. Support element 7. Thermal insulation

Fig. 5. Transversal section of the experimental LTEH with data acquisition modules.

1. Cold side heat exchanger 2. Thermoelectric generator 3. Copper lid 4. Sealing rubber
5. Hot side heat exchanger 6. Support element
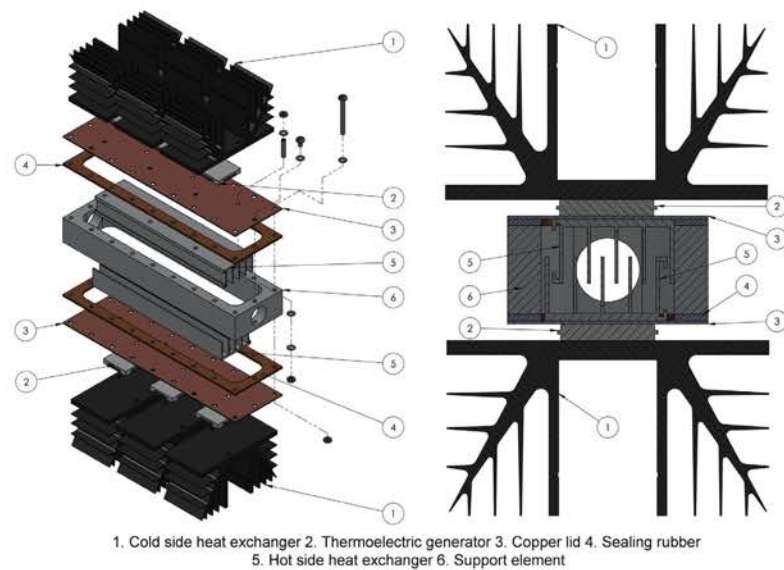
Fig. 6. Exploded and cross sectional view of the experimental setup.

Because of this new model is based on model presented in [17], the same assumptions have been inherited. On the other hand, new ones have been taken: thermal conductivity, electric conductivity and Seebeck coefficient of semiconductors are all assumed to be temperature-independent and adiabatic boundary conditions were supposed on the outside surfaces of TEG element; also thermal conductivity, electrical resistivity and specific heat capacities of non-thermoelectric materials are supposed constants within the operating temperature range; the heat leakage through solder layer and conducting strips are neglected and, finally, heat losses due to radiation and transverse convection through remaining area and lateral walls are also neglected. All TEGs are considered equal and connected to an individual load resistance of the same value. Therefore, series–parallel configuration effects explained in Ref. [16] have not taken into account. In future work these effects will be incorporated.

3. Computer model

The model presented in Section 2 was programmed in Fortran due to the fact that TRNSYS software was chosen to develop the

analysis. TRNSYS [19] is a flexible software tool used to simulate the performance of transient systems. At its heart, TRNSYS is a robust algebraic and differential equation solver that is able to read and process Fortran based components.

Each component is represented by a number of parameters and time-dependent inputs, and produces a number of time-dependent outputs. A given output of a specific component can be used as input to itself or to any number of other components. This is mainly how the system components can be interconnected.

The basic configuration for the LTEH dynamic study follows the general design illustrated in Fig. 4.

As it can be appreciated from Fig. 4, the TRNSYS project developed is composed of several components. The initial conditions block contains the ambient temperature, hot and cold side heat exchanger convective heat transfer coefficients and fluid specific heat and mass flow rate. Besides, the T_{in} and R_L components contain the temperature and load resistance profiles, respectively. Both T_{in} and R_L profiles are treated as system inputs and can be shown in Fig. 7. The three equal components called TEG1 to 3 correspond to the three stages that form the complete LTEH tested in Section 4. Each TEG component contains the thermal and electrical characteristics of a single row and the number of rows per stage.
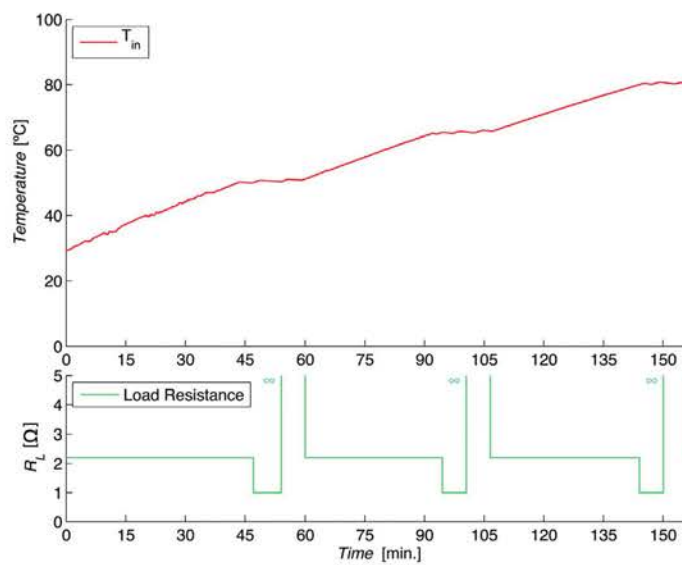
Fig. 7. T_{in} and R_L profiles.
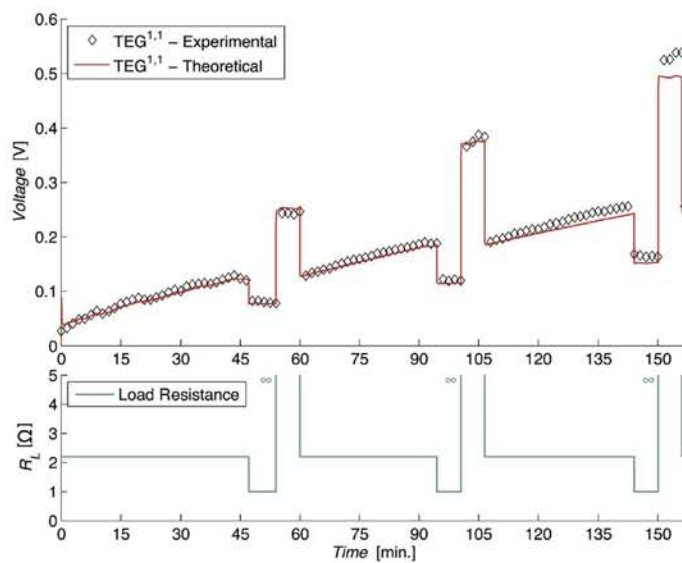
Fig. 8. Correlation of experimental and simulated output voltage of a TEG located in stage 1.

Control component allows selecting the start and finish simulation time and time step. Additionally, the geometric data and the material properties have to be included into the LTEH model as TRNSYS parameter data. All these parameters can be shown in Table 1.

4. Experimental setup

In order to validate the new LTEH model, an experimental setup has been build. This new equipment allowed us to obtain real data to be compared with simulation results. The experimental setup allows establishing thermal and electrical transients of different magnitudes.

Fig. 5 shows the schematic of the experiment. A closed loop water system was designed to supply hot water at different temperatures. The heat source is an electric accumulator that produces hot water up to 80 °C. A recirculating pump moves hot water through the water loop. It picks up the heat in the accumulator and exchanges it through the LTEH system. An ultrasonic flow meter was used to measure the fluid mass flow rate $\dot{m}$. The temperatures T_{in} and T_{out} were measured by two RTD sensors placed, as shown in Fig. 4, on the inlet and outlet of the LTEH system, respectively.

As can be seen in Fig. 6, the LTEH experimental setup is composed of six elements: two hot-side heat exchanger, six cold-side

Fig. 9. Correlation of experimental and simulated output voltage of a TEG located in stage 2.
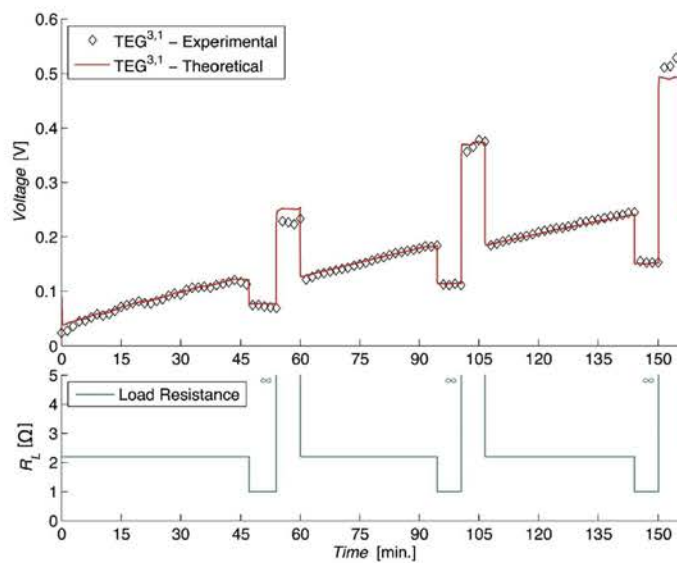
Fig. 10. Correlation of experimental and simulated output voltage of a TEG located in stage 3.

heat exchangers, six thermoelectric modules that convert the waste heat into useful electrical energy, a compression assembly system comprising a top and bottom lid, a support element that permits attachment of the lids and a sealing rubber. TEGs are mounted on the top and the bottom surface and arranged uniformly over the available surface. They are sandwiched between assembly system and cold side heat exchanger; therefore, the model can be treated as a natural convective heat transfer system. The remaining area and the lateral walls are thermally insulated to minimize heat leakage.

In order to validate the model under thermal and electrical dynamics, three temperature steps were established combining steady and transient states. Initially, the fluid temperature was 29.35 °C while the room temperature was measured as 20.10 °C. The mass flow rate of the fluid $\dot{m}$ was 54 kg/h. On the first step, the electrical accumulator was switched on and the pump started moving fluid through the water loop. While T_{in} started increasing, the R_L was set to 2.2 Ω. When temperature achieved 55 °C, T_{in} was maintained while load resistance changed to 1 Ω and to open circuit after. As can be shown in Fig. 7, the same process was repeated for two additional inlet temperatures T_{in} of 65 °C and 80 °C.

During experimental data acquisition, the transient temperatures at the inlet and outlet of the LTEH and the output voltage and current of each TEG were recorded simultaneously into a
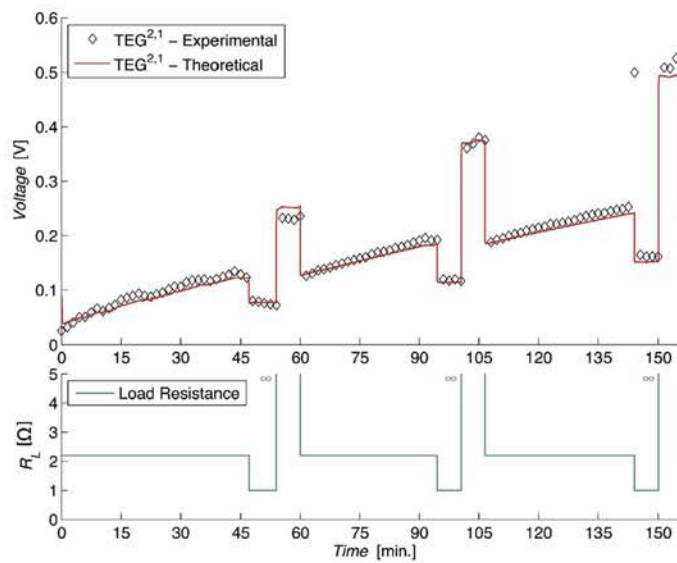

Fig. 11. Correlation of experimental and simulated output electrical power of a TEG located in stage 1.

Fig. 12. Correlation of experimental and simulated output electrical power of a TEG located in stage 2.

digital computer using a data acquisition system (National Instruments-cRIO). The data acquisition was set at a rate of 1 s for about 10,400 s.

Finally, the properties of materials used in the experiment are tabulated in Table 1. The parameters were determined either according to direct measurement, from manufacturer's data or from the existing literature [17]. The Seebeck coefficient, thermal conductivity and electrical resistivity of the p- and n-type elements are listed at steady-state average temperature of $\overline{T} = (T_{f,max} + T_{amb})/2$, which was 50.05 °C.

5. Results and discussion

Based on the transient and steady state experiments explained in Section 4 and TRNSYS simulations, the results and a discussion about their comparison are presented in this section. Due to the fact that TEGs placed in the same stage produce the same output values, only one TEG per stage have been presented. Both the transitory experimental and simulation results are plotted versus the transient time in the same plot. The conditions imposed in the experiment are listed in Table 1.

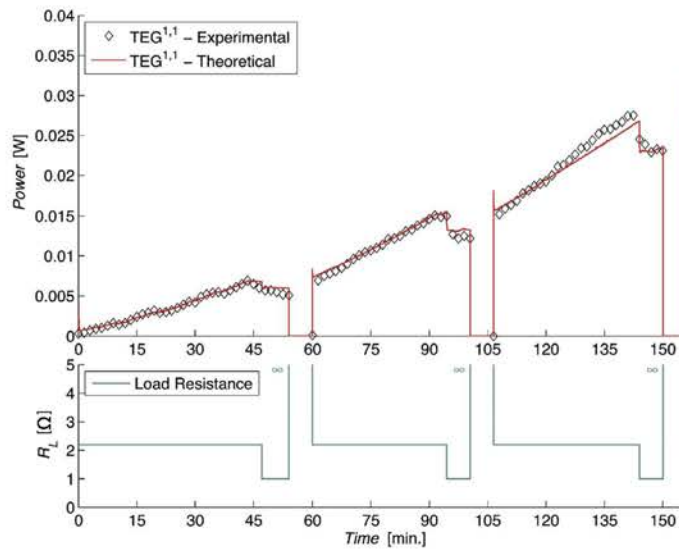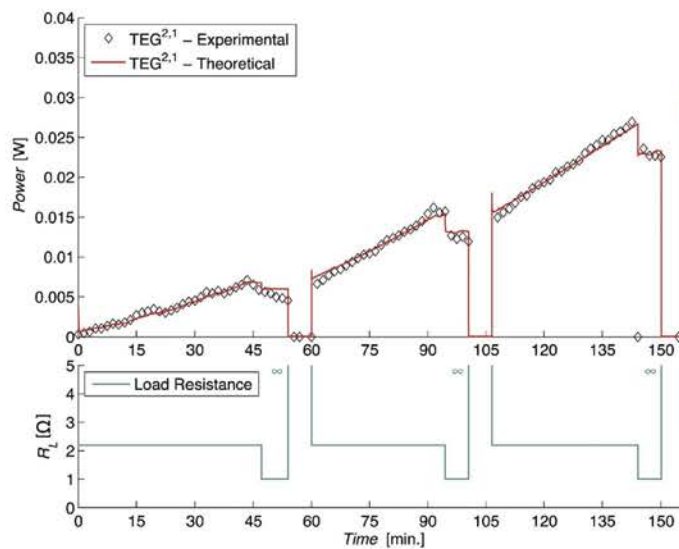**Fig. 13.** Correlation of experimental and simulated output electrical power of a TEG located in stage 3.

Fig. 14. Correlation of experimental and simulated temperature difference between inlet and outlet of LTEH.
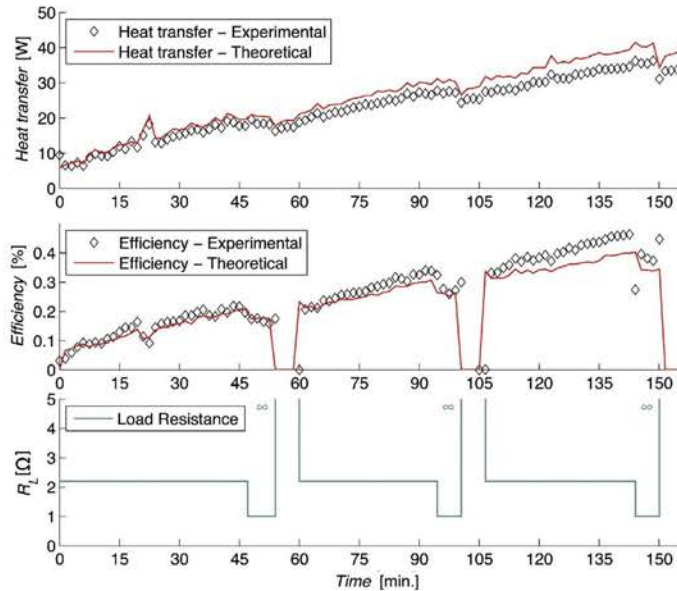
145

Fig. 15. Correlation of experimental and simulated heat transfer and system efficiency of the LTEH.

In Figs. 8–10, the effects of inlet temperature and step changes of load resistance under conditions of Section 4 can be observed. Although there is not appreciable difference between above voltages, an accurately analysis shown that as the stage increase, the output voltage decreases. It is very interesting to note the effect that the load current has on the output voltage, which tends to increase as load current decrease. Maximum output voltages (i.e. open circuit voltages) were obtained when no load resistance was selected.

Simultaneously to the voltage measurements, the electrical output power P_{RL} was obtained. As can be observed from Figs. 11–13, P_{RL} tend to increase as inlet temperature T_{in} increases. Moreover, as the stage increase, the output electrical power decreases. However, electrical power does not only depend on the temperature difference between hot and cold sides of the TEG, but also on the load resistance connected. As explained in Ref. [17], the power generation is highest when the load resistance value is close to the internal resistance $R_L = R_{pn}$, which is measured to be about 2.2 Ω. Consequently, different values of R_L will produce lower electrical powers. This effect can be observed in above figures.

For the purpose of assessing the model, the temperature difference between inlet T_{in} and outlet T_{out} was also measured. Due to the fact that T_{out} differences between experimental and theoretical data were too small, the $\Delta T = T_{in}(t) - T_{out}(t)$ was plotted instead. The comparison of experimental and theoretical data is shown in Fig. 14.

Fig. 14 demonstrates that T_{out} is strongly affected by the load resistance. Every increase in 1 leads to an increase in temperature difference between hot and cold side of TEGs due to the greater value of the Peltier effect. This current increment also produces an increment of hot and cold side heat fluxes. Consequently, every decrease in R_L leads to a reduction in fluid outlet temperature.

As can be shown in Fig. 15, the same effect occurs with heat extracted from LTEH, Eq. (1). It is interesting to note that heat transfer decrease with load resistance. Besides, the LTEH efficiency η also is affected by load resistance but not in the same way. In Fig. 15, it can be observed that R_L values close to internal resistance

produces the maximum system efficiencies η. This not only occurs to power generation but also to system efficiency which is highest when load resistance value is close to the internal resistance $R_L = R_{pn}$.

As it can be appreciated from all figures, the simulation results show good agreement with the experimental results, accurately tracking the electro-thermal coupled effects occurring in the TEG system. However, the plotted curves show highest correlation when inlet temperatures are near to average range. This is due to the fact that thermoelectric parameters (i.e. Seebeck coefficient, thermal conductivity and electrical resistance of TEGs) are constant and obtained from steady-state average temperature $\overline{T} = (T_{f,max} + T_{amb})/2$.

6. Conclusions

In this paper, a new computational model capable to simulate the electro-thermal dynamics of a LTEH is presented, and a thermoelectric energy harvester has been constructed to validate this model. The new component, developed in TRNSYS software, had been analysed and validated under steady and transient states with data obtained from the experimental setup.

Although global maximum output electrical power and efficiency is quite low: 0.162 W and 0.46%, respectively; the comparison of results between theoretic analysis and experiment has approved the reasonability of the new component. The root mean square errors RMSE for heat extracted, electrical power generated and temperature difference between inlet and outlet are 0.566 W, $3.9e^{-3}$ W and $7.4e^{-3}$ °C, respectively. Additionally, the normalized root mean square errors NRMSE are 0.67%, 0.5% and 0.894%, respectively.

Besides, the TRNSYS simulation runs without interruptions or delays, consequently the numerical model and the new component can be considered well optimized. Therefore, this new model can be used in design, performance optimization and further application of thermoelectric energy harvesters.

References

[1] Zhou Y, Paul S, Bhunia S. Harvesting wasted heat in a microprocessor using thermoelectric generators: modeling, analysis and measurement. In: Proc Conf on design, automation and test in Europe; 2008.

[2] Ikoma K, Munckiyo M, Furuya K, Kobayashi M, Isumi T, Shinohara K. Thermoelectric module and generator for gasoline engine vehicles. In: Proc Int Conf thermoelectrics; 1998. p. 464–7.

[3] Love N, Szybist J, Sluder C. Effect of heat exchanger material and fouling on thermoelectric exhaust heat recovery. Appl Energy 2012;89:322–8.

[4] Saqr KM, Mansour MK, Musa MN. Thermal design of automobile exhaust based thermoelectric generators: objectives and challenges. Int J Automotive Technol 2008;9(2):155–60.

[5] Kajikawa T. Status and future prospects on the development of thermoelectric power generation systems utilizing combustion heat from municipal solid waste. In: Proc Int Conf thermoelectrics; 1997. p. 28–36.

[6] Ashwin D, Abhijit D, Chris D, Aliakbar A. Progress of thermoelectric power generation systems: prospect for small to medium scale power generation. Renew Sustain Energy Rev 2014;7(1):245.

[7] Bohn MS. Heat-exchanger effectiveness in thermoelectric power generation. Transactions of the ASME. J Heat Transfer 1981;103(4):693–8.

[8] Esarte J, Min G, Rowe DM. Modelling heat exchangers for thermoelectric generators. J Power Sources 2001;93:72–6.

[9] Crane DT, Jackson GS. Optimization of cross flow heat exchangers for thermoelectric waste heat recovery. Energy Convers Manage 2004;45(9):1565–82.

[10] Crane DT, Jackson GS. Systems-level optimization of low temperature thermoelectric waste heat recovery. In: Proceedings of the intersociety energy conversion engineering conference; 2002. p. 583–91.

[11] Yu J, Zhao H. A numerical model for thermoelectric generator with the parallel-plate heat exchanger. J Power Sources 2007;172(1).

[12] Niu X, Yu J, Wang S. Experimental study on low-temperature waste heat thermoelectric generator. J Power Sources 2009;188(2):621–6.

[13] Wu C. Analysis of waste-heat thermoelectric power generators. Appl Therm Eng 1996;16(1):63–5.

[14] Hsiao YY, Chang WC, Chen SL. A mathematic model of thermoelectric module with applications on waste heat recovery from automobile engine. Energy 2010;35(3):1447–54.

[15] Wang Y, Dai C, Wang S. Theoretical analysis of a thermoelectric generator using exhaust gas of vehicles as heat source. Appl Energy 2013;112:1171–80.

[16] Montecucco A, Siviter J, Knox AR. The effect of temperature mismatch on thermoelectric generators electrically connected in series and parallel. Appl Energy 2014;123:47–54.

[17] Massaguer E, Massaguer A, Gonzalez JR, Montoro L. Development and validation of a new TRNSYS type for the simulation of thermoelectric generators. Appl Energy 2014. http://dx.doi.org/10.1016/j.apenergy.2014.08.010.

[18] Kumar S, Heister SD, Xu X, Salvador JR, Meisner GP. Thermoelectric generators for automotive waste heat recovery systems Part II: parametric evaluation and topological studies. J Electron Mater 2013;42(6):944–55.

[19] Klein SA. TRNSYS 16: a transient system simulation program. USA: University of Wisconsin; 2006.

Bibliography

[1]   S.B. Riffat, X. Ma, Thermoelectrics: A review of present and potential applications, Appl. Therm. Eng. 23 (2003) 913–935. doi:10.1016/S1359-4311(03)00012-7.

[2]   S.A. Omer, D.G. Infield, Design and thermal analysis of a two stage solar concentrator for combined heat and thermoelectric power generation, Energy Convers. Manag. 41 (2000) 737–756. doi:http://dx.doi.org/10.1016/S0196-8904(99)00134-X.

[3]   S. Risse, H. Zellbeck, Close-Coupled Exhaust Gas Energy Recovery In A Gasoline Engine, MTZ Worldw. 74 (2013) 54–61. doi:10.1007/s38313-013-0010-y.

[4]   Y. Wang, C. Dai, S. Wang, Theoretical analysis of a thermoelectric generator using exhaust gas of vehicles as heat source, Appl. Energy. 112 (2013) 1171–1180. doi:10.1016/j.apenergy.2013.01.018.

[5]   C.-C. Weng, M.-J. Huang, A simulation study of automotive waste heat recovery using a thermoelectric power generator, Int. J. Therm. Sci. 71 (2013) 302–309. doi:http://dx.doi.org/10.1016/j.ijthermalsci.2013.04.008.

[6]   D. Champier, J.P. Bédécarrats, T. Kousksou, M. Rivaletto, F. Strub, P. Pignolet, Study of a TE (thermoelectric) generator incorporated in a multifunction wood stove, Energy. 36 (2011) 1518–1526. doi:http://dx.doi.org/10.1016/j.energy.2011.01.012.

[7]   R. Venkatasubramanian, E. Siivola, T. Colpitts, B. O'Quinn, Thin-film thermoelectric devices with high room-temperature figures of merit.,

Nature. 413 (2001) 597–602. doi:10.1038/35098012.

[8]   A.I. Boukai, Y. Bunimovich, J. Tahir-Kheli, J.-K. Yu, W.A. Goddard III, J.R. Heath, Silicon nanowires as efficient thermoelectric materials: Supplementary information, Nature. 451 (2008) 168–171. doi:10.1038/nature06458.

[9]   D.M. Rowe, CRC Handbook of Thermoelectrics, New York. 16 (1995) 1251–1256. doi:10.1016/S0960-1481(98)00512-6.

[10]   L.-D. Zhao, S.-H. Lo, Y. Zhang, H. Sun, G. Tan, C. Uher, et al., Ultralow thermal conductivity and high thermoelectric figure of merit in SnSe crystals., Nature. 508 (2014) 373–7. doi:10.1038/nature13184.

[11]   A. Majumdar, Thermoelectricity in Semiconductor Nanostructures, Science (80-.). 303 (2004) 777–778. doi:10.1126/science.1093164.

[12]   J. Bazinet, The fundamentals of energy harvesting design, 1 Sept. (2011). http://powerelectronics.com/energy-harvesting/fundamentals-energy-harvesting-design (accessed March 12, 2016).

[13]   Ferrotec Corp., Ferrotec's Thermoelectric Technical Reference Guide, (n.d.). https://www.ferrotec.com/technology/thermoelectric/thermalRef13/ (accessed March 12, 2016).

[14]   M. Hodes, On one-dimensional analysis of thermoelectric modules (TEMs), IEEE Trans. Components Packag. Technol. 28 (2005) 218–229. doi:10.1109/TCAPT.2005.848532.

[15]   S. Lineykin, S. Ben-Yaakov, Modeling and analysis of thermoelectric modules, IEEE Trans. Ind. Appl. 43 (2007) 505–512. doi:10.1109/TIA.2006.889813.

[16]   S. Kumar, S.D. Heister, X. Xu, J.R. Salvador, G.P. Meisner, Thermoelectric Generators for Automotive Waste Heat Recovery Systems Part II: Parametric Evaluation and Topological Studies, J. Electron. Mater. 42 (2013) 944–955. doi:10.1007/s11664-013-2472-8.

[17]   X. Gou, S. Yang, H. Xiao, Q. Ou, A dynamic model for

thermoelectric generator applied in waste heat recovery, Energy. 52 (2013) 201–209. doi:10.1016/j.energy.2013.01.040.

[18] F. Meng, L. Chen, F. Sun, A numerical model and comparative investigation of a thermoelectric generator with multi-irreversibilities, Energy. 36 (2011) 3513–3522. doi:10.1016/j.energy.2011.03.057.

[19] Y.Y. Hsiao, W.C. Chang, S.L. Chen, A mathematic model of thermoelectric module with applications on waste heat recovery from automobile engine, Energy. 35 (2010) 1447–1454. doi:10.1016/j.energy.2009.11.030.

[20] C. Wu, Analysis of waste-heat thermoelectric power generators, Appl. Therm. Eng. 16 (1996) 63–69. doi:10.1016/1359-4311(95)00014-5.

[21] D.T. Crane, G.S. Jackson, Optimization of cross flow heat exchangers for thermoelectric waste heat recovery, Energy Convers. Manag. 45 (2004) 1565–1582. doi:10.1016/j.enconman.2003.09.003.

[22] D.T. Crane, G.S. Jackson, Systems-level optimization of low-temperature thermoelectric waste heat recovery, IECEC '02. 2002 37th Intersoc. Energy Convers. Eng. Conf. 2002. (2002). doi:10.1109/IECEC.2002.1392111.

[23] J. Yu, H. Zhao, A numerical model for thermoelectric generator with the parallel-plate heat exchanger, J. Power Sources. 172 (2007) 428–434. doi:10.1016/j.jpowsour.2007.07.045.

[24] X. Niu, J. Yu, S. Wang, Experimental study on low-temperature waste heat thermoelectric generator, J. Power Sources. 188 (2009) 621–626. doi:10.1016/j.jpowsour.2008.12.067.

[25] B. Xiong, L. Chen, F. Meng, F. Sun, Modeling and performance analysis of a two-stage thermoelectric energy harvesting system from blast furnace slag water waste heat, Energy. 77 (2014) 562–569. doi:10.1016/j.energy.2014.09.037.

[26] A. Montecucco, J. Siviter, A.R. Knox, The effect of temperature mismatch on thermoelectric generators electrically connected in series and parallel, Appl. Energy. 123 (2014) 47–54. doi:10.1016/j.apenergy.2014.02.030.

[27] G. Liang, J. Zhou, X. Huang, Analytical model of parallel thermoelectric generator, Appl. Energy. 88 (2011) 5193–5199. doi:10.1016/j.apenergy.2011.07.041.

[28] WEO, World Energy Outlook, Int. Energy Agency. (2012) 690 pp. doi:10.1787/20725302.

[29] W. Projections, BP Energy Outlook 2030, Outlook. 0383 (2011) 230. doi:10.5555/jan.010a.2013.

[30] H2ESOT: waste heat to electrical energy via sustainable organic thermoeletric devices., (2015). www.h2esot.com.

[31] M. and Company, Energy efficiency: A compelling gobal resource, 2010.

[32] G. Skomedal, Thermoelectric Materials for Waste Heat Recovery, 2013.

[33] L. Chen, J. Gong, F. Sun, C. Wu, Effect of heat transfer on the performance of thermoelectric generators, Int. J. Therm. Sci. 41 (2002) 95–99. doi:10.1016/S1290-0729(01)01307-2.

[34] D. Ebling, M. Jaegle, M. Bartel, A. Jacquot, H. Böttner, Multiphysics simulation of thermoelectric systems for comparison with experimental device performance, in: J. Electron. Mater., 2009: pp. 1456–1461. doi:10.1007/s11664-009-0825-0.

[35] A. Montecucco, J.R. Buckle, A.R. Knox, Solution to the 1-D unsteady heat conduction equation with internal Joule heat generation for thermoelectric devices, Appl. Therm. Eng. 35 (2012) 177–184. doi:10.1016/j.applthermaleng.2011.10.026.

[36] N.Q. Nguyen, K. V. Pochiraju, Behavior of thermoelectric generators exposed to transient heat sources, Appl. Therm. Eng. 51 (2013) 1–9. doi:10.1016/j.applthermaleng.2012.08.050.

[37] A. Montecucco, A.R. Knox, Accurate simulation of thermoelectric power generating systems, Appl. Energy. 118 (2014) 166–172. doi:10.1016/j.apenergy.2013.12.028.

[38] et al. S.A. Klein, TRNSYS 16: A Transient System Simulation Program, Univ. Wisconsin USA. (2006).

[39] X. Gou, H. Xiao, S. Yang, Modeling, experimental study and

optimization on low-temperature waste heat thermoelectric generator system, Appl. Energy. 87 (2010) 3131–3136. doi:10.1016/j.apenergy.2010.02.013.

[40] S. Kim, Analysis and modeling of effective temperature differences and electrical parameters of thermoelectric generators, Appl. Energy. (2012). doi:10.1016/j.apenergy.2012.09.006.

[41] A. Rodríguez, J.G. Vián, D. Astrain, A. Martínez, Study of thermoelectric systems applied to electric power generation, Energy Convers. Manag. 50 (2009) 1236–1243. doi:10.1016/j.enconman.2009.01.036.

[42] C.H. Cheng, S.Y. Huang, T.C. Cheng, A three-dimensional theoretical model for predicting transient thermal behavior of thermoelectric coolers, Int. J. Heat Mass Transf. 53 (2010) 2001–2011. doi:10.1016/j.ijheatmasstransfer.2009.12.056.

[43] Y. Zhou, S. Paul, S. Bhunia, Harvesting Wasted Heat in a Microprocessor Using Thermoelectric Generators: Modeling, Analysis and Measurement, 2008 Des. Autom. Test Eur. (2008) 98–103. doi:10.1109/DATE.2008.4484669.

[44] K. Ikoma, M. Munekiyo, K. Furuya, M. Kobayashi, T. Izumi, K. Shinohara, Thermoelectric module and generator for gasoline engine vehicles, Seventeenth Int. Conf. Thermoelectr. Proc. ICT98 (Cat. No.98TH8365). (1998) 464–467. doi:10.1109/ICT.1998.740419.

[45] N.D. Love, J.P. Szybist, C.S. Sluder, Effect of heat exchanger material and fouling on thermoelectric exhaust heat recovery, Appl. Energy. 89 (2012) 322–328. doi:10.1016/j.apenergy.2011.07.042.

[46] K.M. Saqr, M.K. Mansour, M.N. Musa, Thermal design of automobile exhaust based thermoelectric generators: Objectives and challenges, Int. J. Automot. Technol. 9 (2008) 155–160. doi:10.1007/s12239-008-0020-y.

[47] T. Kajikawa, Status and future prospects on the development of thermoelectric power generation systems utilizing combustion heat from municipal solid waste, Thermoelectr. 1997. Proc. ICT '97. XVI Int. Conf. (1997) 28–36. doi:10.1109/ICT.1997.666971.

[48] A. Date, A. Date, C. Dixon, A. Akbarzadeh, Progress of thermoelectric power generation systems: Prospect for small to medium scale power generation, Renew. Sustain. Energy Rev. 33 (2014) 371–381. doi:10.1016/j.rser.2014.01.081.

[49] M. S. Bohn, Heat-Exchanger Effectiveness in Thermoelectric Power Generation, in: J. Heat Transfer, 1981: pp. 693–698.

[50] J. Esarte, G. Min, D.M. Rowe, Modelling heat exchangers for thermoelectric generators, J. Power Sources. 93 (2001) 72–76. doi:10.1016/S0378-7753(00)00566-8.

[51] A. Montecucco, J. Siviter, A.R. Knox, The effect of temperature mismatch on thermoelectric generators electrically connected in series and parallel, Appl. Energy. 123 (2014) 47–54. doi:10.1016/j.apenergy.2014.02.030.

[52] E. Massaguer, a. Massaguer, L. Montoro, J.R. Gonzalez, Development and validation of a new TRNSYS type for the simulation of thermoelectric generators, Appl. Energy. 134 (2014) 65–74. doi:10.1016/j.apenergy.2014.08.010.

[53] M. a. Karri, E.F. Thacher, B.T. Helenbrook, Exhaust energy conversion by thermoelectric generator: Two case studies, Energy Convers. Manag. 52 (2011) 1596–1611. doi:10.1016/j.enconman.2010.10.013.

[54] H. Xiao, K. Qiu, X. Gou, Q. Ou, A flameless catalytic combustion-based thermoelectric generator for powering electronic instruments on gas pipelines, Appl. Energy. 112 (2013) 1161–1165. doi:10.1016/j.apenergy.2013.01.078.

[55] Y.Y. Hsiao, W.C. Chang, S.L. Chen, A mathematic model of thermoelectric module with applications on waste heat recovery from automobile engine, Energy. 35 (2010) 1447–1454. doi:10.1016/j.energy.2009.11.030.

[56] a. Goudarzi, a. Mozaffari, P. Samadian, a. Rezania, L. a. Rosendahl, Intelligent design of waste heat recovery systems using thermoelectric generators and optimization tools, Meccanica. 49 (2014) 1211–1223. doi:10.1007/s11012-014-9878-0.

[57] F. Meng, L. Chen, F. Sun, B. Yang, Thermoelectric power

generation driven by blast furnace slag flushing water, Energy. 66 (2014) 965–972. doi:10.1016/j.energy.2014.02.018.

[58] N.R. Kristiansen, G.J. Snyder, H.K. Nielsen, L. Rosendahl, Waste Heat Recovery from a Marine Waste Incinerator Using a Thermoelectric Generator, J. Electron. Mater. 41 (2012) 1024–1029. doi:10.1007/s11664-012-2009-6.

[59] X.F. Zheng, Y.Y. Yan, K. Simpson, A potential candidate for the sustainable and reliable domestic energy generation– Thermoelectric cogeneration system, Appl. Therm. Eng. 53 (2013) 305–311. doi:10.1016/j.applthermaleng.2012.03.020.

[60] M.P. Codecasa, C. Fanciulli, R. Gaddi, F. Gomez-Paz, F. Passaretti, Update on the Design and Development of a TEG Cogenerator Device Integrated into Self-Standing Gas Heaters, J. Electron. Mater. 42 (2013) 2243–2248. doi:10.1007/s11664-013-2598-8.

[61] E. Massaguer, A. Massaguer, L. Montoro, J.R. Gonzalez, Modeling analysis of longitudinal thermoelectric energy harvester in low temperature waste heat recovery applications, Appl. Energy. 140 (2015) 184–195. doi:10.1016/j.apenergy.2014.12.005.

$$\text{①} \quad T_m^p + 2 f_0 \, \ell_2 \, T_{h0} = T_m^{p+1}(2 f_0 + \ell_2 \ell_2^2 f_0 + \ell_2) - 2 f_0 \, T_{m+1}$$

$$\text{②} \quad T_m^p = (1 + 2 f_0) T_m^{p+1} - f_0 \, T_{m-1}^{p+1} - T_{m+1}^{p+1} \qquad \text{ⓐ}$$

$$\text{③}$$

$$\frac{(P_1 c_1 + f_2 c_2) \cdot A \frac{\Delta x}{2} \cdot T_m^{p+1} - \left(P_1 c_1 + f_2 c_2 \right) A \frac{\Delta x}{2} \cdot T_m^p}{\Delta t} = \qquad \text{ⓑ}$$

$$\frac{A}{\Delta x} \cdot T_{m-1}^{p+1} - \frac{k_1 A}{\Delta x} \cdot T_m^{p+1} + \frac{k_2 A_2}{\Delta x} T_{m+1}^{p+1} - \frac{k_2 A_2}{\Delta x} \cdot T_m^{p+1} +$$

$$\frac{u^2 d^2 \left\{ T_{m+1}^{p+1} \cdot T_m^{p+1} \right\}}{R_2 + f_2 \frac{\Delta x}{A_2}} - \frac{u^2 d^2 \left(T_m^{p+1} \right)}{R_2 + f_2 \frac{\Delta x}{A_2}} + \frac{1}{2} \frac{u^2 d^2 \left(T_{m+1}^{p+1} \right)^2}{\left(R_2 + f_2 \frac{\Delta x}{A_2} \right)^2} \cdot f_2 \frac{\Delta x}{A_2}$$

$$\frac{\frac{1}{2} \frac{u^2 d^2 \left(T_m^{p+1} \right)^2}{\left(R_2 + f_2 \frac{\Delta x}{A_2} \right)^2} \cdot f_2 \frac{\Delta x}{A_2} - \frac{1}{2} \frac{u^2 d^2 \cdot 2 \left(T_{m+1}^{p+1} \right) \cdot \left(T_m^{p+1} \right)}{\left(R_2 + f_2 \frac{\Delta x}{A_2} \right)^2} f_2 \frac{\Delta x}{A_2}}{}$$

$$\frac{A_1}{\Delta x} T_{m-1}^{p+1} + \left(-\frac{k_1 A_1}{\Delta x} + \left(-\frac{k_2 A_2}{\Delta x} \right) + \frac{u^2 d^2 \cdot T_{m+1}^{p+1}}{R_2 + f_2 \frac{\Delta x}{A_2}} + \left(-\frac{u^2 d^2 \, T_m^{p+1}}{R_2 + f_2 \frac{\Delta x}{A_2}} \right) +$$

$$u \frac{\Delta x}{2} + \frac{1}{2} \cdot \frac{u^2 d^2 \, T_m^{p+1}}{\left(R_2 + f_2 \frac{\Delta x}{A_2} \right)^2} \cdot f_2 \frac{\Delta x}{A_2} - \frac{1}{2} \frac{u^2 d^2 \cdot 2 \, T_{m+1}^{p+1}}{\left(R_2 + f_2 \frac{\Delta x}{A_2} \right)^2} f_2 \frac{\Delta x}{A_2} \right) \cdot T_m^{p+1}$$